Forest&Wood Products Australia
Knowledge for a sustainable Australia

PROCESSING

PROJECT NUMBER: PNB045-0809 AUGUST 2011

Evaluation of super-heated steam vacuum drying viability and development of a predictive drying model for four Australian hardwood species

This report can also be viewed on the FWPA website
www.fwpa.com.au
FWPA Level 4, 10-16 Queen Street,
Melbourne VIC 3000, Australia
T +61 (0)3 9927 3200 F +61 (0)3 9927 3288
E info@fwpa.com.au W www.fwpa.com.au

Evaluation of super-heated steam vacuum drying viability and development of a predictive drying model for four Australian hardwood species

Prepared for

Forest & Wood Products Australia

by

Adam Redman

Forest&Wood Products Australia
Knowledge for a sustainable Australia

Publication: Evaluation of super-heated steam vacuum drying viability and development of a predictive drying model for four Australian hardwood species

Project No: PNB045-0809

ISBN: 978-1-921763-38-0

Researcher:
A. Redman
DEEDI
Salisbury Research Centre
50 Evans Road Salisbury

Final report received by FWPA in August, 2011

Forest & Wood Products Australia Limited
Level 4, 10-16 Queen St, Melbourne, Victoria, 3000
T +61 3 9927 3200 F +61 3 9927 3288
E info@fwpa.com.au
W www.fwpa.com.au

1 Executive Summary

The primary objectives of this study were to:

- Establish the viability of vacuum drying for four high commercial volume Australian hardwood species in terms of drying quality, time and cost. The four species investigated were: *Corymbia citriodora* (spotted gum), blackbutt (*Eucalyptus pilularis*), messmate (*Eucalyptus obliqua*) and jarrah (*Eucalyptus marginata*)
- Develop an economic model to compare the drying costs of vacuum and conventional drying.
- Develop a predictive vacuum drying heat and mass transfer deterministic model using fundamental principles. Investigate the model limitations and sensitivities.
- Validate the drying model against data derived from applied drying trials.

We investigated the viability of vacuum drying by conducting a series of four trials per species and developing an economic model application. For each trial 25 x 100 mm nominal cross-section dimension boards were kiln dried in a 2 m^3 capacity vacuum kiln and compared with end-matched boards kiln dried in commercial conventional driers. We used the economic model to investigate the comparative costs of small (10 m^3), medium (35 m^3) and large (50 m^3) vacuum and conventional operations using the best quality results from the drying trials as input data, and data provided by industry.

The results of drying trials show that vacuum drying produces material of the same or better quality than is currently being produced by conventional methods within 41 to 66 % of the drying time, depending on the species. Economic analysis indicates positive or negative results depending on the species and the size of drying operation. Definite economic benefits exist by vacuum drying over conventional drying for all operation sizes, in terms of drying quality, time and economic viability, for *E. marginata* and *E. pilularis*. The same applies for vacuum drying *C. citriodora* and *E. obliqua* in larger drying operations (kiln capacity 50 m^3 or above), but not for smaller operations at this stage. Further schedule refinement has the ability to reduce drying times further and may improve the vacuum drying viability of the latter species in smaller operations.

A comprehensive heat and mass transfer drying model was developed with the ability to accurately simulate vacuum and conventional drying of Australian hardwood species. Measurement of essential wood drying properties required for the model revealed that water movement within these species occurs mostly by diffusion. Subsequently diffusion measurements were critical for refining the model accuracy. Validation of the model resulted in excellent simulated accuracy where the predicted drying times agreed with the kiln trial drying times by 91 to 98 %, depending on the species. This has the ability to greatly accelerate the time required for further vacuum and conventional drying research, and to quickly design new drying schedules.

Overall, the outcomes of this research provide industry with the confidence to make informed decisions regarding their potential investment in vacuum drying technology. With the aid of the economic model application and the results of the drying trials, industry has the ability to investigate the viability of vacuum drying over conventional drying dependant in their own specific requirements.

Table of Contents

2 Introduction

Drying timber to produce material for high quality applications is an expensive and time-consuming operation. It is often referred to as the 'bottleneck' of the production process. The drying process consumes approximately 70% of the energy required to convert green logs into dried, value added products. Additionally, estimates suggest that up to 10% degrade occurs in dried wood due to the drying process because of checking, collapse, distortion, and moisture variation. Over the years the timber industry worldwide, in conjunction with researchers, engineers and manufacturers, have strived to dry quality timber as quickly and cheaply as possible to maximise profitability. Therefore, the timber industry pursues any technologies that can improve the quality and reduce timber drying times and costs.

Conventional kiln drying with controlled heating, humidity and air-flow under atmospheric pressure conditions is the primary method for drying timber in Australia (Nolan *et al.*, 2003). In recent years, with emerging technological advancements in construction, computer control and less expensive materials, vacuum drying of hardwood timber has been proven (particularly in Europe and USA) in many applications to be a more economical alternative to drying using conventional methods, with similar or better quality outcomes (Savard *et al.*, 2004). For this reason, Queensland Government's Department of Employment, Economic Development and Innovation (DEEDI) - Agri-Science Queensland expanded its seasoning research and development capacity through the purchase of a 2 m^3 research vacuum kiln to investigate the viability of vacuum drying technology for drying Australian hardwood species. Initial kiln trials drying native forest *Corymbia citriodora* (spotted gum) and young plantation *Eucalyptus cloeziana* (Gympie messmate) have proven that these species can be vacuum dried approximately 60% faster than conventional drying, within acceptable grade quality limits (Redman, 2007).

The results obtained from these preliminary vacuum drying trials generated much interest from the Australian hardwood timber industry. In response, Forest and Wood Products Australia (FWPA) in conjunction with various industry partners and DEEDI invested in this project to establish the viability of vacuum drying technology for drying four high commercial volume Australian hardwood species in terms of drying quality, time and cost. The first part of this work involved a series of applied drying trials and an applied economic model application to establish vacuum drying viability in terms of dried quality, time and cost. The industry partners involved in this part of the research were:

- Dale and Meyers (QLD)
- Burnett Sawmilling (QLD)
- Boral Timber (NSW)
- J. Notaras and Sons (NSW)
- Hurford Hardwood (NSW)
- ITC Timber (TAS)
- Gunns (TAS)
- Gunns (WA)
- Brunner-Hildebrand (Germany)

We recognised that a better knowledge of the material and associated drying behaviour was required to optimise the vacuum drying process in the future. Therefore, we chose to development a hardwood vacuum drying model. This required collaboration with a number of renowned experts in the field. The modelling collaborators and their areas of expertise were:

- Queensland University of Technology (QUT) – mathematical modelling and visualisation
- Wood Science at École Nationale du Génie Rural des Eaux et des Forêts (ENGREF) in Nancy, France – drying modelling, instrumentation and wood property measurement
- Queensland Cyber Infrastructure Foundation (QCIF) – High performance computing and model optimisation

Some of the wood property measurements, essential to develop an accurate model, required the use of specifically designed equipment only available in the ENGREF laboratory, France. With the aid of funding from an FWPA Denis Cullity fellowship, this author travelled to the ENGREF laboratory to perform the required tests. The results are reported by Redman (http://fwpa.com.au, 2008). For the modelling component, QCIF provided external funding to optimise the model convergence times and use of High Performance Computers (HPC). The results of which are reported by Redman (http://www.qcif.edu.au, 2010). Additionally, the vacuum drying model was developed and implemented as part of this authors PhD project offered by QUT. At the stage of writing Redman's PhD is pending.

2.1 Applied drying – Experimental drying trials

The following report presents the results of sixteen vacuum drying trials and corresponding end–matched conventional drying trials for *C. citriodora*, *E. pilularis*, *E. marginata* and *E. obliqua* (four trials per species). The structure of applied drying trials' reporting is such that the materials and methods section is generic across all trials and species. Results and conclusions are reported separately for each species, allowing the reader to peruse their specific area (species) of interest.

2.2 Applied trials - Economic model

For the hardwood sawn timber industry, drying is the single processing step that adds the greatest value. However, there is significant variation in this cost between processors and methods. Therefore, processors who operate with higher efficiency, have greater profitability than their competitors.

This section of the report investigates economic comparisons between conventional and vacuum kiln drying from the green condition. This was facilitated via the creation and use of an economic model based on fundamental economic and wood drying principles. The objective of this work was to determine the economic viability of vacuum drying Australian hardwoods compared to current conventional methods. This was achieved by using the 'best case scenario' vacuum drying trial for each species studied. The best case for each species was chosen based on the best dried quality outcome (comparable to conventional trials) and fastest drying time. Comparisons were based on determining the vacuum drying time producing the same cost of drying as for conventional trials and comparing this to the vacuum drying times achieved for the best case trials per species.

We present a number of case studies for different sized operations.

2.3 Drying modelling - Measurement of kiln conditions and wood drying properties

We used specialised instruments on test boards during vacuum drying trials to obtain, through continuous 'real–time' measurements, a greater understanding of the kiln conditions and

wood drying properties. This is essential to validate and provide actual kiln and wood property data for the modelling component of this project and hence optimise the process. As such the proposed model is 'deterministic', whereby actual wood property and kiln data are required to 'feed' the model to obtain the most accurate simulations possible. A deterministic model is one in which outcomes are determined through known relationships among states or events, without any room for random variation. In such models, a given input will always produce the same output.

The wood drying properties measured were: internal wood temperature at various depths using thermocouples, global shrinkage and stress/strain characterisation using strain gauges and jig, mass/moisture content using load cells, and internal pressure using pressure gauges. The kiln conditions measured during vacuum drying were atmospheric pressure, temperature, relative humidity, and air velocity.

2.4 Drying modelling - Measurement of essential wood properties

For each species, we measured a number of wood properties deemed essential input data for the model. They were deemed essential, based on previous modelling research relating to model sensitivities (Perré, 1996, Salin, 2010). We calculated other wood properties required for modelling, either from theory or inferred from essential measured wood properties. The essential wood properties measured to achieve accurate modelling results, were:

- wood density – from drying trials
- initial wood moisture content – from drying trials
- fibre and vessel porosity – from microscopy imaging
- gas permeability (radial, tangential and longitudinal directions) – using specialised equipment
- diffusivity (radial, tangential and longitudinal directions) – using specialised equipment
- shrinkage (radial and tangential) and sorption isotherm – using specialised equipment.

2.5 Drying modelling - Vacuum drying modelling

As the anatomical configuration of wood is complex, we must write transport equations at the macroscopic scale. This leads to the definition of empirical laws of migration that can be demonstrated to a large extent by averaging over representative volumes (Perré, 1996). At this level, we observe the porous medium as a fictitious, continuous medium. By using this approach, most fluxes can be written as the product of a coefficient times the driving force, both for the porous medium and the surrounding air. The conservation of liquid, water vapour, air and enthalpy enable a set of equations governing transfer in porous media to be derived (Whitaker, 1977). These equations have subsequently been used to model the softwood drying process (Perré, 1996, Perré and Turner, 1999b), where their ability to describe several different drying configurations has been proven.

The most recent application of the model describes the heat and mass transfer drying of single boards applied to the growth rings of softwood (Perré and Turner, 2008). This model describes the drying process for both homogeneous and heterogeneous cross sections, where density and transport differences due to the presence of growth rings are accounted. As the species investigated in this study are relatively homogenous, the majority of the transport model equations are from the homogenous model reference.

This softwood model, known as *TransPore 2D* was used as a basis for the hardwood model. MatLab was the predominant platform used to write the heat and mass transfer model code, with some components written in C++ to enable fast convergence (completion).

3 Methodology

3.1 Applied drying – Experimental drying trials

The efficiency of vacuum drying emanates from the fact that operating at low pressures reduces the boiling point of water, enabling generation of an overpressure, maintained within the product throughout drying. This overpressure accelerates internal liquid and vapour migration, producing a very efficient drying rate. Despite the fact that the effectiveness of external heat transfer decreases at low pressure, it is still necessary to supply adequate supply to the material for the purposes of evaporation. The DEEDI kiln uses convective, superheated steam for this purpose. The kiln operates between 0.1-0.2 bar, whereby the boiling point of water is around 45^{o}C. The convectively heated vacuum dryer uses a mixture of superheated steam and air between 40-80^{o}C, with a relative humidity of 90%.

3.1.1 Sourcing material and preparation

Table 1 summarises the species names (scientific and common), source (state, sawmill and forest type), conventional drying type and abbreviated notation for each trial. We will use this notation from this point forward to identify each trial. For each trial, we performed end-matched vacuum and conventional trials, where conventional trials consisted of either kiln drying from the green condition or a combination of air and final kiln drying.

Table 1. Trial number, source, abbreviated notation and drying treatment results reported

	Species name		Source			Conventional	
Trial number	Scientific	Common	State	Sawmill	Forest type	Drying Type	Abbreviation
1	*C. citriodora*	spotted gum	QLD	Dale and Myers, Maryborough	native	green	SPG1
2	*E. marginata*	jarrah	WA	Gunns Timber, Manjimup	native	green	JAR1
3	*E. pilularis*	blackbutt	NSW	Hurford Hardwood, Casino	native	air	BBT1
4	*E. obliqua*	messmate	TAS	ITC Timber, Huonville	native	air	MES1
5	*C. citriodora*	spotted gum	QLD	Burnett Sawmill, Bundaberg	native	air	SPG2
6	*E. marginata*	jarrah	WA	Gunns Timber, Manjimupp	native	green	JAR2
7	*E. pilularis*	blackbutt	NSW	Boral Timber, Murwillumbah	native	green	BBT2
8	*E. obliqua*	messmate	TAS	ITC Timber, Huonville	native	green	MES2
9	*C. citriodora*	spotted gum	QLD	Dale and Myers, Maryborough	native	green	SPG3
10	*E. marginata*	jarrah	WA	Gunns Timber, Manjimupp	native	green	JAR3
11	*E. pilularis*	blackbutt	NSW	Boral Timber, Murwillumbah	native	green	BBT3
12	*E. obliqua*	messmate	TAS	Gunns Timber, Launceston	native	green	MES3
13	*C. citriodora*	spotted gum	QLD	Dale and Myers, Maryborough	native	green	SPG4
14	*E. marginata*	jarrah	WA	Gunns Timber, Manjimupp	native	green	JAR4
15	*E. pilularis*	blackbutt	NSW	Boral Timber, Murwillumbah	native	green	BBT4
16	*E. obliqua*	messmate	TAS	Gunns Timber, Launceston	native	green	MES4

The boards used for each trial came from mature native forest logs. Sawmills supplied 350 green–off–saw boards (heart free) of nominal dimension 25 x 100 x 4500 mm, except for trial BBT2 where board cross sections were 25 x 125 mm. We crosscut the boards in half using a chainsaw (Plate 1), labelled (identical label for each end–matched board, Plate 2) and end painted with a wax emulsion sealer.

Plate 1. Preparation of end matched boards

Plate 2. End coated and labelled boards

One-half of the end–matched boards remained on–site for industry standard conventional drying. The conventional drying treatment differed between trials depending on each site's general practice (i.e. kiln drying from green or a combination of air and final kiln drying). We wrapped the other half of the boards in impermeable plastic to prevent drying during transportation and dispatched to the DEEDI Salisbury Research Centre (SRC) for vacuum drying. The conventionally dried material was transported to SRC for dried quality assessment upon the completion of drying.

For each trial 100 end–matched sample boards were randomly[1] chosen for detailed wood property and quality assessment. We chose this number of boards based on our experience to account for the natural variation of wood properties.

3.1.2 Drying properties and quality

Table 2 outlines the wood properties and dried quality assessments performed on the 100 sample boards for both conventional and vacuum drying trials. Figure 1 illustrates the sampling breakdown, showing length of samples and properties measured, for each trial. We conducted all tests in accordance with:

- Australian and New Zealand standards *AS/NZS 1080.1:1997 Timber–Methods of test–Method 1: Moisture content* (Standards Australia, 1997),
- *AS/NZS 1080.3:2000 Timber–Methods of Test–Method 3: Density* (Standards Australia, 2000),
- *AS 2796:1999 Timber–Hardwood–Sawn and milled products* (Standards Australia, 1999) and *AS/NZS 4787:2001 Timber–Assessment of drying quality* (Standards Australia, 2001).

We did not measure wood properties on the conventionally dried boards in the green condition as we assumed that over a sample size of 100 boards the average end–matched sample properties would be similar to those measured for the vacuum dried boards in the green condition. All properties measured for the vacuum dried sample boards were on the undressed timber, except for surface checking which were undertaken after dressing. Boards were evenly dressed on both wide faces to the common strip flooring thickness of 19 mm. For the purpose of this study, dried quality in accordance with *AS/NZS 4787:2001* (Standards Australia, 2001) was deemed acceptable if 90% of samples fell into quality class B or better, unless otherwise stated.

[1] Numbers randomly generated using Research *Randomizer* internet program, see http://www.randomizer.org/form.htm.

Table 2. Wood properties and dried quality measurements for each trial

Properties measured (standard)	Vacuum		Conventional
	Green	Dry	Dry
Cross-sectional MC (AS/NZS 1080.1, AS/NZS 4787, AS 2796)	✓	✓	✓
MC gradient (AS/NZS 1080.1, AS/NZS 4787)	✓	✓	✓
Distortion (AS 2796)	✓	✓	✓
Surface checking (AS 2796)	✓	✓	✓
Internal checking (AS/NZS 4787)		✓	✓
End split (AS/NZS 4787)	✓	✓	✓
Drying stress (AS/NZS 4787)		✓	✓
Collapse (AS/NZS 4787)		✓	✓

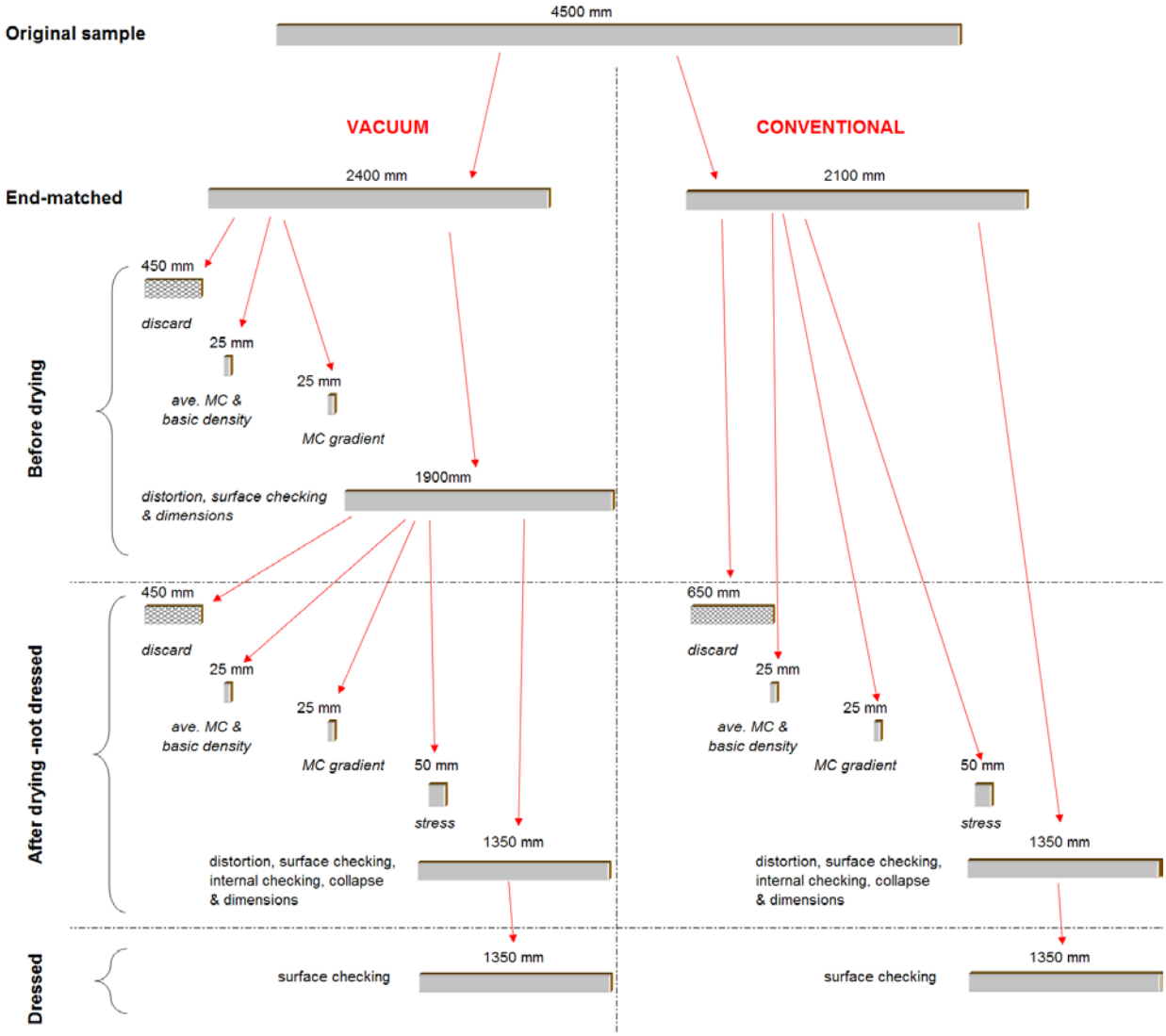

Figure 1. Schematic of sampling breakdown

Moisture content

Before vacuum drying, we removed 25 mm long cross sections for initial green cross–sectional MC determination while docking sample boards to 1.9 m, the maximum board length governed by the vacuum kiln. Moisture content was determined using the oven-dry method in accordance with *AS/NZS 1080.1:1997* (Standards Australia, 1997).

Final dried cross–sectional MC was determined from sections removed from each board, no closer than 400 mm from the board end. Two 25 mm long sections per board enabled cross-

sectional MC and MC gradients to be calculated (by ripping into approximate 1/3 thickness pieces and calculating MC in accordance with *AS/NZS 1080.1:1997* (Standards Australia, 1997). Both cross–sectional MC and MC gradient were assessed in accordance with *AS/NZS 4787:2001* (Standards Australia, 2001). Final cross–sectional MC was also assessed in accordance with *AS 2796:1999* (Standards Australia, 1999), which specifies all boards (for strip flooring) must have a MC between 9 and 14%, unless otherwise agreed.
The target final cross-sectional MC was 11% for all trials.

Basic Density

The green MC sections described above were also used to measure basic density in accordance with *AS/NZS 1080.3:2000* (Standards Australia, 2000). Density was determined by measuring the MC of the test piece (in accordance with *AS/NZS 1080.1:1997*), and the volume of the test piece before oven drying.

Distortion

Each sample board was graded for distortion (i.e. twist, spring, bow and cup) in accordance with Australian Standard *AS 2796:1999* (Standards Australia, 1999).

Surface and internal checking

When kiln drying was complete, each board was assessed for surface checking (on both wide faces) in accordance with Australian Standard *AS2796.3:1999* (Standards Australia, 1999), whereby a board was deemed to make select (best) grade if no surface checks on either face were greater than 250 mm long or 1 mm wide. We assessed surface checking on boards in the dressed condition at a thickness of 19 mm.

The presence of internal checking was determined on a present or absent basis by visually inspecting the freshly sawn end of each board (i.e. after we removed the 400 mm and MC sections). Internal checking was assessed in accordance with *AS/NZS 4787:2001* (Standards Australia, 2001).

End split

End splits were measured and assessed (both ends) in accordance with Australian and New Zealand Standard *AS/NZS 4787:2001* (Standards Australia, 2001).

Drying stress

When drying was complete, a 25 mm cross–section was removed (as adjacent to the MC sample location) and used to quantify residual drying stress in accordance with *AS/NZS 4787:2001* (Standards Australia, 2001).

We quantified drying stress by measuring the width of each cross section before ripping the section down the middle and measuring the gap between the freshly sawn concave/convex faces (Figure 2). The degree of drying stress is the ratio of gap width and section width expressed as a percentage as follows:

$$D_{stress} = (D_{gap} / W) \times 100 \qquad \textbf{(I)}$$

where,

D_{stress} = degree of residual stress as a percentage (%)
D_{gap} = gap between concave / convex faces (mm)
W = board width (mm)

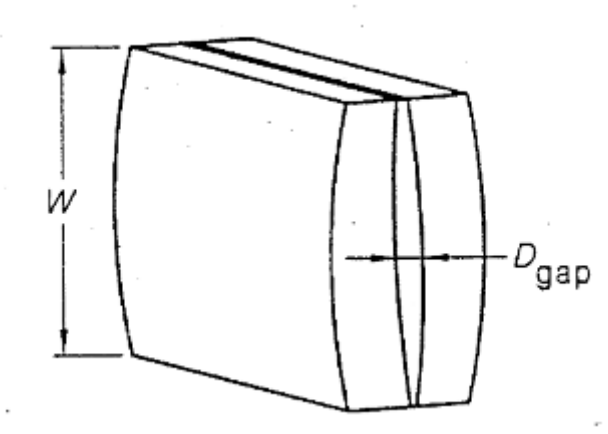

Figure 2. Diagram of ripping method for assessing drying stress (image taken from AS/NZS 4787:2001)

Collapse

Collapse observations occurred for each sample board at the completion of drying, on a present or absent basis, by inspecting the wide face surfaces. For the vacuum trial drying *E. obliqua* (MES1), a highly collapse prone species, scanned cross sections were analysed using *MeshPore* (Perré, 2005a), an image analysis software package developed to characterise the morphology and produce finite element meshes of wood anatomy. For the purpose of this study, we used *MeshPore* to determine the area of board cross sections as an aid to quantify collapse. In line with industry practice, we deemed collapse present in boards after dressing to be unacceptable.

Sawn orientation

We classified sawn orientation into three groups: q (quarter sawn), t (transitionally sawn) and b (backsawn). Transitionally sawn boards are boards with a sawn orientation between quarter and backsawn.

Gross shrinkage

We measured width and thickness at the centre of each of the sample board's length before drying. This was repeated at the same position for the undressed dry boards. We used these measurements to calculate the gross percentage shrinkage from green to dry using equations 2 and 3.

$$\text{Width shrinkage (\%)} = \left(\frac{W_g - W_d}{W_g}\right) \times 100 \quad \textbf{(2)}$$

$$\text{Thickness shrinkage (\%)} = \left(\frac{T_g - T_d}{T_g}\right) \times 100 \quad \textbf{(3)}$$

Where,
W_g = board width green
W_d = board width dry
T_g = board thickness green
T_d = board thickness dry.

Drying quality class descriptions

Standard *AS/NZS 4787:2001* (Standards Australia 2001) assigns drying quality classes for cross–sectional MC, MC gradient, drying stress, end split/check and internal check measurements. The standard bases quality classes on 90% of samples adhering to predetermined allowable limits dependent on the final target value for each property measured. It ranks classes from A to E as described below:

Class A – caters for specific end uses and very specific requirements for drying quality
Class B – applies where tight control over drying is required to limit 'in service' movement resulting from changes in equilibrium moisture content
Class C – applies where higher drying quality is required and the final use environment is clearly defined
Class D – applies when the final use environment is more clearly defined but the drying quality requirements are not considered high, and
Class E – applies when the final use and drying quality requirements are not high.

Table 3 shows the limits for the various quality classes as described within the standard. In accordance with general industry requirements, **dried quality was deemed acceptable if 90% of sample populations fell into quality class B or better**. The target final average cross–sectional MC was 11% for all trials.

Table 3. Allowable limits for MC, drying stress, end split/check and internal check per quality class

Quality class	Allowable range for 90% of samples				
	Cross-sectional MC (11%)	MC Gradient (11%)	Drying stress (D_{stress})	End check/split length (mm)	Internal check (% loss of cross-section)
A	10 - 13	2.0	0.5	0	0
B	9 - 14	3.0	1.0	50	0
C	8 - 15	3.5	2.0	100	5
D	7 - 16	4.0	3.0	200	10
E	6 - 18	5.0	4.0	300	15

3.1.3 Kiln drying

We performed vacuum drying using a 2 m^3 superheated steam vacuum drying kiln supplied by Brunner-Hildebrand, Germany. The kiln is powered entirely from electricity. This would generally not be the case for an industrial kiln that would use cheaper onsite energy alternatives (e.g. steam, hot oil or gas).

Conventional drying was conducted by the company from which the material was sourced using standard industry practice Table 1.

Kiln charge preparation for vacuum drying

Sample boards were stripped in the kiln between evenly spaced rows of non-sample boards using recommended 19 mm thick stickers (Nolan *et al.*, 2003). Six *test boards* were selected to measure MC during drying using resistance probes inserted at varying depths. Two sets of probes were inserted into each test board (Plate 3). One set was inserted at a depth of 1/2 board thickness (core). For three of the boards the second set of probes was inserted at a depth of 5 mm (surface), and for the other three at a depth of 1/3 board thickness. The kiln was controlled using the average core MC of the six test boards to determine each change point.

Plate 3. MC resistance probes inserted into a test board

The second set of probes was used to determine MC gradient of boards during drying. Plate 4 illustrates the stack preparation method implemented for this study. The 100 sample boards are those with end labels. Shown are the position and labelling of the six test boards where the test boards with the red arrows included specialised instrumentation, and the positioning of the *flying wood* test board (see section: *3.3.1 Shrinkage and flying wood*).

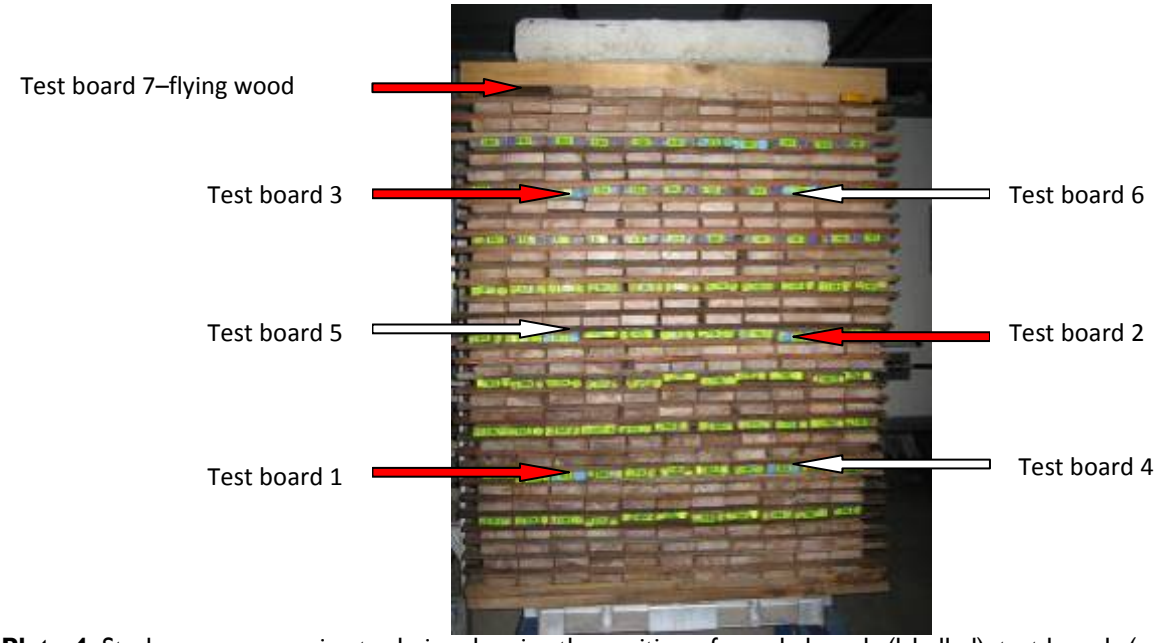

Plate 4. Stack appearance prior to drying showing the position of sample boards (labelled), test boards (red arrows indicate test boards incorporating specialised instrumentation) and the 'flying wood' board

For the *E. obliqua* MES1 vacuum drying trial, we stripped boards in two packs separated by bearers. When the average MC of the vacuum dried boards was approximately 15% we removed the top half of the stack from the kiln and reconditioned in a conventional research kiln at 97°C and 100% relative humidity for 6 hours. After reconditioning, the reconditioned and non-reconditioned boards re-entered the vacuum kiln to complete drying. This allowed observations of the effect of reconditioning on collapsed vacuum dried boards and compared with non-reconditioned boards.

Specialised instrumentation including anemometers, strain gauges, thermocouples and load cells measured the kiln conditions and wood properties during vacuum drying to test the modelling component of this project. For all trials except SPG1, a 300 mm length section was sawn from the middle of a seventh test board to perform a *flying wood* test (Brandao and Perré, 1996).

The methods and results recorded from these instruments are reported separately in this report.

For trials SPG1, SPG2, JAR1, BBT1 and MES1 we placed a concrete weight of approximately 500 kg on bearers on the top of the stack to reduce distortion. Due to unacceptable twist distortion recorded on dried boards for trial JAR1, we used two concrete weights for all subsequent trials in an attempt to reduce distortion to within permissible limits, with an approximate combined weight of 1000 kg.

Drying schedules

In keeping this *methodology* section generic between trials, we have reported the justification and presentation of the drying schedules separately in the *results* section of this report, for each species group.

3.1.4 Explanation of statistical analysis and presentation techniques

Scatter plots

We use *scattergrams* to present much of the quantitative data in this report. Scattergrams are a visual representation of quantitative results and are particularly useful for visually comparing paired numerical data. Individual, disconnected symbols represent data on a scattergrams. The plot allows the reader to observe the distribution of quantitative data around the mean, represented by a red line.

Normality test

Before statistical comparison of results between end-matched trials, normality tests were required and performed on much of the quantitative data. Normality tests show if a quantitative data set is normally distributed and hence determines the statistical method used to compare and analyse paired data. For instance, if both sets of paired data are normally distributed, *parametric* tests are required for statistical comparisons. Similarly, if one or both sets of paired data are not normally distributed, *nonparametric* tests are required. The normality test used in this report was the *Shapiro–Wilk* test, testing normality to a 95% confidence limit.

Parametric test

Parametric tests compare normally distributed quantitative data. The parametric test used in this report is the *Student t test*. The test statistically compares if significant differences exist between the means of paired data of end-matched boards for both conventional and vacuum drying treatments.

Nonparametric test

Nonparametric tests compare non-normally distributed quantitative data. We used two nonparametric tests in this report: the *Wilcoxin signed–rank test* and the *Mann–Whitney test*. The Wilcoxin signed–rank test statistically compares if significant differences exist between the paired data populations of end-matched boards for both conventional and vacuum drying treatments. The Mann–Whitney test statistically compares if significant differences exist between the unpaired data populations between trials of the same species.

Significance

The standard 95% confidence limit applied to all paired comparisons. Therefore, significance is indicated by $p<0.05$.

3.2 Applied drying - Economic model

The following method section describes how to use the economic model, and details the input and output variables and mechanisms that generate the output data.

3.2.1 How to use the model

The following section is a user guide explaining how to use the economic model.

Running model

To run the model, open (double click) the file '*KilnCompare.exe*'.

Opening files

To open a previously saved data file select *File/Open* when running the model. Select the directory and file you wish to open. A default file called '*Kiln data*' can be opened when the model is run. This is a read only file. This file provides sensible data and can be used as a starting point for further model manipulation.

Saving files

To save a file under the same name you have previously opened select *File/Save*. You cannot save to the default file '*Kiln data*' as it is a read only file. To save the file under a different filename select *File/Save As* and enter the new file name in the *Filename* box.

Entering data

Data can be entered into the first four pages selected via the tabs labelled *Finance*, *Capacity*, *Operations* and *Wood*. Numerical data only are allowed.

Observing model outputs

Model outputs can be observed by selecting the fifth tab labelled *Calculation*.

Information

Input variable information can be observed by 'double clicking' the input variable headings.

3.2.2 Inputs

Drying costs are analysed using a number of input variables allowing the total drying costs to be estimated. The model application consists of four input variable pages accessed by the tabs labelled: *Finance*, *Capacity*, *Operations* and *Wood*. The following provides an explanation of the input variables required.

Finance variables

Project life – Depreciation period where the capital cost of the kiln is straight line depreciated over project life (years).

Kiln capital ($) – The capital cost of a single kiln

Interest rate (%) – The interest charged on stock holdings

Wood value ($/$m^3$) – The value of a cubic metre of green-sawn stacked wood

Electrical($) - The price of electricity

Heat ($/MJ) - The price of a mega joule of heat energy

Thermal Efficiency (%) - An estimate of average operational heat loss from a kiln as percentage

Capacity

No. of Kilns - The number of kilns you want to work with

Kiln Capacity (m^3) - The maximum cubic metres of wood in a kiln

No. of Fans - The number of fans in a kiln

Fan Rating (kW) - The average power rating of a single fan

Vacuum Pump Rating (kW) - The average power rating of the vacuum pump

Vacuum Pump Usage (%) - An estimate of run time of the vacuum pump as a percentage

Condenser Fan Rating (kW) - The average power rating of the condenser fan

Condenser Fan Usage (%) - An estimate of run time of the condenser fan as a percentage

Operations

Pre-Drying - Refers to an initial air-drying stage. This is used when drying time is greater than zero

Air Drying Time (weeks) - The air drying time

Initial Moisture Content (%) - The initial moisture content of wood entering this drying stage

Final Moisture Content (%) - The moisture content of wood at the end of this drying stage *(%)*

Final Drying - Refers to the kiln drying stage

Final Drying Time (hrs) - The time in kiln drying

Drying Max. Temp. (°C) - The highest temperature attained during kiln drying

Operational Year (days) - The days per year of operating time

Run Time (hrs) - The sum of air and kiln drying times

Wood

Wood Basic Density (kg/m^3) - The basic density of the wood resource to be dried

3.2.3 Calculated outputs

The model application calculated outputs are presented in the ‘Calculation’ tab located at the bottom right corner of the program. The following section details the calculations used to determine the values presented on the ‘Calculation’ tab. As per the model output, the

calculations are split between the *Capital calculations, Operational calculations* and *Total costs* where any differences between conventional and vacuum drying calculations are noted.

Annual throughput

We define the annual throughput as:

$$total\ capacity\ (m^3) = no.of\ kilns \times kiln\ capacity \quad \textbf{(4)}$$

$$annual\ throughput\ (m^3/yr) = total\ capacity \times kiln\ cycles\ per\ year \quad \textbf{(5)}$$

Where,

$$kiln\ cycles\ per\ year = operational\ year \times \frac{24}{run\ time} \quad \textbf{(6)}$$

Capital calculations – depreciation

We calculate the annual cost of plant capital or depreciation using:

$$cost\ plant\ capital\ (\$/yr) = \frac{no.of\ kilns \times kiln\ capital}{project\ life} \quad \textbf{(7)}$$

$$cost\ plant\ capital\ (\$/m^3) = \frac{cost\ plant\ capital\ (\$/yr)}{annual\ throuput} \quad \textbf{(8)}$$

Capital calculations –stock interest cost

If the air-drying time is set to a value greater than zero weeks, the following calculations are performed to determine the annual interest and interest per cubic metre on the dry yard stock:

$$volume\ air\ dry\ yard\ stock\ (m^3) = total\ capacity \times \frac{air\ drying\ time \times 7 \times 24}{final\ drying\ time} \quad \textbf{(9)}$$

$$cost\ of\ air\ dry\ stock\ interest\ (\$/yr) = volume\ air\ dry\ yard\ stock \times wood\ value \times \frac{interest\ rate}{1000} \quad \textbf{(10)}$$

$$cost\ of\ air\ dry\ stock\ interest\ (\$/m^3) = \frac{cost\ of\ air\ dry\ stock\ interest\ (\$/yr)}{annual\ throughput} \quad \textbf{(11)}$$

Similarly, the following calculations are performed to determine the annual interest and interest per cubic metre on the kiln stock:

$$cost\ of\ kiln\ stock\ interest\ (\$/yr) = total\ capacity \times wood\ value \times \frac{interest\ rate}{1000} \quad \textbf{(12)}$$

$$cost\ of\ kiln\ stock\ interest\ (\$/m^3) = \frac{cost\ of\ kiln\ stock\ interest\ (\$/yr)}{annual\ throughput} \quad \textbf{(13)}$$

Capital calculations – totals

The total capital costs are calculated as follows:

$$total\ capital\ cost\ (\$/yr) = cost\ plant\ capital + cost\ air\ dry\ stock\ interest + cost\ of\ kiln\ stock\ interest \quad \textbf{(14)}$$

$$total\ capital\ cost\ (\$/m^3) = \frac{total\ capital\ cost\ (\$/yr)}{annual\ throughput} \quad (15)$$

Operations calculations – Air Flow

The cost of running the kiln fans is calculated using:

$$air\ \ flow\ cost\ (\$/yr) = kiln\ cycles\ per\ year \times no.\ of\ \ fans \times fan\ rating \times number\ of\ \ kilns \times kiln\ drying\ time \times electricity\ cost \quad (16)$$

$$air\ \ flow\ cost\ (\$/m^3) = \frac{air\ \ flow\ cost\ (\$/yr)}{annual\ throughput} \quad (17)$$

Operations calculations – Heat

The quantity of heat energy used per cubic metre for heating the wood, heating the water within the wood and vaporisation of water during kiln drying are calculated using:

$$energy\ to\ heat\ wood\ (MJ/m^3) = wood\ basic\ density \times \frac{specific\ heat\ of\ \ wood}{1000} \times \Delta T \quad (18)$$

Where the specific heat of hardwood is 1.2 kJ/(kg°C) and ΔT is the maximum – minimum drying temperature (°C). For the purpose of this study the minimum drying temperature is assumed ambient temperature at 25°C.

$$energy\ to\ heat\ water\ (MJ/m^3) = \frac{initial\ MC}{100} \times wood\ basic\ density \times \frac{specific\ heat\ of\ \ water}{1000} \times \Delta T \quad (19)$$

Where the specific heat of water is 4.186 kJ/(kg°C).

$$energy\ to\ heat\ water\ (MJ/m^3) = \frac{initial\ MC\ -\ final\ MC}{100} \times wood\ basic\ density \times heat\ of\ \ vaporisation \quad (20)$$

Where the heat of vaporisation of water is 2.25 MJ/kg (Serway, 1998).

$$energy\ to\ vaporise\ water\ (MJ/m^3) = \frac{initial\ MC\ -\ final\ MC}{100} \times wood\ basic\ density \times heat\ of\ \ vaporisation \quad (21)$$

The total amount of heat per cubic meter, taking into account the thermal loss is calculated using:

$$total\ heat\ energy\ (MJ/m^3) = \left(energy\ to\ heat\ wood + energy\ to\ heat\ water + energy\ to\ vaporise\ water\right) \times \left(\frac{1 - thermal\ loss}{100}\right) \quad (22)$$

The total cost of heat energy is calculated as follows

$$heat\ cost\ (\$/yr) = \left(kiln\ cycles\ per\ \ year \times total\ capacity \times total\ heat\ energy\right) \times cost\ of\ \ heat \quad (23)$$

$$heat\ cost\ (\$/m^3) = \frac{heat\ cost\ (\$/yr)}{annual\ throughput} \quad (24)$$

Operational costs – Extra vacuum drying energy calculations

Unlike conventional kilns, vacuum kilns are equipped with a vacuum pump to maintain vacuum during drying. Additionally, for the type of vacuum kiln used in this study a condenser fan is used to maintain the desired relative humidity during drying. To operate these devices electrical energy is required. This energy is calculated using:

$$vacuum\ pump\ energy\,(kJ) = vacuum\ pump\ rating \times \frac{vacuum\ pump\ usage}{100} \times drying\ time \quad \textbf{(25)}$$

$$condensor\ \ fan\ energy\,(kJ) = condensor\ \ fan\ rating \times \frac{condensor\ \ fan\ usage}{100} \times drying\ time \quad \textbf{(26)}$$

The total extra energy is calculated using:

$$total\ extra\ energy\,(kJ) = vacuum\ pump\ energy + condensor\ \ fan\ energy \quad \textbf{(27)}$$

The total cost of extra vacuum drying energy is determined by:

$$vacuum\ specific\ energy\,(\$/yr) = total\ extra\ energy \times kiln\ cycles\ per\ year \times no.\,of\ \ kilns \times electricity\ cost \quad \textbf{(28)}$$

$$vacuum\ specific\ energy\,(\$/m^3) = \frac{vacuum\ specific\ energy\,(\$/yr)}{annual\ throughput} \quad \textbf{(29)}$$

Operational costs – totals

The total operational cost per year for **conventional** drying is determined by:

$$total\ operational\ cost\,(\$/yr) = air\ \ flow\ cost\,(\$/yr) + heat\ cost\,(\$/yr) \quad \textbf{(30)}$$

The total operational cost per year for **vacuum** drying is determined by:

$$total\ operational\ cost\,(\$/yr) = air\ \ flow\ cost\,(\$/yr) + heat\ cost\,(\$/yr) + vacuum\ specific\ energy\,(\$/yr) \quad \textbf{(31)}$$

For both drying types, the total operational cost per cubic metre is calculated using:

$$total\ operational\ cost\,(\$/m^3) = \frac{total\ operational\ cost\,(\$/yr)}{annual\ throughput} \quad \textbf{(32)}$$

Total costs

The total cost of drying is calculated using:

$$total\ \ drying\ cost\,(\$/yr) = total\ capital\ cost\,(\$/yr) + total\ operational\ cost\,(\$/yr) \quad \textbf{(33)}$$

$$total\ drying\ cost\,(\$/m^3) = \frac{total\ drying\ cost\,(\$/yr)}{annual\ throughput} \quad \textbf{(34)}$$

3.2.4 Case studies

We investigated three (3) case studies to determine the economic viability of vacuum drying compared to conventional drying. Each case study relates to three different sized operations; small, medium and large. For each size of operation, three different sized kilns, typically used by industry, were investigated. The three sizes investigated were 10, 35 and 50 m^3 wood

capacity kilns. Obviously many more scenarios exist, however these sizes were chosen based on typical sized hardwood operations in Australia.

For each case study the following assumptions were made:

Throughput

Throughput is calculated and used to normalise drying cost comparisons. For instance, if we compare a 50 m^3 kiln for both conventional and vacuum drying operations, given the vacuum drying rate is faster, the vacuum drying operations will have a greater throughput. This is taken into account for all $/$m^3$ calculations.

Cost of green-off-saw wood

The cost of green-off-saw wood was set at a constant value of $426 for all case studies. This figure was calculated from the most recent native sawlog price index of $149 / m^3 (http://abare/publications_html/afwps, 2010) divided by the approximate average green-off-saw recovery for Australian hardwoods of 35% (Leggate *et al.*, 2000).

Project life – depreciation time

The capital depreciation time was fixed at a typical 20 years for each case study.

Interest on stock

The stock interest was fixed at a typical 7% for each case study.

Energy costs

Heat energy costs were fixed at 0.05 $/MJ, a typical average value of natural gas in Australia at the time of writing this report (Anon, 2011). Obviously, this figure will differ between different operations and can be adjusted to reflect other heating mediums such as steam, wood waste or heated oil etc. The heat energy costs are made up of a combination of heating required to heat the wood, heat the water within the wood and vaporise the water into steam at the wood surface. The total heat energy cost is also a function of the thermal loss undergone by a certain kiln type.

Electricity costs

Electricity costs were fixed at 0.2 $/kWh, a typical average value in Australia at the time of writing this report (Anon, 2011).

Thermal efficiency

The project collaborator Brunner-Hildebrand provided data for the thermal efficiency for each kiln type. The values used are detailed in the results section: *4.2 Applied drying* - Economic model.

Kiln capacities

For each case study three kiln capacity sizes were investigated: 10, 35 and 50 m^3 of wood volume.

Fans, vacuum pump and condenser fan details

The project collaborator Brunner-Hildebrand provided data for the number of fans, average fan ratings, vacuum pump and condenser fan usage and ratings for each case study. **Please note that the fan, pump and condenser ratings are estimated average values over a single kiln run**. The values used are detailed in the results section: *4.2 Applied drying* - Economic model.

Kiln drying time and wood conditions

Conventional and kiln drying times were based on the best case scenario vacuum drying trial per species, in terms of quality and drying time. For each scenario, we used the actual initial and final MC values, basic densities and maximum drying temperatures. The same values were used for a single species between each case study. The values used are detailed in the results section: *4.2 Applied drying* - Economic model.

Operational year

For each case study, the operational year was fixed at 328 days. This equates to a full year operation minus four weeks. We based this assumption on the fact that many sawmills shutdown over the Christmas and early New Year period.

3.3 Drying modelling - Measurement of kiln conditions and wood drying properties

We used specialised instruments on test boards during vacuum drying trials to obtain, through continuous 'real–time' measurements, a greater understanding of the kiln conditions and wood drying properties. This is essential to validate and provide actual kiln and wood property data for the modelling component of this project and hence optimise the process. As the proposed model is 'deterministic', actual wood property and kiln data are required to 'feed' the model to obtain the most accurate simulations possible.

This section describes the specialised instrumentation used to measure both wood boundary condition properties and internal wood properties we used for model input. It should be noted that a certain level of 'trial and error' and 'prototyping' of these instruments occurred between drying trials, the account of which is presented in Milestone Report 2. This part of the experimental design is not included in this report as we deemed it unnecessary.

Three test boards were selected for each trial to measure internal temperature using thermocouples, MC using load cells and shrinkage using strain gauges. Except for the first trial SPG1, one of the three test boards was modified to perform a 'flying wood' test, described later in this section. The flying wood test board utilised the specialised instrumentation in the same manner described below, as the other two test boards.

Each test board was loaded onto two load cells, one at each end, to measure the MC of these boards based on board weight.

We measured the overall shrinkage for the same three boards using specialised 'omega' shaped strain gauges attached to the board edges using a jig developed by DEEDI. Two strain gauges were used for each test board.

Internal temperature was measured for the test boards using 1 mm diameter thermocouples. Measurements were made at 1/3 thickness and 1/2 thickness inserted 50 mm into the side of the boards, and at the centre of the board end at a depth of 50 mm.

Inlet and outlet airflows were measured using two anemometers placed at approximately ½ the stack height on the second board in from the stack edge at each side of the stack.

The output of these devices was obtained using DataTaker™ data acquisition equipment.

3.3.1 Shrinkage and flying wood

Generally, drying stresses are assessed at stages or at the end of drying using prong or cup tests. However, it is very difficult to gather information on the stress field within boards during drying. The flying wood test was developed in the laboratory of Wood Science at École Nationale du Génie Rural des Eaux et des Forêts (ENGREF) in Nancy, France and is a well documented test method for gathering information on the stress field during drying and the phenomenon of stress reversal (Aguiar and Perré, 2000, Brandao and Perré, 1996). The data gathered from this test method, although not used in this report will be used for future modelling work incorporating a mechanical (degrade) component. The flying wood test consists of non-symmetrical drying of small boards. Five surfaces of the sample are sealed, so that the moisture migration occurs only in one direction. This strategy transforms a part of the drying stresses encountered during drying into a global deformation of the sample (Figure 3).

Three successive stages are observed: the first drying period with liquid water at the surface with no shrinkage and hence no deformation; the second period with shrinkage at the surface and positive curvature; and the final stage which starts when shrinkage occurs close to the impermeable face. Due to the memory effect of wood, which is responsive to stress reversal in normal boards, the curvature becomes negative in the case of non–symmetrical drying. Given the same external conditions, the response of each specimen to this test strongly depends on the species, the sawing pattern and the position in the tree (Perré, 2007a).

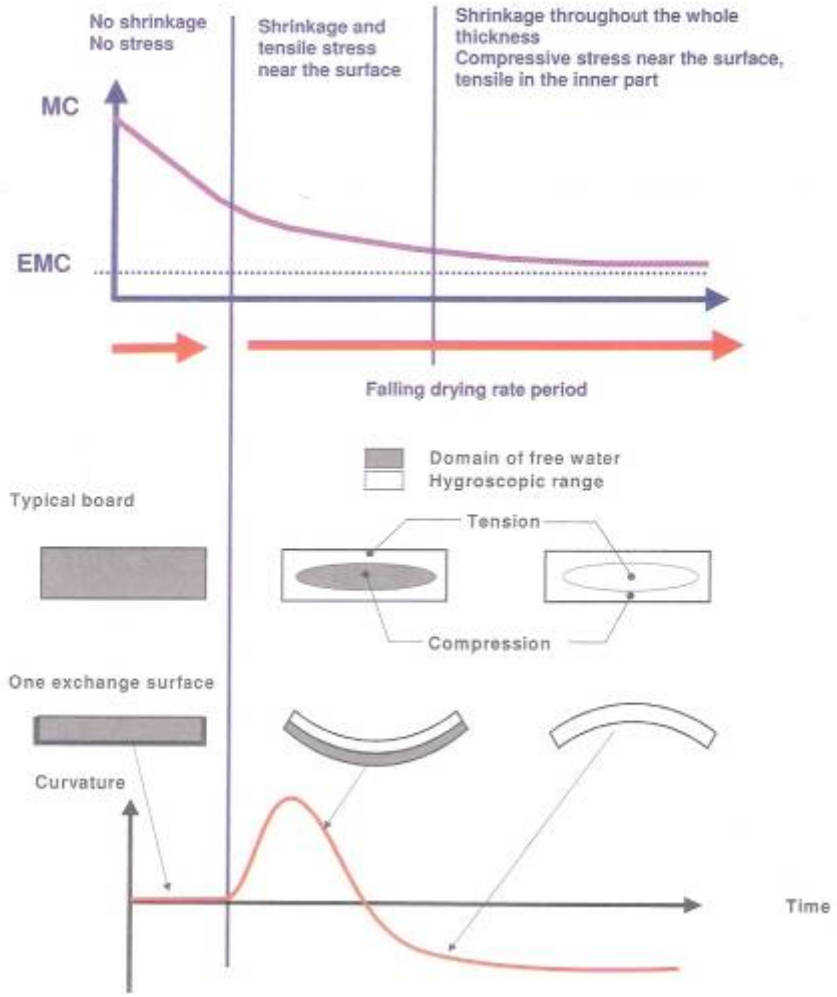

Figure 3. Principle of the *flying wood* test, diagram extracted from Perré & Passard (2008)

To prepare the sample board for the flying wood test, we cut a 300 mm length section from the middle of the test board. The section was ripped down the centre along the narrow edge surface to produce two (2) boards of similar dimension (approximately 14 x 110 x 300 mm). One half was chosen for the 'flying wood' test and was coated on five surfaces with epoxy resin excluding the wide freshly ripped face. During drying, we used two strain gauges to measure the test board's shrinkage/curvature. Additionally, we inserted three thermocouples into the board, as previously discussed, and the weight of the board was measured using two load cells. The flying wood test board was originally placed in the gap between the top of the stack and the concrete weight, but was later placed within the kiln stack and surrounded by boards to maintain more representative airflow (Plate 5).

Plate 5. Position of flying wood test board during drying

We measured the gross shrinkage for each test board using *Sokki Kenkyujo PI–2–50* specialised 'omega' shaped strain gauges fixed to the centre of the board edges. The strain gauges are usually used industrially to measure crack propagation in concrete. Thus, the potential for these strain gauges to measure surface checking was realised. We used two strain gauges for each test board, one on the top and another underneath.

We developed the strain gauge assembly to allow flying wood test board distortion to be captured. This also has allowed the measurement of cup distortion on the full dimension test boards. They are attached to vertical aluminium plates screwed to the narrow sides of the board, via nylon extensions, eye hooks and split pins (Plate 6 and Plate 1). Even though no slack was evident between the hooks and pins, the assembly wasn't so tight as to impede the movement of the strain gauge in the vertical direction so accurate curvature of the flying wood board could be captured (Plate 7). This assembly allows the strain gauges to move freely at the attached joint during both natural board shrinkage and cupping.

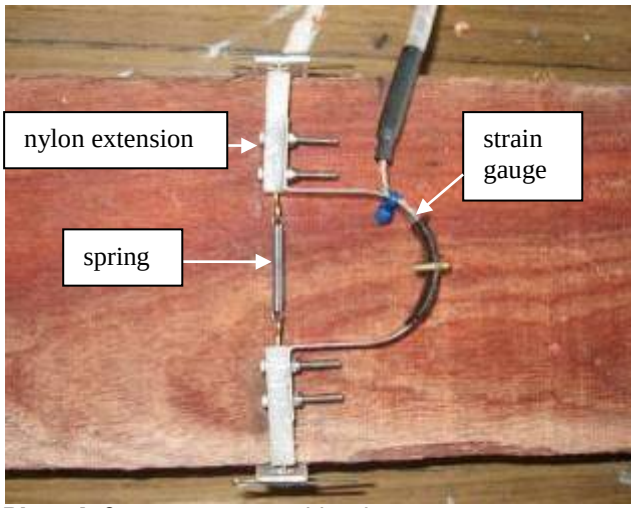

Plate 6. Strain gauge assembly–plan view

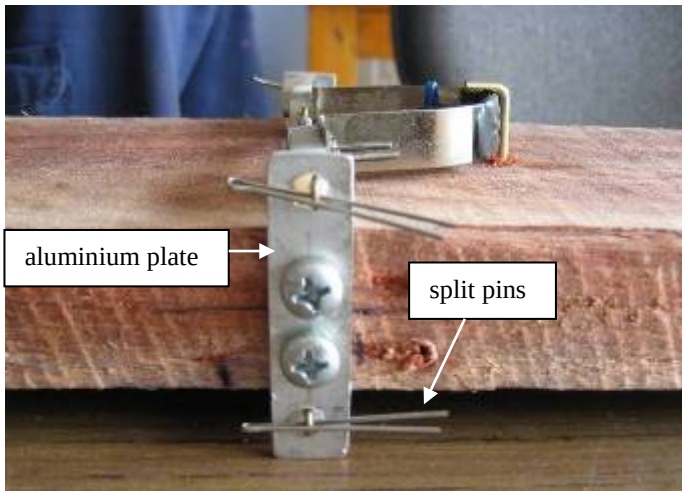

Plate 7. Strain gauge assembly–side view

3.3.2 Load/moisture content

Each test board was loaded onto two load cells (20 kg capacity each, supplied by Scaime (model F60F), one at each end, to measure the MC of these boards based on initial board MC and subsequent weight reduction during drying. Due to the larger size of the load cells and associated weighing frames, the ends of the board below the test boards were removed to accommodate them (Plate 8). We removed the strippers and board above the test boards to allow a large degree of unrestrained distortion (Plate 9).

Plate 8. Load cell placement

Plate 9. Test board/ load cell arrangement

3.3.3 Airflow

We measured inlet and outlet airflows using two *Schiltnecht MiniAir60* anemometers placed at ½ the stack height on the second board in from the stack edge at each side of the stack. The anemometers were attached to the boards using 'u' brackets (Plate 10).

Plate 10. Anemometer placement

3.3.4 Board temperature

We used three thermocouples per test board for each trial. Thermocouples were placed at 1/3 and ½ thickness of boards, 50 mm in from the side and at the centre thickness inserted 50 mm in from the end (Plate 11).

Plate 11. Thermocouple inserted into the end of a test board

3.4 Drying modelling - Measurement of essential wood properties

Drying is a complex operation combining intricate physical and mechanical processes that include external heat and mass flow, coupled heat and mass transfer within wood, shrinkage induced stress deformation, and the mechanical memory behaviour of wood. The model developed for this work represents the heat and mass transfer component only. Previous research (Salin, 2010, Perré, 1996) has shown that a number of wood properties exist that must be measured to have provide the necessary structure for developing an accurate drying model. A number of other wood properties that govern wood heat and mass transfer exist, but can be either inferred from essential wood properties or calculated via theory.

The following describes the methods used to measure the essential wood properties for accurate heat and mass transfer modelling.

3.4.1 Wood density and initial MC

For the vacuum drying trials simulated, we used the average wood density and initial MC measured from the 100 sample boards. The method for which has been previously described in section *3.1 Applied drying* – ***Experimental drying trials***.

3.4.2 Fibre porosity

Fibre porosity is essentially a measure of the ratio of fibre lumen area to woody tissue in the transverse (radial/tangential) plane. We determined fibre porosity by using specialised image analysis software on environmental scanning electron microscope scans of each species in the transverse direction. We also measured the density of scanned sections to investigate the relationship between fibre porosity and wood density. The following describes the methods used.

Environmental Scanning electron microscope

An environmental scanning electron microscope (ESEM) is a type of electron microscope that images a sample surface by scanning it with a high-energy beam of electrons, usually under partial vacuum. The electrons interact with the atoms that make up the sample producing signals that contain information about the sample's surface topography, composition and other properties such as electrical conductivity.

An ESEM can produce very high-resolution images of a sample surface revealing details about 1 to 5 nm in size. Due to the way these images are created, SEM micrographs have a very large depth of field yielding a characteristic three-dimensional appearance useful for understanding the surface structure of a sample. A wide range of magnifications is possible, from about x 25 (about equivalent to that of a powerful hand-lens) to about x 250,000, about 250 times the magnification limit of the best optical microscopes.

The ESEM used for this research was a Quanta 200 3D manufactured by FEI[2] (Plate 12). The microscope has a resolution of 3 nm and its main components consist of: a vacuum pump, electron emission column, sealed specimen chamber and image processing facilities.

[2] See http://www.fei.com/products/families/quanta-family.aspx for more information.

Plate 12. FEI Quanta 200 3D environmental electron scanning microscope.

Meshpore

Meshpore (Perré, 2005b) is a powerful software package used to apply image-based meshing techniques to anisotropic and heterogeneous porous media. This application allows a comprehensive finite element mesh to be prepared from digital images and can be used to determine important morphological properties of porous media, such as average cell wall thickness and media porosity. Using a number of mathematical algorithms the application is able to automatically describe cell contours by segment chains, allowing additional chains to be added, deleted, and altered.

Sample preparation

For each species, we cut small heartwood samples from unseasoned, median density sample boards used for the vacuum drying trials. One sample per species was cut using a laboratory bandsaw to the approximate dimensions: 4 mm (radial) x 4 mm (tangential) x 20 mm (longitudinal). The samples were cut in half lengthwise to produce two matched samples of dimension: 4 mm x 4 mm x 10 mm. One section was used for ESEM analysis while the other section was used to determine basic density. One image was analysed per species.

The ESEM samples were soaked in water at room temperature for at least 24 hours, before further processing, to soften the wood tissue prior to image surface preparation. One of the radial/tangential surfaces was prepared for ESEM imaging using a precision MICROM HM 440™ sledge/sliding microtome (Plate 13). This process provides a flat, sharply sliced surface essential for producing high quality ESEM images. We loaded samples into the ESEM specimen chamber (Plate 14), levelled and scanned at 200X 400X and 800X magnifications. Images at 800X magnification were cropped to include only the wood fibres (not ray parenchyma or vessel cells).

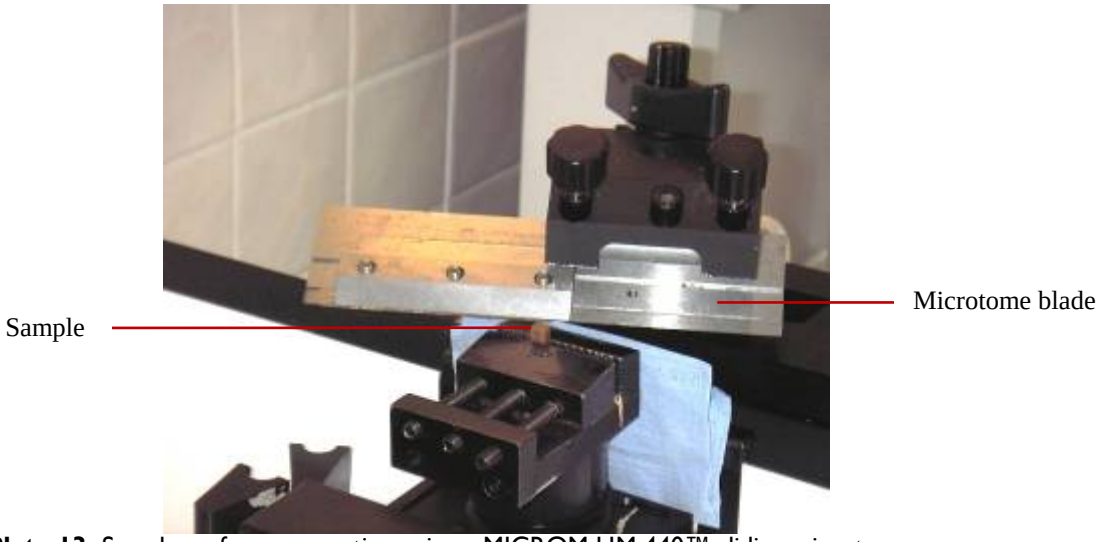

Plate 13. Sample surface preparation using a MICROM HM 440™ sliding microtome

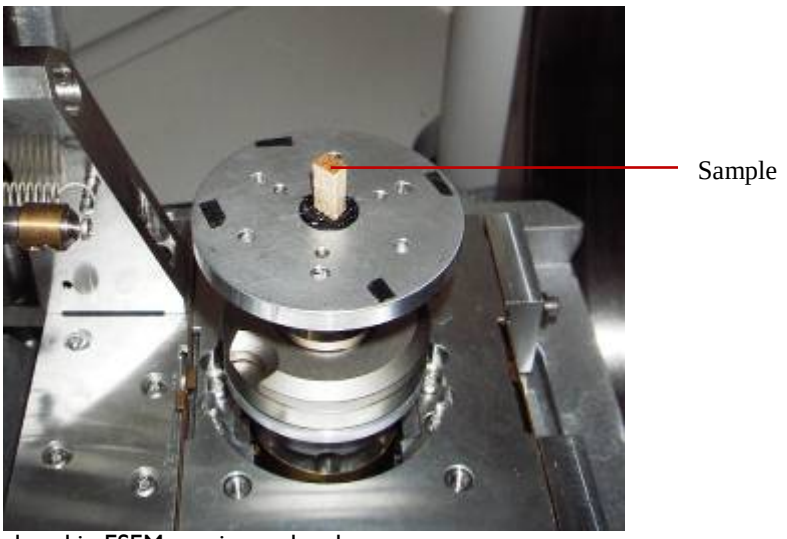

Plate 14. Sample placed in ESEM specimen chamber

Using *MeshPore*, cell lumen contours were automatically generated (Figure 4) to determine the average fibre porosity. The fibre porosity (%) was calculated by *MeshPore* as the sum of the voids divided by the total image area, as follows:

$$f_p = \frac{\sum_{i=1}^{n} A_{vj}}{A_i} \times 100 \quad \textbf{(35)}$$

Where f_p is the fibre porosity (%), A_{vj} is the void (lumen) area (m^2) of lumen number j, n is the number of lumens in the image, and A_i is the area of the image (m^2).

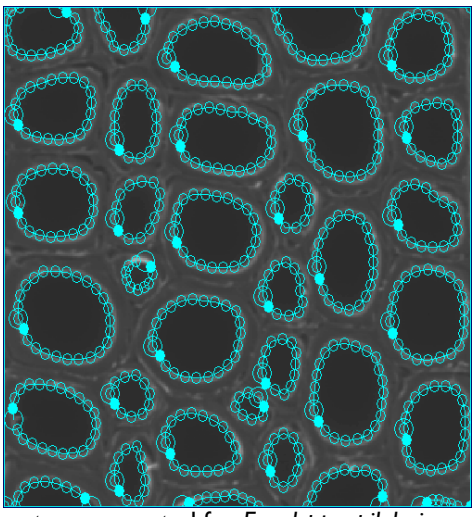

Figure 4. Automated Meshpore contour generated for *Eucalyptus pilularis*.

We calculated basic density by determining a samples green volume and dry weight in accordance with *Australian and New Zealand Standard AS/NZS 1080.3:2000 – Timber – Methods of Test – Method 3: Density* (Standards Australia 2000). To ensure samples were fully saturated we placed them in a beaker of water, which we positioned in an airtight container surrounded by an ice/water mixture (Plate 15). The ice water was used to maintain the samples at low temperature to minimise leaching of extractives and provide accurate density measurements. We connected the container to a small vacuum pump and a vacuum pressure of 15 mbar was drawn. The samples remained in this state for approximately 1 hour before slow depressurisation. This was repeated 3 times to ensure the samples were fully saturated. The green volume of the samples was determined using the water immersion method. We dried the samples in a laboratory oven at 103 ± 2°C for 48 hours and weighed to determine the oven dry weight. We calculated sample basic density using:

$$\rho_b = \frac{m_d}{V_g} \quad \textbf{(36)}$$

Where ρ_b is the basic density (kg/m^3), m_d is the oven dry mass (kg), and V_g is the green volume (m^3).

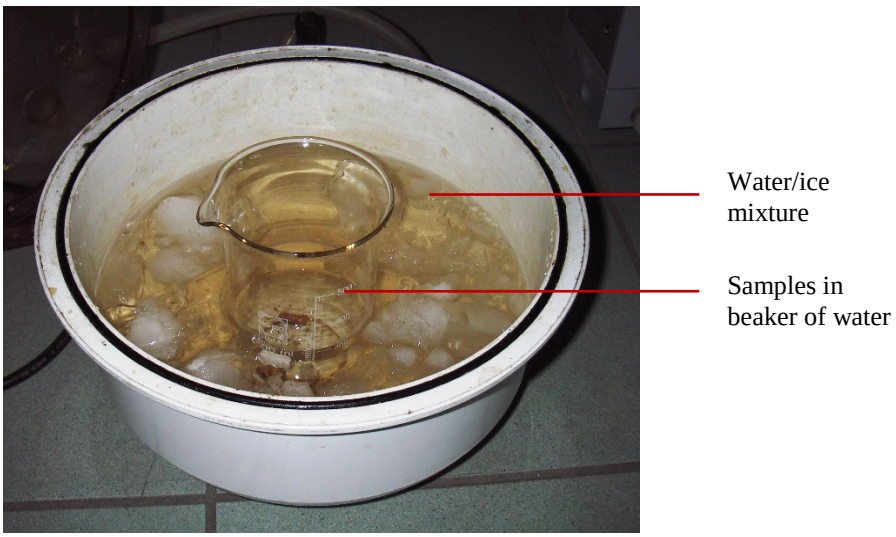

Plate 15. Samples prepared for vacuum saturation (container uncovered for photo)

Using the measured fibre porosities, density was calculated to determine if density can be predicted using only these parameters. The formula uses the oven dried density of wood

tissue, suggested to be constant for all wood species, the value of which is reported to be approximately 1500 kg/m^3 (Siau, 1984). The following equation was used to calculate density:

$$\rho_{calc} = \rho_{wt}\left(1-\phi_f\right) \quad \textbf{(37)}$$

Where ρ_{calc} is the calculated density, ρ_{wt} is the density of wood tissue (1500 kg/m^3) and φ_f is the fibre porosity.

3.4.3 Gas permeability

Permeability is the property of a material that indicates how freely fluids flow in response to a pressure gradient. Permeability of wood to liquids and gases plays an important role in a number of technical processes such as wood treatment with preservative chemicals, the pulping process and wood drying. The more permeable the wood the more easily it can be processed or treated. Drying time and conditions are driven by the permeability making it a crucial factor for the resulting product quality (Hansmann *et al.*, 2002).

Wood permeability in hardwoods is affected mainly by anatomical features such as vessel size and obstructions (tyloses), pit aspiration, and the presence of extractives in heartwood.(Milota *et al.*, 1995). For Australian eucalyptus species, as previous researchers suggest, water movement during conventional drying is restricted predominantly to diffusion, (Innes, 1996, Blakemore and Langrish, 2008).

Sampling procedure

For each species, we prepared one quartersawn and one backsawn board with dimensions 300 x 100 x 8 mm using boards from the vacuum drying trials of this project. Three 74 mm diameter samples were cut using an 80 mm diameter hole-saw for each board producing three radial and three tangential (in thickness direction) samples per species. For each species, one 200 x 100 x 28 mm thick sample was prepared. From those boards we cut three 19 mm diameter, 40 mm long cylinders using a 24 mm hole-saw in the same longitudinal symmetry plane (Figure 5). We used these samples to determine longitudinal permeability. Due to the impermeability of these species, the longitudinal samples were cross-cut in half to produce 20 mm long samples. We coated the side surfaces of all specimens with epoxy resin to guarantee the air tightness of the lateral surfaces during measurement.

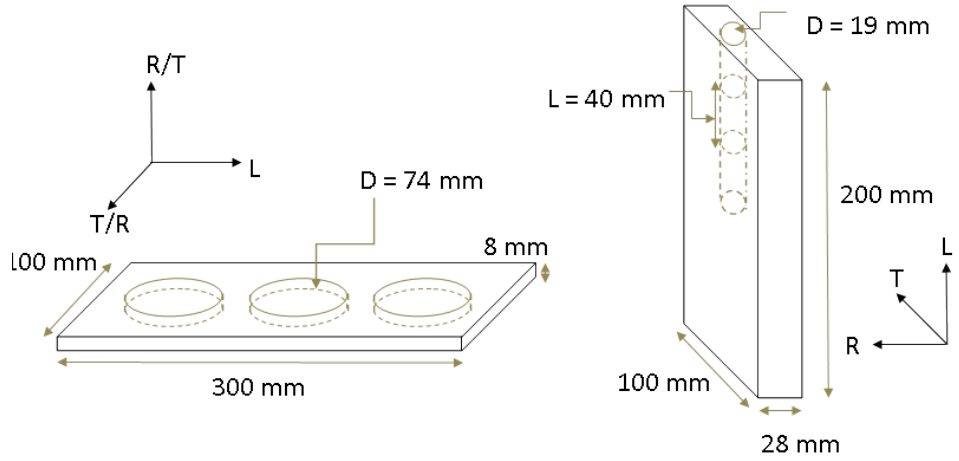

Figure 5. Sample preparation for permeability tests: Left – radial and tangential permeability sampling. Right – longitudinal permeability sampling

Test apparatus

The need to carry out measurements of permeability to air of various species, along the three material directions and at different pressure levels requires an accurate and reliable device capable of measurement over a wide range of permeability values (from 10^{-10} down to 10^{-18} m^2). For this purpose, the team at AgroParisTech-ENGREF developed a system called ALU-CHA at LERMAB. The originality of this medium lies in a high reliability of lateral air tightness, the rapid operation and the possibility to measure permeability with the same geometry, thus on the same samples as those employed for the diffusion measurement (Figure 6). This device allows us to apply an accurate and constant pressure difference between the two faces of the sample. We can determine the corresponding gas flux by the measurement of the thermal perturbation due to the air flux when it passes through a capillary tube.

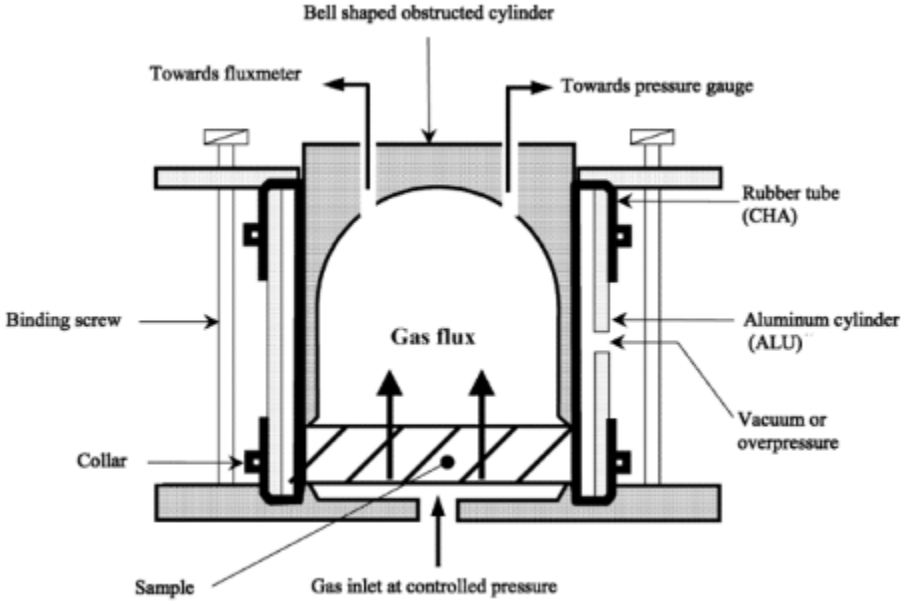

Figure 6. Schematic of sample support with ALU-CHA system. Diagram courtesy of (Rousset *et al.*, 2004)

Note the presence of a rubber tube around the sample. Partial vacuum phase is applied in the chamber between the rubber tube and the aluminum tube to easily place or remove the sample. Then, during measurement, a typical pressure of 2–3 bar is applied in this chamber to press the rubber joint against the lateral face of the sample for air tightness. In addition, before placing the specimen in the ALU-CHA system, a silicone-based grease of high viscosity (vacuum grease) was applied on the specimen's lateral surfaces to inhibit surface flow in the micro-porosity layer formed between the epoxy resin and rubber surfaces. The measurement was carried out by applying a controlled and constant pressure difference (ΔP) between two faces of the specimen, and then measuring the corresponding airflow (Q). All measurements were performed in a temperature-controlled room with minimum temperature fluctuations. Due to the effect of temperature on the air viscosity, the room temperature was also recorded for each measurement. The air flux permeating through the specimen was recorded when the flowmeter exhibited a nearly constant airflow. The air permeability of each sample was then calculated by Darcy's law (Dullien, 1992):

$$K = \frac{Q.\mu.e.P}{A.\Delta P.\overline{P}} \quad \textbf{(38)}$$

Where K is intrinsic permeability (m^2), Q is flux ($m^2 s^{-1}$), μ is dynamic viscosity of the air (Pa. s), e is sample thickness (m), P is pressure at the flux Q (Pa), A is sample area (m^2), ΔP is

pressure difference (Pa), and $\overline{P}$ is average pressure (Pa). The validity of Darcy's law was proved for all test samples by the linear correlation found between the pressure difference (ΔP) and air flux (Q).
Two ALU-CHA systems were used to cater for the two diameter class of specimens. One system was used for the longitudinal samples (Figure 7) and another for the larger diameter transverse samples. (Figure 8).

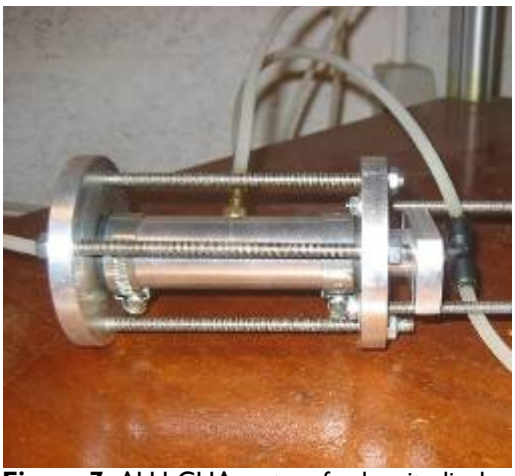

Figure 7. ALU-CHA system for longitudinal samples

Figure 8. ALU-CHA system for transverse samples

For most species, permeability measurements in the radial and tangential directions could not be achieved using the regular experimental set-up as the permeability was too low, below the limitation of the flux-meter (10^{-18} m^2). So instead the flux-meter was disconnected and a simple 'venturi type' tube was connected to the gas output of the ALU-CHA system. This entailed a flexible silicon hose connected to a glass tube with an internal radius of 2.87 mm. The radius of the tube was accurately calibrated using a laboratory pipette. The glass tube was placed in a beaker of water next to a 0.5 mm increment metal ruler (Figure 9). We could then measure permeability as before by measuring the volume of the displacement of water in the tube as a function of time (measured using a chronometer) at different pressures. Instead of measuring permeability over a matter of seconds, minutes or hours were required to obtain accurate measurements using this method. This method, although using relatively fundamental practices, was able to increase the range of permeability measurement 4 orders of magnitude, from 10^{-18} to 10^{-22}.

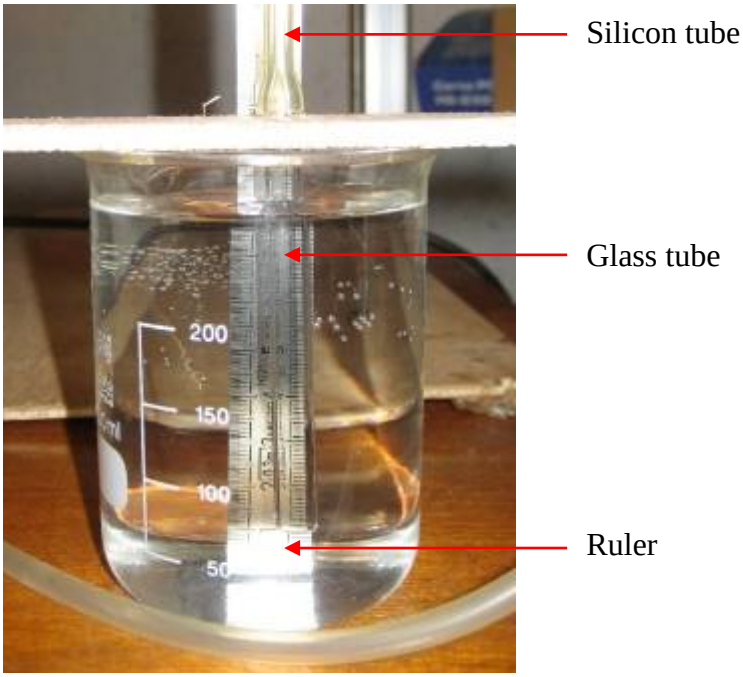

Figure 9. Apparatus used to measure low permeability samples

3.4.4 Bound Water Diffusion (D_b)

Avrimidis (2007) suggests that unsteady-state diffusion coefficient values are of more interest for drying modelling. However, through personal communication with experts in this field, Rémond (2010), suggested that for thick specimens of high density hardwood, measured diffusion coefficients under steady-state conditions would be equal to those in unsteady-state conditions. Therefore, as the species tested are of high density relative to most commercial species and steady-state measurements require less complex and cheaper equipment, we chose the steady-state regime to calibrate and refine the theoretical values described in section *3.5.7. Physical Properties*.

We used the same specimens to determine diffusion co-efficient values as those used to measure permeabilities in each direction for each species (see sampling methodology above).

Wood specimens were initially equalised in a constant humidity and temperature chamber at 75 ± 2% relative humidity and 35 ± 0.1 ºC to produce equilibrium conditions of 14% MC.

The principle of measurement in the steady-state regime uses the technique of the vaporimeter (Plate 16). Specimens were placed onto similar diameter cylindrical glass vessels containing a saturated solution of deionised/purified water and chemical grade (>99.9%) NaCl. For a given temperature, the partial pressure of vapour relates directly to relative humidity. A saturated salt solution inside the vessel generates a relative humidity (RH2) of 75% at 35 ºC.

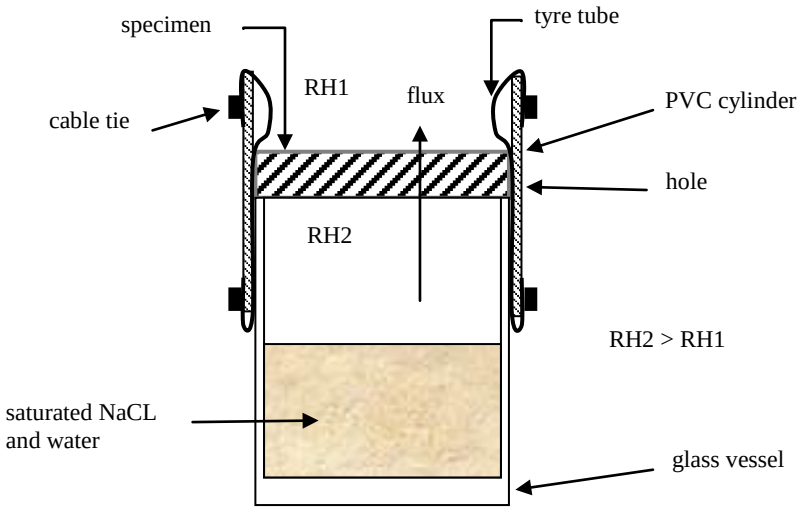

Plate 16. Vaporimeter schematic

To create an airtight seal around the device, we used a cylinder of PVC with an attached piece of tyre tube inside the PVC clamped using cable ties. A small hole was drilled into the side of the PVC pipe. Using a vacuum, air was aspirated through the hole, thus sucking the tyre tube against the PVC pipe. This enabled us to lower the apparatus over the specimen and glass. By releasing the vacuum, the tyre tube relaxes tightly against the specimen and vessel creating an airtight seal.

We placed the vaporimeter devices into the constant environment chamber at 35 ºC and 40% relative humidity (RH1) to produce equilibrium conditions of 7% MC. With this device assembly, two different relative humidities occur on each side of the wood specimen to create a diffusive flux driving force through the sample. We measured the flux by weighing the device periodically over time and measuring the overall weight loss of the device. The samples were weighed inside the constant environment chamber via sealed glove gauntlets in the chamber door, and a mass balance, accurate to 1mg, placed inside the chamber. This allows mass flux measurements without disruption of conditions of temperature and humidity, and assures their good stability whatever the length of testing.

By plotting the weight change as a function of time, after a few days a steady-state relationship occurs where the plot becomes a straight line (linear relationship between weight change and time). The diffusion coefficient through gross wood (D_b) is then calculated from the following formula (Siau, 1979),

$$D_b = \frac{100mL}{tAG\rho_w \Delta X} \quad \textbf{(39)}$$

Where m is the mass vapour transferred through the specimen (g), L is the specimen thickness (m), t is time (s), A is the specimen surface area (m^2), G is the specific gravity of the specimen at moisture content X, ρ_w is the normal density of water (kg/m^3), and ΔX is the moisture difference between two parallel surfaces of the specimen (%) calculated by:

$$\Delta X = \frac{X_b + X_t}{2} \quad \textbf{(40)}$$

Where *Xb* is the bottom specimen surface MC (%) and *Xt* is the top specimen surface MC (%).

3.4.5 Shrinkage

The shrinkage of wood during drying is one of the most important properties as it is responsible for deformations during drying (twist, spring, bow and cupping), dimensional variations in situ, and is the driving force for stress. Shrinkage induced drying stress is one of the main reasons for poor quality of dried products.

Due to this project's timeframe and model complexities, a mechanical modelling component was not included; heat and mass transfer only. An accurate heat and mass transfer model is however necessary to develop an accurate drying mechanics model. Even though the shrinkage values derived were not required for the heat and mass transfer model, the measurements were necessary to determine sorption isotherms and hysteresis for each species for accurate board MC predictions. Salin (2010) proposes that traditional models that use an average MC sorption curve (derived across a range of species) are problematic because different species have different sorption isotherms of which drying models are very sensitive.

The work presented in this section aims to characterise the wood-water relations of each in particular shrinkage and sorption isotherms. We performed tests on small micro-samples using specialised precision apparatus designed and built to determine the drying behaviour of small micro-samples. By using such small samples, the stress level during testing is not high enough to produce checks and, more importantly, the sample can be considered relatively homogeneous particularly in terms of moisture content variation. As far as the author is aware, there are no other methods available to continuously follow the evolution of wood samples as a function of external conditions. The highly accurate results produced by this method are imperative as input parameters for theoretical modelling.

Test apparatus

The apparatus used for these tests was designed and built specifically to accurately determine the wood-water relations on micro-samples, by members of the ENGREF team. Plate 17 and Figure 10 present the experimental set-up. The dimensions of micro-samples are measured using a non-contact laser system while continuously measuring the MC of samples.

The system incorporates a highly sensitive electronic microbalance (MC2, Sartorius) with a capacity of 2 g and typical sensitivity of 0.1 µg. Two high-speed laser micrometers (Keyance, LS-5000 series) are incorporated to measure changes in the width and height samples without contact. The laser micrometers can measure within a range of 0.2 – 40 mm at a scanning rate of 1200 scans/s, resolution of 0.05 µm and accuracy of 2 µm. The outputs from both devices are fed back to a PC.

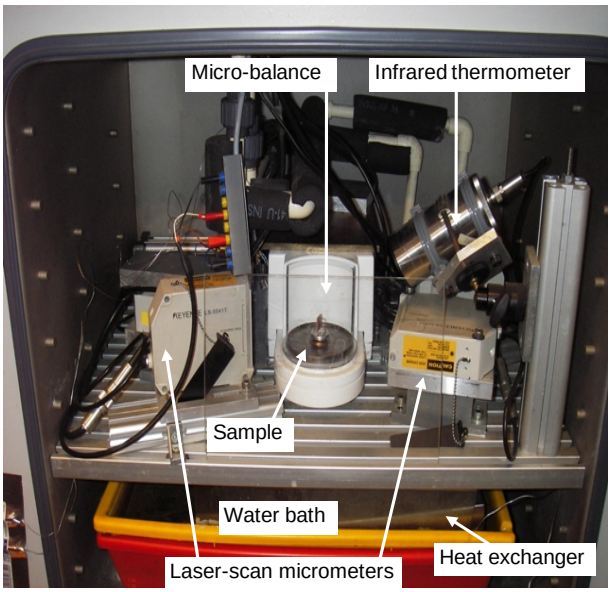

Plate 17. Experimental set-up overview

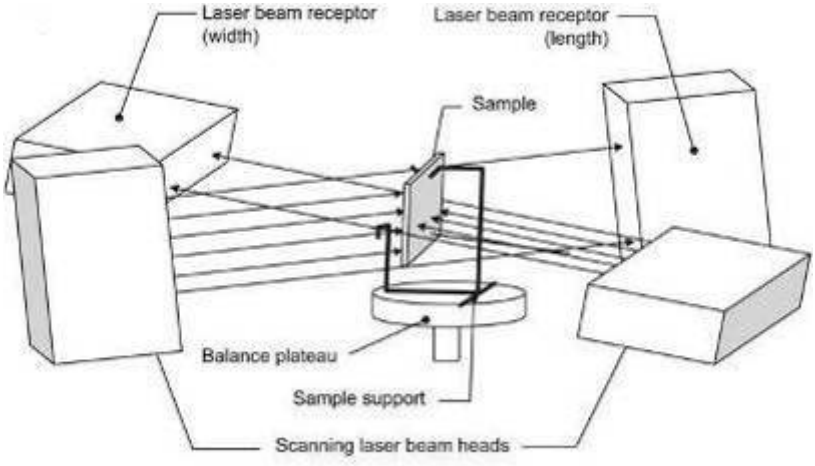

Figure 10. Schematic diagram of scanning laser micrometers and sample positioning. Diagram extracted from Perré (2007b).

The surface temperature of samples is measured using an infrared thermometer (pyrometer). It uses a germanium lens with a measurement spot size of 2 mm, and measures to an accuracy of 0.6 % of the measured value (in °C).

The measurement system is placed in a climatic chamber where the dry-bulb temperature is held constant at 30°C by a proportional-integral-derivative (PID) controller. Relative humidity inside the chamber is controlled using a water bath maintained at the desired dew point temperature. A refrigerating circulator is used to maintain the bath temperature. A small fan ensures satisfactory airflow is maintained across the bath and provides even temperature and humidity conditions throughout the chamber. The dew point and water temperature are measured to an accuracy of 0.1°C using a dew point analyser.

Sampling

Particular care was required when preparing samples for the apparatus. For each species, a small block of unseasoned material was initially prepared with the approximate dimensions: 13 mm in the tangential (T) direction, 10 mm in the radial (R) direction and 40 mm in the longitudinal direction (L). We sliced the block in the longitudinal direction using a diamond

wire saw (Plate 18) to obtain 1 mm thick samples. Due to collapse occurring in the 1mm thick *E. obliqua* micro-samples, further 2mm, 1mm and 0.5mm thick *E. obliqua* samples were prepared to investigate the effect of sample thickness on collapse during testing.

As the name suggests, the diamond wire saw features a high tensile wire of 0.3 mm diameter in which diamonds, approximately 60 µm wide are impregnated. The wire unwinds and winds between two bobbins. Cutting is performed under a constant load and the wire is submerged in water to minimise heating and drying of the sample. We soaked the samples in water and stored in a refrigerator to avoid fungal attack.

Immediately prior to testing, we inserted samples into a specially designed sample support (Plate 19). The sample support was designed so it does not interfere with the laser beams shrinkage measurements are made at the same material locations, and the sample is sufficiently restrained to avoid flexure while maintaining freedom to shrink.

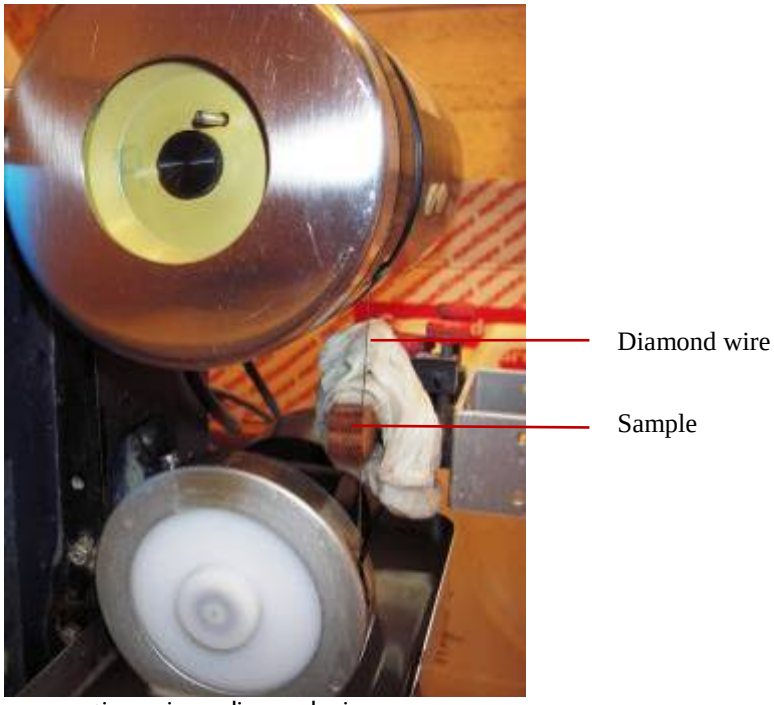

Plate 18. Sample preparation using a diamond wire saw

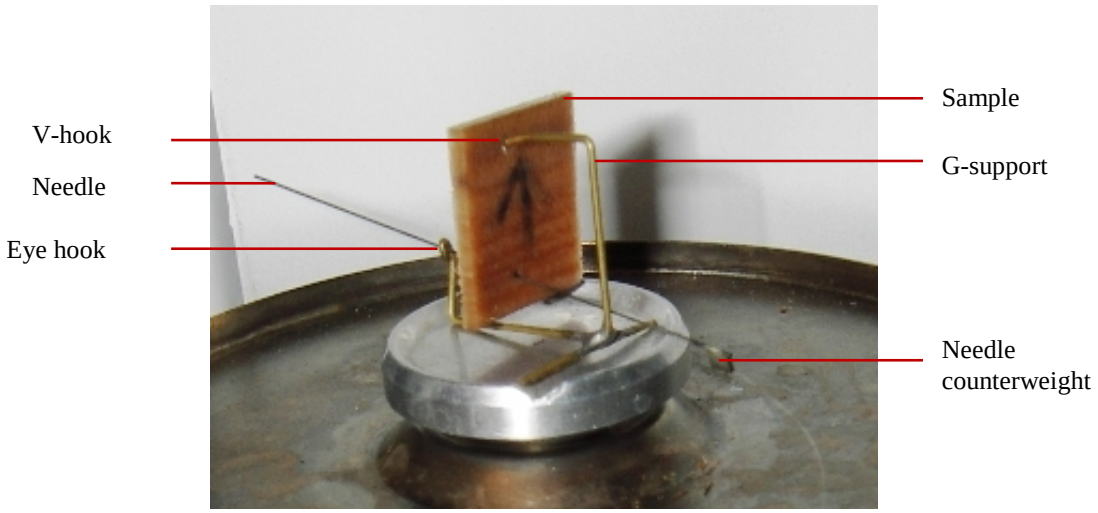

Plate 19. Sample support

The support is made from soldered brass. Samples are hung from a G-shaped support via a 1 mm diameter hole drilled in the upper part. The upper branch of the G-support is curved to create a V shaped hook. The V-shaped hook inhibits sample movement in the direction of the support branch to which the V-hook is connected (sample thickness direction). Rotation around the V-hook (sample width direction) is inhibited by using a needle and attached counterweight. The needle is inserted in a second hole (0.8 mm diameter) drilled in the bottom of the sample. One end of the needle is held by an eye-hook at the bottom part of the G-support. The two holes are both offset from the central width of the sample, so that gravity forces the sample to rotate around the V-hook until the needle leans against the G-support. Due to friction, as a result of the needle counterweight, the sample is also blocked from rotating in the direction of the needle. Even though rotational movement of the sample is blocked in all directions, it is still free to shrink.

Experimental procedure

We investigated radial and tangential shrinkage on two 1 mm samples for each species, except for *Corymbia citriodora*, where three samples were tested due to an unreliable test. An additional, two shrinkage samples per 0.5 mm, 1 mm and 2 mm thickness were investigated for *Eucalyptus obliqua*, due to collapse shrinkage compromising initial samples.

We placed each sample on the support in the centre of the balance, ensuring that the vertical laser passed along the two holes. Drying of the sample before data acquisition was inhibited by regularly adding liquid water to the surfaces using atomised water spray during set-up. For each test, the water bath was initially set to a temperature of 27°C for 10 hours, then ramped to 9°C over 12 hours, held at these conditions for 3 hours, then returned to 27°C over a 6 hr ramp. The final conditions were held for at least 3 hours. The corresponding relative humidity values were 88% and 30% (Figure 11).

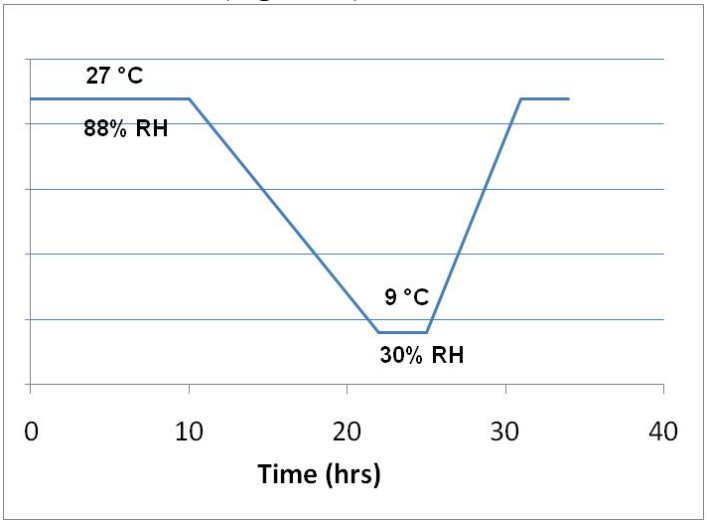

Figure 11. Climatic schedule used for shrinkage tests – dew point temperature and relative humidity are shown

During each test, we recorded shrinkage, temperature and sample weights at regular intervals. At the end of the experiment, the sample was dried at 103 ± 2°C in accordance with *AS/NZS 1080.1* (2001) to determine the current MC of the sample and previous MC evolution during the test. Investigations of sample MC versus external relative humidity were conducted to observe the sorption/desorption characteristics and hysteresis. The desorption phase is more applicable to wood drying. Therefore, the desorption RH and MC data were used to solve the

sorption isotherm equation **(53)** for constants c1 and c2. This provided the model with accurate desorption isotherms specific for each species.

3.5 Drying modelling - Vacuum drying modelling

The vacuum drying model was developed and implemented as part of this authors PhD project offered by QUT.

At the time of running model simulations, not all vacuum drying trials were completed. For model validation, one vacuum drying trial was chosen per species. We chose the trial that, to date, had produced the best-dried quality outcome in the quickest drying time (most optimised). The vacuum drying trials chosen were the *E. obliqu*a trial MES8, *C. citriodora* trial SPG9, *E. marginata* trial JAR10 and *E. pilularis* trial BBT11.

As the anatomical configuration of wood is complex, one must write transport equations at the macroscopic scale. This leads to the definition of empirical laws of migration that can be demonstrated to a large extent by averaging over representative volumes (Perré, 1996). At this level, we observe the porous medium as a fictitious, continuous medium. By using this approach, we can write most fluxes as the product of a coefficient times the driving force, both for the porous medium and the surrounding air. The conservation of liquid, water vapour, air and enthalpy enable a set of equations governing transfer in porous media to be derived (Whitaker, 1977). These equations have subsequently been used to model the softwood drying process (Perré, 1996, Perré and Turner, 1999b), where their ability to describe several different drying configurations has been proven.

The most recent application of the model describes the drying of single boards applied to the growth rings of softwood (Perré and Turner, 2008). This model, known as *TransPore 2D* describes the drying process for both homogeneous and heterogeneous cross sections, where density and transport differences due to the presence of growth rings accounted for. As the species investigated in this study are relatively homogenous, the majority of the transport model equations derive from the homogenous model reference as summarised:

3.5.1 Liquid conservation

$$\frac{\partial}{\partial t}(\varepsilon_w\rho_w + \varepsilon_v\rho_v + \overline{\rho}_w) + \nabla\cdot(\rho_w\overline{\mathbf{v}}_w + \rho_g\overline{\mathbf{v}}_g\,\overline{\rho_b\mathbf{v}_b}) = \nabla\cdot(\rho_g\overline{\overline{\mathbf{D}}}_{eff}\nabla\omega_v) \qquad \textbf{(41)}$$

3.5.2 Energy conservation

$$\begin{aligned}&\frac{\partial}{\partial t}(\varepsilon_w\rho_w h_w + \varepsilon_g(\rho_v h_v + \rho_a h_a) + \overline{\rho}_b\overline{h}_b + \rho_0 h_s - \varepsilon_g P_g) \\ &+\nabla\cdot(\rho_w h_w\overline{\mathbf{v}}_w + (\rho_v h_v + \rho_a h_a)\overline{\mathbf{v}}_g + g h_b\overline{\rho_b\mathbf{v}_b}) \\ &=\nabla\cdot(\rho_g\overline{\overline{\mathbf{D}}}_{eff}(h_v\nabla\omega_v + h_a\nabla\omega_a + \overline{\overline{\mathbf{K}}}_{eff}\nabla T) + \Phi\end{aligned} \qquad \textbf{(42)}$$

3.5.3 Air conservation

$$\frac{\partial}{\partial t}(\varepsilon_g\rho_a) + \nabla\cdot(\rho_a\overline{\mathbf{v}}_g) = \nabla\cdot(\rho_g\overline{\overline{\mathbf{D}}}_{eff}\nabla\omega_a) \qquad \textbf{(43)}$$

The Generalised Darcy's Law gives the gas and liquid phase velocities:

$$\overline{\mathbf{v}}_l = -\frac{\overline{\overline{\mathbf{K}}}_l\overline{\overline{\mathbf{k}}}_l}{\mu_l}\nabla\varphi_l \qquad \nabla\varphi_l = \nabla P_l - \rho_l g\nabla\chi \quad , \qquad \textbf{(44)}$$

Where $l = w, g$

The quantities φ in equation (44) represents the phase potentials and χ is the depth scalar. The nomenclature section of this report defines all other symbols.

This formulation accounts for the evolution of internal pressure through the air balance (equation (43)) and is thus able to deal with high temperature convective drying, vacuum drying and dielectric drying.

3.5.4 Closure conditions

Wood is a highly hygroscopic porous medium; therefore, we must separate bound water from free water as defined by:

$$X = X_w + X_b \equiv \frac{\varepsilon_w \rho_w}{\rho_o} + \min(X_{fsp}, X). \quad \textbf{(45)}$$

The volume fractions of the liquid and gaseous phases are defined as: $\varepsilon_w = \phi S_w$, $\varepsilon_g = \phi(1 - S_w)$, $\varepsilon_w + \varepsilon_g = \phi$, where ϕ is the porosity. We define the intrinsic phase air density as $\overline{\rho}_a = \varepsilon_g \rho_a$ and the gaseous phase is a binary mixture of air and vapour, which we assume to behave like an ideal gas. The saturation variable involved in the relative permeability functions is calculated according to the free water content only:

$$S_w = \frac{X_w}{X_{w\max}}. \quad \textbf{(46)}$$

As both liquid and gaseous water phases are present during drying of wood, and because of the curvature of the interface that exists between the liquid and gas phases within the pores of the medium, the liquid pressure is less than the gas pressure. The capillary pressure represents the difference:

$$P_w = P_g - P_c. \quad \textbf{(47)}$$

The values for fibre saturation point (X_{fsp}) are essential wood properties for the development of an accurate wood drying model and were therefore, measured as part of this study. The methodology for which is detailed in section *3.4 Drying modelling* - Measurement of essential wood properties.

3.5.5 Boundary Conditions

The boundary conditions for the external drying surfaces are assumed to be of the following form (Turner and Perré, 2004):

$$\mathbf{J}_w\big|_{x=0^+} \cdot \hat{\mathbf{n}} = k_m c M_v \ln\left(\frac{1 - x_{v\infty}}{1 - x_v\,|_{x=0^+}}\right) \quad \textbf{(48)}$$

$$\mathbf{J}_e\big|_{x=0^+} \cdot \hat{\mathbf{n}} = q(T - T_\infty) + h_v k_m c M_v \ln\left(\frac{1 - x_{v\infty}}{1 - x_v\,|_{x=0^+}}\right) \quad \textbf{(49)}$$

$$P_g\,|_{x=0^+} = P_\infty, \quad \textbf{(50)}$$

Where $\mathbf{J}_w$ and $\mathbf{J}_e$ represent the fluxes of total moisture and total enthalpy at the boundary. The pressure P_∞ and temperature T_∞ at the external drying surfaces are fixed at the kiln vacuum pressure and operating temperature. As one of the primary variables used for the computations is the average air density, modification of the boundary pressure condition (50) is required to form an appropriate nonlinear equation for this primary variable:

$$\varepsilon_g (P_v - P_\infty) + \frac{\overline{\rho}_a RT}{M_a} = 0. \qquad \textbf{(51)}$$

Equation (51) must be resolved, along with the conservation laws, during the nonlinear iterations for every external boundary control volume within the computational domain.

Introducing symmetry planes into the model (i.e., a quadrant of a board) reduces the overall computational times. We assume all fluxes of liquid, vapour, air, and heat are zero at the symmetry planes. Initially the board has some prescribed moisture content, with the pressure and temperature being constant throughout the board at the initial kiln pressure and temperature.

The values for external pressure and temperature are essential boundary condition parameters for the development of an accurate deterministic wood drying model and were therefore, measured as part of this study. The methodology for which is detailed in section *3.3 Drying modelling - Measurement of kiln conditions and* wood drying properties.

3.5.6 Numerical Solution Procedure

The numerical procedure used to resolve the drying model has been extensively published, and the reader is referred to the most relevant literature for the finer details (Perré and Turner, 1999a, Perré and Turner, 1999b). In summary, to discretise the conservation laws, we implement the *finite volume* method on a structured mesh. Triangular meshes were calculated over symmetry plane dimensions using the software application GMSH version 2.4.2. Thereafter, we used an efficient inexact Newton method to resolve in time the complicated and often large nonlinear system that describes the drying process. Flux limiting is used to determine the spatial weighting schemes for all advection/convection terms in the equations in order to reduce numerical dispersion of the drying fronts, and the introduction of the fixed phase ensures that full saturation $S_w = 1$ is never reached at the surface of the medium. These are important advancements in the computational model that can enhance convergence of the nonlinear iterations and ensure accurate resolution of the drying fronts on relatively coarse meshes and are particularly useful for simulating the vacuum drying process (Turner and Perré, 2004). For this project, we performed drying simulations in the radial-tangential (R-T) plane.

3.5.7 Physical Properties

The following physical properties are necessary scalar or tensor input variables for the drying model computations. The expressions and/or values provided have been used to simulate homogenous modelling of softwoods (Turner and Perré, 2004, Perré and Turner, 1999b), and their adaptability to the proposed hardwood model will be tested and modified where necessary. Some of the properties discussed are specific to the wood direction (Plate 20) termed longitudinal (up the stem of the tree parallel to the wood fibres), radial (from the outside of the tree towards the centre) and tangential (perpendicular to the radial direction). A backsawn board has the tangential direction along the wide face of the board and a quartersawn board has the radial direction along the wide face of the board.

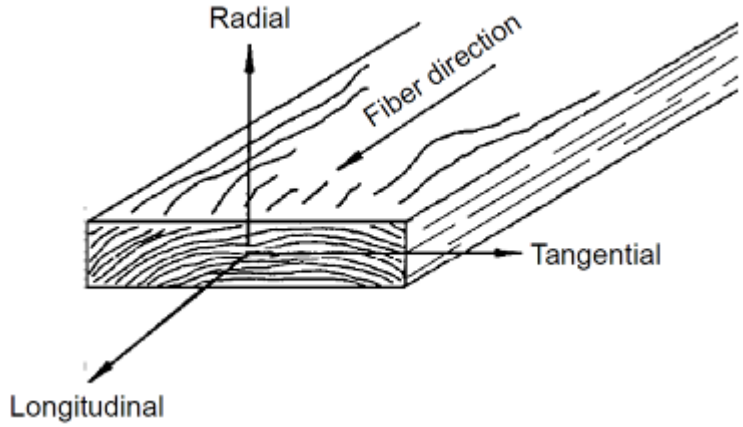

Plate 20. Three principal axes of wood direction with respect to grain direction and growth rings

Porosity (φ)

Porosity values are essential wood properties for the development of an accurate wood drying model and were therefore, measured as part of this study. Porosity values were determined via image analysis of environmental scanning electron microscope (ESEM) images. The methodology for which is detailed in section *3.4 Drying modelling* - Measurement of essential wood properties.

Wood Density (ρ)

Density values are essential wood properties for the development of an accurate wood drying model and were therefore, measured as part of this study. The methodology for which is detailed in section *3.4 Drying modelling* - Measurement of essential wood properties.

Heat Capacity ($\overline{\rho c_p}$)

The heat capacity is defined as (Perré and Turner, 2008):

$$\overline{\rho c_p} = \rho_w(1113 + 4.85T + 4185X). \quad \textbf{(52)}$$

Sorption Isotherm

The sorption isotherm is defined as (Perré and Turner, 2008):

$$\frac{P_v}{P_{vs}} = 1 - \exp(-c_1 A - c_2 A^2), \text{ where } \quad c_1 \text{ and } c_2 \text{ are constants and } A = X_b / X_{fsp}. \quad \textbf{(53)}$$

The values c_1 and c are essential species dependant constant properties for the development of an accurate wood drying model and were therefore, measured as part of this study. The methodology for which is detailed in section *3.4 Drying modelling* - Measurement of essential wood properties.

Capillary Pressure (P_c)

The capillary pressure is defined as (Perré and Turner, 2008):

$$P_c = 1.24\times10^5 \times \sigma(T) \times (S_w + 1\times10^{-0.61}), \text{ where } \quad \sigma(T) = (77.5 - 0.185T)\times10^{-3} \quad \textbf{(54)}$$

represents the surface tension.

Relative Permeability (k_r)

The relative **liquid** permeability is defined respectively in the tangential, radial and longitudinal directions as (Perré and Turner, 2008):

$$k_{rl}^{T} = (S_w)^3, \quad k_{rl}^{R} = k_{rl}^{T}, \quad k_{rl}^{L} = (S_w)^8. \tag{55}$$

The relative **gas** permeability is defined respectively in the tangential, radial and longitudinal directions as:

$$k_{rg}^{T} = 1 + (2S_w - 3)(S_w)^2, \quad k_{rg}^{R} = k_{rg}^{T}, \quad k_{rg}^{L} = 1 + (4S_w - 5)(S_w)^4. \tag{56}$$

Intrinsic Permeability

Intrinsic permeability values are essential wood properties for the development of an accurate wood drying model and were therefore, measured as part of this study. We measured the gas permeabilities for each species as detailed in section *3.4 Drying modelling* - Measurement of essential wood properties. The liquid permeability values were given the same values as for the gas permeabilities as pit aspiration does not apply for hardwoods.

Gaseous Diffusion (D_{eff})

The gaseous diffusion is defined respectively in the tangential, radial and longitudinal directions as (Perré and Turner, 2008):

$$D_{eff}^{T} = 10^{-3} \times k_{rg}^{T} \times D_v, \quad D_{eff}^{R} = 2 \times D_{eff}^{T}, \quad D_{eff}^{L} = 100 \times D_{eff}^{T} \tag{57}$$

, where D_v is the mass diffusivity of vapour in the air phase.

Diffusivity of vapour (D_v)

The diffusivity of vapour in gas is defined as (Perré and Turner, 2008, Bird *et al.*, 1960):

$$D_v = 2.2 \times 10^{-5} \left(\frac{1.013 \times 10^5}{P} \right) \left(\frac{T}{273} \right)^{1.75} \tag{58}$$

Bound Water Diffusion (D_b) – Theory

Initial simulations used theoretical bound liquid diffusivities, detailed by Perré and Turner (2008) and summarized below. In this section, we assume the gradient of bound water is the driving force. This allows two pseudo-diffusivities to be defined (bound water in the cell wall and air in the pores):

$$\hat{D}_b = \rho_s D_b, \quad \hat{D}_v = \frac{M_v}{RT} D_v \frac{\partial P_v}{\partial X_b}, \quad \hat{D}_b = \rho_s \exp\left(-12.8183993 + 10.8951601 X_b - \frac{4300}{T + 273.15} \right) \tag{59}$$

Using homogenisation results, we propose the following correlations:

$$\tilde{D}_b^R = A_{series}(1+1.6(\varepsilon_g)^{1.8}, \quad \tilde{D}_b^T = 1.8 * A_{series}, \quad \text{with} \quad A_{series} = \frac{1}{\frac{\varepsilon_s}{\hat{D}_b} + \frac{\varepsilon_g}{\hat{D}_v}} \tag{60}$$

A small percentage of ray cells have to be in parallel to the cell arrangement giving the final form of the radial macroscopic diffusivity as:

$$\rho_0 D_b^R = (1-\varepsilon_{ray})\tilde{D}_b^R + \varepsilon_{ray} \times \tilde{D}_{ray}^R \tag{61}$$

Typical values for ε_{ray} and $\tilde{D}_{ray}^R$ are 0.05 and 0.1 x $\hat{D}_v$ respectively (Perré and Turner, 2008). To be consistent, the same amount of ray cells is put in series with tracheids in the tangential direction:

$$\rho_0 D_b^T = \frac{1}{\frac{1-\varepsilon_{ray}}{\tilde{D}_b^T} + \frac{\varepsilon_{ray}}{\tilde{D}_{ray}^T}} \tag{62}$$

Due to the considerable length of wood fibres, the longitudinal macroscopic diffusivity is derived using a parallel model of the form:

$$\rho_0 D_b^L = \varepsilon_s \hat{D}_b + \varepsilon_g \hat{D}_v \tag{63}$$

Thermal Conductivity (λ_{eff})

The thermal conductivity is defined using homogenisation in the R-T plane and using a parallel flow model in the longitudinal direction (Perré and Turner, 2008):

$$\tilde{\lambda}_0^R = 0.46 \times \lambda_{series} + 0.54 \times \lambda_{parallel}, \quad \tilde{\lambda}_0^T = \left(\varepsilon_g \lambda_{air}^n + \varepsilon_s \hat{\lambda}_{s\perp}^n\right)^{\frac{1}{n}}, \quad \text{with n} = 0.6, \quad \lambda_0^L = \varepsilon_g \lambda_{air} + \varepsilon_s \hat{\lambda}_{s//} \quad \text{with } \hat{\lambda}_{s//} \approx 2 \times \hat{\lambda}_{s\perp}, \tag{64}$$

where $\lambda_{series} = \frac{1}{\frac{\varepsilon_s}{\hat{\lambda}_{s\perp}} + \frac{\varepsilon_g}{\lambda_{air}}}$ and $\lambda_{parallel} = \varepsilon_s \hat{\lambda}_{s\perp} + \varepsilon_g \lambda_{air}$.

Properties with a subscript of 0 denote thermal conductivities at a moisture content equal to zero. Constant values λ_{air} = 0.023 W m^{-1} K^{-1} and $\hat{\lambda}_{s\perp}$ = 0.5 W m^{-1} K^{-1}.

The effect of ray cells are into account such that:

$$\lambda_0^R = \left(1-\varepsilon_{ray}\right)\tilde{\lambda}_0^R + \varepsilon_{ray} \times \tilde{\lambda}_{ray//}, \qquad (65)$$

$$\lambda_0^T = \frac{1}{\frac{1-\varepsilon_{ray}}{\tilde{\lambda}_0^T} + \frac{\varepsilon_{ray}}{\tilde{\lambda}_{ray\perp}}} \quad \text{with n = 0.6.}$$

$\lambda_{ray\perp}$ and $\lambda_{ray//}$ are evaluated using equations (**64**) respectively with a density of 500 kg m^{-3}. For any value of moisture content, the final expression for conductivity read:

$$\lambda^T(\rho, X) = \left(\left(1-S_w\right)\left(\lambda_0^T\right)^n + S_w\left(\phi\lambda_{air}^n + \varepsilon_s\hat{\lambda}_{s\perp}^n\right)\right)^{\frac{1}{n}}, \qquad (66)$$

$$\lambda^R(\rho, X) = \left(\left(1-S_w\right)\left(\lambda_0^R\right)^n + S_w\left(\phi\lambda_{air}^n + \varepsilon_s\hat{\lambda}_{s\perp}^n\right)\right)^{\frac{1}{n}}, \qquad \text{with n = 0.6}$$

$$\lambda^L(\rho, X) = \left(\left(1-S_w\right)\left(\lambda_0^L\right)^n + S_w\left(\phi\lambda_{air} + \varepsilon_s\lambda_{s//}\right)^n\right)^{\frac{1}{n}},$$

where n =0.6 for the three expressions.

Heat transfer coefficient (h_h)

The heat transfer coefficient is computed from classic boundary layer theory and is defined as (Bird *et al.*, 1960):

$$h_h = 0.023\frac{\lambda_a}{L}\mathrm{Pr}^{1/3}\left(\frac{v_g XP}{\mu_g RT}\right)^{0.8}, \qquad (67)$$

where the humid air viscosity is defined as (Bird *et al.*, 1960):

$$\mu_g = \frac{P_a\mu_a\sqrt{M_a} + P_v\mu_v\sqrt{M_v}}{P_a\sqrt{M_a} + P_v\sqrt{M_v}}, \qquad (68)$$

the dry air viscosity is (Bird *et al.*, 1960):

$$\mu_a = A_0 + A_1T, \quad \text{where} \quad \begin{matrix} A_0 = 0.59\times10^{-5} \\ A_1 = 4.2\times10^{-8} \end{matrix}, \qquad (69)$$

the water vapour viscosity is (Perré and Turner, 2008):

$$\mu_v = A_0 + A_1T + A_2T^2, \quad \text{where} \quad \begin{matrix} A_0 = -3.189\times10^{-6} \\ A_1 = 4.145\times10^{-8} \\ A_2 = -8.272\times10^{-13} \end{matrix}, \qquad (70)$$

and the Prandtl number is defined as:

$$\mathrm{Pr} = \frac{c_p\mu}{k}. \qquad (71)$$

Mass transfer coefficient (h_m)

The mass transfer coefficient is computed from classic boundary layer theory and is defined as (Bird *et al.*, 1960):

$$h_m = \frac{h_h}{\rho c_p}. \quad \textbf{(72)}$$

4 Results

4.1 Applied drying – Experimental drying trials

The results of the vacuum and conventional drying trials are presented in this section. The results of each species are reported separately.

4.1.1 *Corymbia citriodora* – spotted gum

Drying schedules

The vacuum kiln used for the study incorporates a standard software package that includes a number of pre-set schedules for various species (predominantly American and European species) of varying thickness. Only two pre-set schedules pertaining to native Australian eucalypts exist (*E. regnans* and *E. globulus)*. The drying properties of these *ash* type species are very different from those for *C. citriodora*. For this reason, we judged existing vacuum drying schedules for Australian species unsuitable.

The schedules used for each trial are shown (Table 4) including for each MC change point, the dry bulb temperature (DBT), wet bulb depression (WBD) and equilibrium moisture content (EMC). The schedule chosen for vacuum drying trial SPG1 was the same schedule reported by Redman (2006) to have successfully vacuum dried native forest *Corymbia citriodora* (spotted gum) during commissioning of the vacuum kiln. This schedule was a preset schedule provided for *Hymenaea courbaril* (courbaril) and we chose this on the understanding (supported by Simpson and Verill, 1997) that in general; timbers of similar densities often have similar drying characteristics. The average dried density (12% MC) of mature *H. courbaril* is 910 kg/m^3 (Lincoln 1991), which is similar to 1010 kg/m^3 reported for mature *C. citriodora* (http://www.dpi.qld.gov.au, 2008). Although presented as a conventional stepwise schedule, the dry and wet bulb temperatures were actually ramped between MC change points. We performed a 48-hour equalisation phase at the end of drying at an EMC of 12%.

For the second *C. citriodora* vacuum drying trial (SPG2), we repeated the schedule used for the SPG1 vacuum drying trial as, although we achieved acceptable dried quality results, the drying rate for the first trial was compromised (slowed) due to a kiln vacuum leak. Therefore, it was deemed necessary to repeat the trial.

Due to favourable dried quality resulting from the first two trials, we increased the DBT throughout for the SPG3 trial with the intention of reducing the drying time. As is generally the case when drying Australian hardwoods, the material was dried 1-2% below the target average MC and then re-wet during the equalisation phase to reach the target MC to minimise MC gradients and associated residual drying stresses. The fact that re-wetting timber (sorption) leads to lower values of MC at the same EMC than drying timber (desorption) is known as sorption hysteresis (Siau, 1984). For this reason, we increased the equalisation EMC for the SPG3 trial from 12% to 13%, to bring the final average MC closer to the target 11% and reduce unacceptable stress levels encountered in the first two trials.

For the SPG4 vacuum trial we chose the same schedule used for the SPG3 trial except the equalisation time was increased from 48 to 72 hours. We made this change in an attempt to alleviate drying stress, which was not within acceptable limits for the SPG3 vacuum trial.

Dale and Meyers Sawmill (Maryborough, Queensland) supplied material for conventional trials SPG1, SPG3 and SPG4 and Burnett Sawmill (Bundaberg, Queensland supplied material for conventional trial SPG2. Commercial confidentiality prevents details of the conventional drying schedule used by either sawmill from being discussed.

Table 4. Vacuum drying schedules – *Corymbia citriodora*

Trial	SPG1 and SPG2			SPG3			SPG4		
MC change points (%)	DBT (°C)	WBD (°C)	EMC (%)	DBT (°C)	WBD (°C)	EMC (%)	DBT (°C)	WBD (°C)	EMC (%)
Heat-up	60	2.4	17.0	64	1.8	18.0	64	1.8	18.0
Green - 70	60	5.0	12.0	64	5.0	12.0	64	5.0	12.0
70 - 60	61	5.4	12.0	65	5.4	12.0	65	5.4	12.0
60 - 50	63	6.0	11.0	66	5.8	11.0	66	5.8	11.0
50 - 40	64	6.2	11.0	66	6.2	11.0	66	6.2	11.0
40 - 30	65	7.1	10.0	67	7.1	10.0	67	7.1	10.0
30 - 25	67	9.1	9.1	69	8.9	9.1	69	8.9	9.1
25 - 20	69	12.0	7.4	71	12.0	7.4	71	12.0	7.4
20 - 15	72	18.0	5.4	75	18.0	5.5	75	18.0	5.5
15 - final	77	13.0	6.9	80	13.0	6.9	80	13.0	6.9
Equalise (48 hrs)	70	4.8	12.0	80	4.7	13.0	80	4.5	13.5 (72 hrs)

Moisture content

Initial MC results are shown in Table 5. For trial SPG1, initial MC populations are normally distributed, but are not normally distributed for the other trials, likely because of high MC outliers (Figure 12). Multiple pairwise comparisons produced no significant differences between sample populations of trials SPG1 and SPG4. All other pairwise comparison combinations produced significant differences between sample populations. This is evident by observation, where the initial cross-sectional MC average of trials SPG2 and SPG3 was approximately 3% lower for each successive trial compared with trials SPG1 and SPG4.

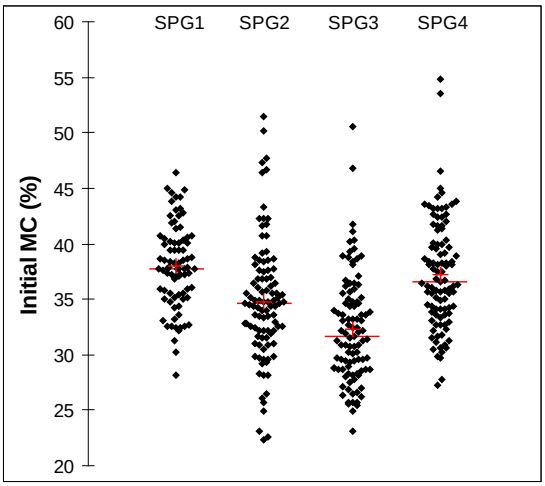

Figure 12. Scattergram of initial MC – *C. citriodora*

Table 5. Initial MC results – *C. citriodora*

	Initial MC (%)			
Trial	SPG1	SPG2	SPG3	SPG4
Average	37.9	34.8	32.3	37.3
Maximum	46.4	51.5	50.6	54.8
Minimum	28.2	22.4	23.1	27.3
Standard deviation	3.8	5.5	4.8	5.0

The final cross-sectional MC results are presented in Figure 13 and Table 6. Except for trial SPG4, there are significant differences between the final cross-sectional MC means of end-matched conventional and vacuum trials. In accordance with *AS/NZS: 4787* each vacuum trial, and SPG2 conventional trial achieved acceptable grade quality B results for final cross-sectional MC (target = 11%). Both conventional SPG1 and SPG3 trials achieved unacceptable grade quality C due to,

- under-drying in the case of the SPG1 trial (average 13.6%) and
- over-drying in the case of the SPG3 trial (average 7.9%).

Except for the SPG1 and SPG4 vacuum trials and SPG4 conventional trial, unacceptable average cross-sectional MC results were recorded for all other trials in accordance with Australian Standard *AS 2796:1999*. For the SPG2 and SPG3 conventional and vacuum trials this was due to under-drying and not the spread of final MC.

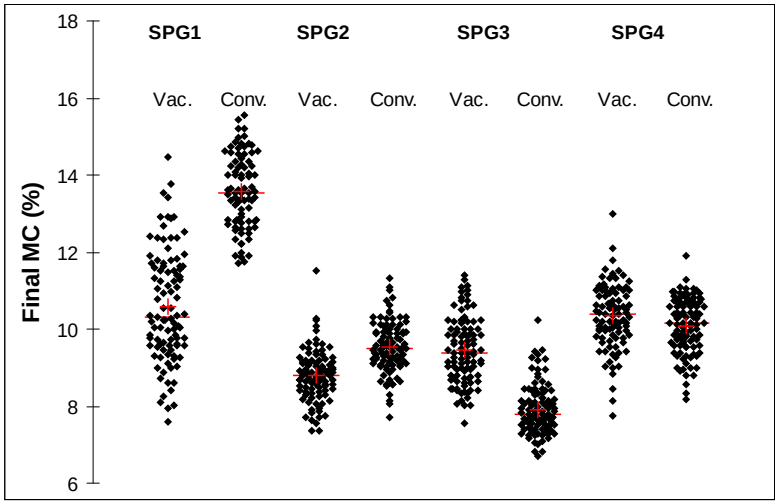

Figure 13. Scattergram of final MC – *C. citriodora*

Table 6. Final MC results - *C. citriodora*

	Final MC (%)							
	SPG1		SPG2		SPG3		SPG4	
	Vacuum	Conventional	Vacuum	Conventional	Vacuum	Conventional	Vacuum	Conventional
Average	10.7	13.6	8.8	9.5	9.5	7.9	10.4	10.2
Maximum	14.5	15.5	11.5	11.3	11.4	10.2	13.0	11.9
Minimum	8.0	11.7	7.3	7.7	7.6	6.7	7.7	8.2
Standard deviation	1.4	1.0	0.7	0.7	0.9	0.7	0.8	0.7
Significance (p)	< 0.0001		< 0.0001		< 0.0001		0.056	
Grade quality (*AS/NZS 4787*)	B	C	B	B	B	C	B	B
% permissible (*AS 2796*)	90	66	36	84	70	9	96	95

The final MC gradient results are displayed in Figure 14 and Table 7. For each trial there are significant differences between the final MC gradient means of end-matched conventional and vacuum trials. For all trials, the MC gradient results were acceptable in accordance with *AS/NZS: 4787*. All trials achieved the best grade quality A except for the SPG3 vacuum and SPG4 conventional trials, which achieved grade quality B. The SPG3 vacuum trial B grade is likely because the harshest and fastest, drying schedule was used for this trial. From this author's experience, generally harsher more accelerated drying schedules tend to amplify the final spread of final average MC, MC gradient and residual drying stress. Thus, drying schedules are often limited by the acceptance level of these parameters.

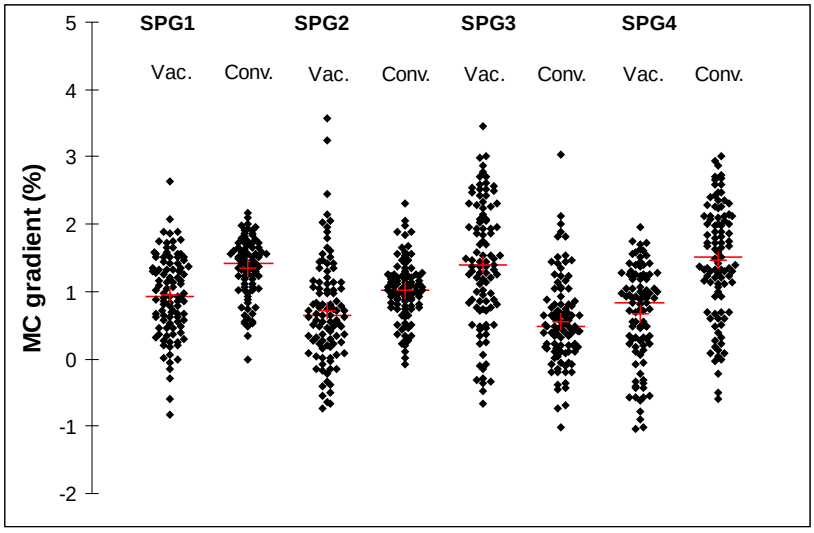

Figure 14. Scattergram of MC gradient – *C. citriodora*

Table 7. MC gradient results – *C. citriodora*

	Final MC gradient (%)							
	SPG1		SPG2		SPG3		SPG4	
	Vacuum	Conventional	Vacuum	Conventional	Vacuum	Conventional	Vacuum	Conventional
Average	1.0	1.3	0.7	1.0	1.4	0.6	0.7	1.5
Maximum	2.1	2.2	3.6	2.3	3.5	3.0	2.0	-0.6
Minimum	-0.8	0.0	-2.2	-0.1	-0.7	-1.0	-1.0	3.0
Standard deviation	0.6	0.5	0.8	0.5	0.9	0.7	0.7	0.8
Significance (p)	< 0.0001		0.0002		< 0.0001		< 0.0001	
Grade quality (*AS/NZS 4787*)	A	A	A	A	B	A	A	B

Basic density

The basic density results are displayed in Figure 15 and Table 8. Multiple pairwise comparisons produced no significant differences between basic density populations of trials SPG1 and SPG2, and SPG2 and SPG3. All other pairwise comparison combinations produced significant differences between sample populations. The average basic density of trial SPG4 is significantly lower than the other trials. The average basic density recorded for each trial is similar to the value recorded (http://www.fwpa.com.au, 2003) of 865 kg/m^3 for mature native forest *C. citriodora*.

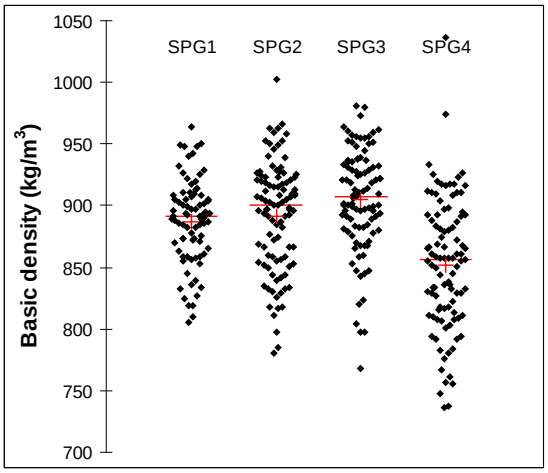

Figure 15. Scattergram of basic density – *C. citriodora*

Table 8. Basic density results – *C. citriodora*

	Basic density (kg/m^3)			
Trial	SPG1	SPG2	SPG3	SPG4
Average	887.4	891.7	904.8	852.2
Maximum	963.4	1002.7	981.2	1036.5
Minimum	805.0	780.1	768.2	735.7
Standard deviation	34.4	44.3	42.2	53.3

Distortion

We measured distortion on undressed boards before and after drying. For all trials, cupping was not included in the total percentage of boards within acceptable limits as all cupping was removed after dressing. Significant differences do not exist between paired conventional and vacuum population means of bow, twist and cup for trial SPG1, bow for trial SPG2, cup for trial SPG3, and bow and cup for trial SPG4 (Table 9). All other comparisons exhibited significant differences. Distortion results were acceptable (total > 90%) after drying for all trials except for the SPG3 and SPG4 conventional trials. Twist was the predominant type of distortion for boards failing to meet the standard (Table 10).

Table 9. Distortion results after drying – *C. citriodora*

		Distortion (mm)							
Trial		Vacuum				Conventional			
		Spring	Bow	Twist	Cup	Spring	Bow	Twist	Cup
SPG1	Average	3.0	3.6	1.8	0.0	2.4	3.5	1.7	0.0
	Maximum	10.0	13.0	9.0	0.0	12.0	10.0	8.0	0.0
	Minimum	0.0	1.0	0.0	0.0	0.0	0.0	0.0	0.0
	Standard deviation	1.9	2.2	1.4	0.0	2.2	2.7	1.8	0.0
	Significance (p)	0.013	0.640	0.747	1.000				
SPG2	Average	1.9	5.4	2.0	0.0	2.5	5.4	3.3	0.2
	Maximum	8.0	15.0	8.0	0.0	10.0	16.0	11.0	2.0
	Minimum	0.0	0.0	0.0	0.0	0.0	0.0	0.0	0.0
	Standard deviation	1.9	2.6	2.0	0.0	2.3	3.3	2.5	0.5
	Significance (p)	0.024	0.961	0.001	< 0.0001				
SPG3	Average	2.2	2.2	1.5	0.8	4.3	5.0	5.1	0.8
	Maximum	12.0	10.0	8.0	2.0	21.0	21.0	35.0	6.0
	Minimum	0.0	0.0	0.0	0.0	0.0	0.0	0.0	0.0
	Standard deviation	1.8	1.9	1.4	0.7	3.5	3.9	5.4	0.9
	Significance (p)	< 0.0001	< 0.0001	< 0.0001	0.878				
SPG4	Average	2.7	5.2	1.3	0.4	3.3	4.8	2.8	0.3
	Maximum	11.0	16.0	11.0	3.0	12.0	17.0	15.0	7.0
	Minimum	0.0	0.0	0.0	0.0	0.0	0.0	0.0	0.0
	Standard deviation	2.6	2.8	2.0	0.7	2.7	3.9	3.2	1.0
	Significance (p)	0.049	0.146	< 0.0001	0.171				

Table 10. Distortion grade results – *C. citriodora*

		Distortion - % In grade									
Trial		Vacuum					Conventional				
		Spring	Bow	Twist	Cup	**Total**	Spring	Bow	Twist	Cup	**Total**
SPG1	Before drying	100	100	100	100	**100**	NA	NA	NA	NA	**NA**
	After drying	100	99	99	100	**99**	100	100	98	100	**98**
SPG2	Before drying	100	99	95	100	**94**	NA	NA	NA	NA	**NA**
	After drying	100	98	96	100	**94**	100	97	97	97	**93**
SPG3	Before drying	100	99	100	100	**99**	NA	NA	NA	NA	**NA**
	After drying	100	100	98	90	**98**	99	98	87	81	**86**
SPG4	Before drying	100	95	100	100	**95**	NA	NA	NA	NA	**NA**
	After drying	100	98	97	91	**96**	99	93	84	97	**83**

Surface and internal checking

Significant differences do not exist between the surface checking populations of the SPG1 and SPG3 conventional and vacuum trials (Table 11). For every vacuum drying trial and the SPG3 conventional trial, an acceptable (> 90%) number of boards achieved select grade for surface checking in accordance with *AS 2796:1999* (Table 12). For the SPG2 conventional trial only 8% of boards achieved this grade. This result may be due to this trial being pre-air dried in an uncontrolled environment prior to final kiln drying. The other conventional trials were kiln dried from the green condition. In most cases, we achieved better surface checking grade recovery through vacuum drying than conventional drying.

All of the boards from each trial were free of internal checking.

Table 11. Surface checking results – *C. citriodora*

	Surface checking (mm)							
	SPG1		SPG2		SPG3		SPG4	
	Vacuum	Conventional	Vacuum	Conventional	Vacuum	Conventional	Vacuum	Conventional
Average	10.9	14.1	2.9	973.9	44.5	47.6	34.8	60.4
Maximum	1055.0	800.0	240.0	1980.0	1850.0	1370.0	839.0	1011.0
Minimum	0.0	0.0	0.0	0.0	0.0	0.0	0.0	0.0
Standard deviation	85.0	72.2	24.0	646.7	182.7	160.4	126.9	185.8
Significance (p)	0.0560		< 0.0001		0.571		0.019	

Table 12. Surface checking grade results – *C. citriodora*

	SPG1		SPG2		SPG3		SPG4	
Grade	Vacuum	Conventional	Vacuum	Conventional	Vacuum	Conventional	Vacuum	Conventional
Select (%)	99	89	100	8	92	93	93	87
Medium feature (%)	0	10	0	0	0	0	0	0
High feature (%)	1	1	0	92	8	7	7	13
Surface check free boards (%)	93	84	96	3	85	83	86	72
Internal check free boards (%)	100	100	100	100	100	100	100	100

End splits

Significant differences exist between vacuum and conventional drying end split populations for trials SPG3 and SPG4 Table 13. All trials achieved acceptable grade quality results for end-split. In all cases significantly less end split was recorded for the vacuum drying trials than the conventional trials (no end split for vacuum trials SPG1 and SPG2). It may be due to extra internal overpressure caused by the vacuum itself, more end drying is present during vacuum drying compared to conventional methods. This theory is reinforced by the test board thermocouple results presented in section *4.3.4 Board temperature*. The thermocouple results show noticeably lower temperatures at the board ends than the centres indicating a higher degree of free water at the ends of the boards. This would certainly reduce the level of shrinkage variation at the board ends and hence reduce the incidence and severity of end-splitting.

Table 13. End split results – *C. citriodora*

	End splits (mm)							
	SPG1		SPG2		SPG3		SPG4	
	Vacuum	Conventional	Vacuum	Conventional	Vacuum	Conventional	Vacuum	Conventional
Average	0.0	2.0	0.0	18.8	1.0	2.2	8.2	7.8
Maximum	0.0	200.0	0.0	170.0	41.0	68.0	904.0	258.0
Minimum	0.0	0.0	0.0	0.0	0.0	0.0	0.0	0.0
Standard deviation	0.0	16.4	0.0	33.2	5.1	8.7	66.5	30.6
Significance (p)	< 0.0001		< 0.0001		0.043		0.014	
Grade quality (*AS/NZS 4787*)	A	A	A	A	A	B	A	B

Drying stress

Significant differences exist between the drying stress population means of all conventional and vacuum end-matched trials (Table 14). Both conventional and vacuum SPG1 trials and the SPG2 and SPG4 vacuum trials achieved the acceptable grade quality B for average drying stress. All other trials achieved the unacceptable grade quality C. It is not possible to determine if the harsher drying schedule used for the SPG3 vacuum trial contributed to the unacceptable grade quality as we obtained similar results for the corresponding conventional trial. However, we used the same schedule for the SPG4 trial but with a longer equalisation period (72 hrs instead of 48 hrs). This resulted in improved, and acceptable drying stress results for the SPG4 vacuum trial. Improvements due to schedule manipulation are visually evident in Figure 16.

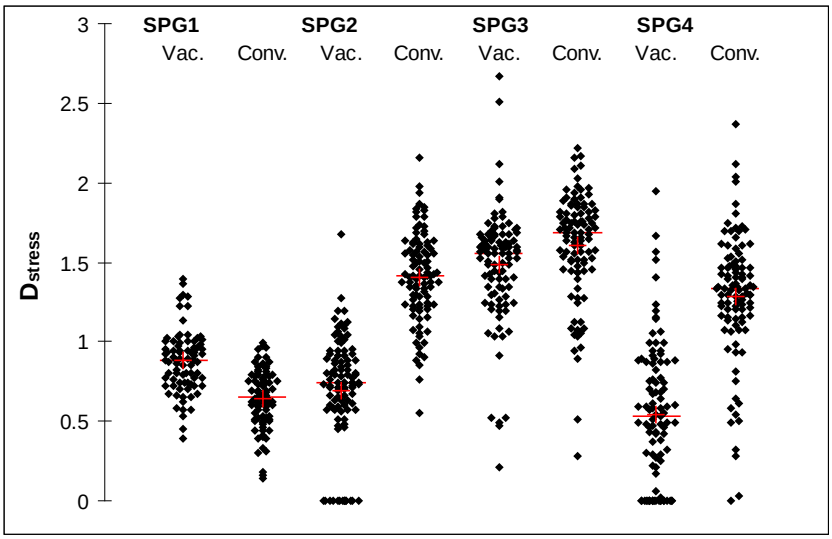

Figure 16. Scattergram of drying stress – *C. citriodora*

Table 14. Drying stress results – C. citriodora

	Drying stress (D_{stress})							
	SPG1		SPG2		SPG3		SPG4	
	Vacuum	Conventional	Vacuum	Conventional	Vacuum	Conventional	Vacuum	Conventional
Average	0.9	0.6	0.7	1.4	1.5	1.6	0.5	1.3
Maximum	1.4	1.0	1.7	2.2	2.7	2.2	1.9	2.4
Minimum	0.4	0.1	0.0	0.6	0.2	0.3	0.0	0.0
Standard deviation	0.2	0.2	0.3	0.3	0.4	0.3	0.4	0.4
Significance (p)	< 0.0001		< 0.0001		< 0.0001		< 0.0001	
Grade quality (*AS/NZS 4787*)	B	B	B	C	C	C	B	C

Collapse

No signs of collapse were present for any boards from any trial.

Sawn orientation

The majority of boards were a combination of back sawn and transitionally sawn Table 15. Backsawing is the desired cutting pattern for this species as it usually provides a higher green off-saw (GOS) recovery than quartersawing, and better aesthetics because of growth ring orientation.

Table 15. Sawn orientation results – *C. citriodora*

	Sawn orientation (%)			
	SPG1	SPG2	SPG3	SPG4
Quartersawn	9	2	3	2
Backsawn	41	71	73	78
Transitional	50	27	24	20

Gross shrinkage

There is no difference between the width and thickness gross shrinkage means for the SPG1 and SPG3 vacuum trials but do exist for the SPG2 and SPG4 vacuum trials (Table 16). This suggests that in terms of shrinkage in the radial and a tangential direction; *C. citriodora* has less transverse anisotropy compared with the other species reported. The results are in agreement with published tangential (6.1%) and radial (4.3%) shrinkages (http://www.dpi.qld.gov.au, 2008).

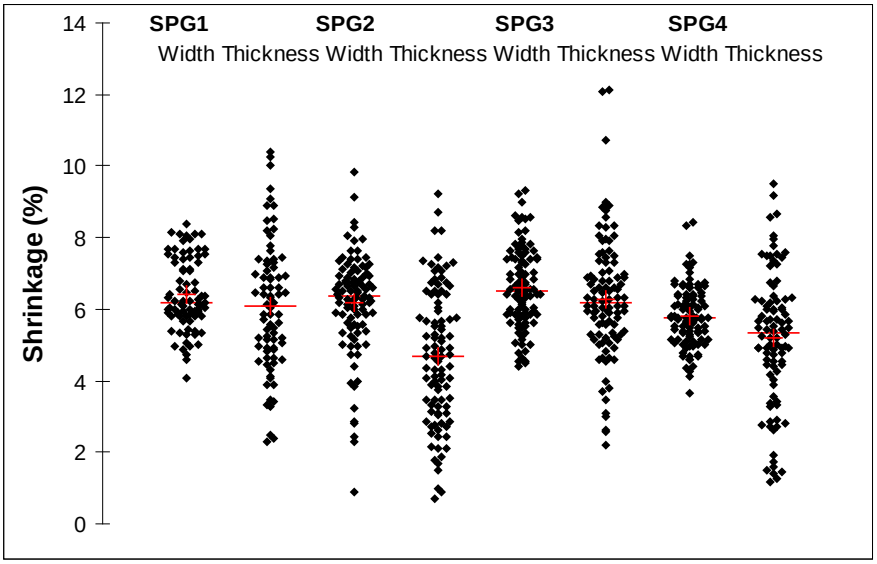

Figure 17. Scattergram of gross shrinkage – *C. citriodora*

Table 16. Gross shrinkage results – *C. citriodora*

	Gross shrinkage (mm)							
	SPG1		SPG2		SPG3		SPG4	
	Width	Thickness	Width	Thickness	Width	Thickness	Width	Thickness
Average	6.4	6.1	6.2	4.7	6.6	6.3	5.8	5.2
Maximum	8.4	10.4	9.9	9.2	9.3	12.1	8.4	9.5
Minimum	4.1	2.3	0.9	0.7	4.4	2.2	3.6	1.2
Significance (p)	0.1670		< 0.0001		0.1550		0.0020	
Standard deviation	1.0	1.8	1.4	1.9	1.1	1.7	0.9	1.9

Drying times and vacuum kiln output

For the conventional SPG1, SPG3 and SPG4 trials the total kiln drying time from the green condition was 21 days. The total drying times, including equalisation for the vacuum trials SPG1, SPG2, SPG3 and SPG4 were 14.0, 17.2, 12.0 and 13.8 days respectively. The drying rate for the first six days of the SPG1 vacuum trial was potentially slowed due to a kiln vacuum leak. This is evident by observing the pressure and core MC curves (Figure 18). By inspection of the slope of the MC core curve after the leak was repaired (day 6), we estimate that the drying time for SPG1 vacuum trial may have been shortened by at least 2 days using the same schedule. This did not seem to hold true for the SPG2 vacuum trial using the same schedule (Figure 19), however the final average cross-sectional MC for vacuum trial SPG2 was lower (8.8%) compared with that of vacuum trial SPG1 (10.7%). Average core MC resulting from the resistance probes shows a period of 2.5 days was required to reduce the SPG2 MC from 10.7% to 8.8% during the final stages of drying. Thus, the SPG2 vacuum drying time is comparable to trial SPG1 (14 days). The SPG3 vacuum drying schedule was the harshest in terms of DBT and subsequently had the fastest drying rate, drying 57% faster than the end-matched conventional boards from the green condition (Figure 20). We used the same schedule for the SPG4 trial except the equalisation time was extended by 24 hours (Figure 21). This trial produced the best dried quality than any other vacuum or conventional trial.

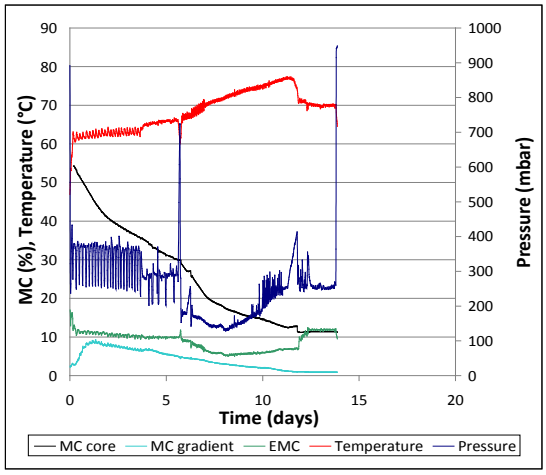

Figure 18. Vacuum drying chart – SPG1 trial

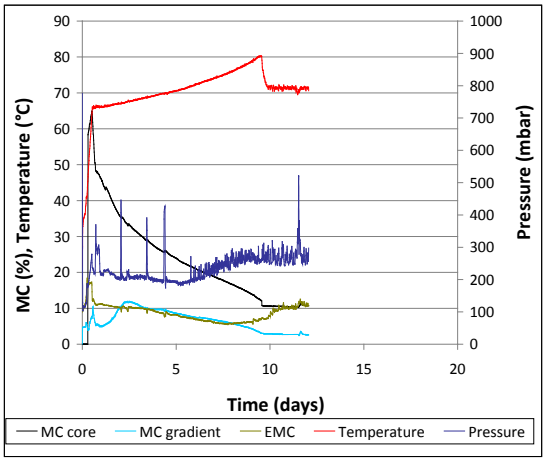

Figure 20. Vacuum drying chart – SPG3 trial

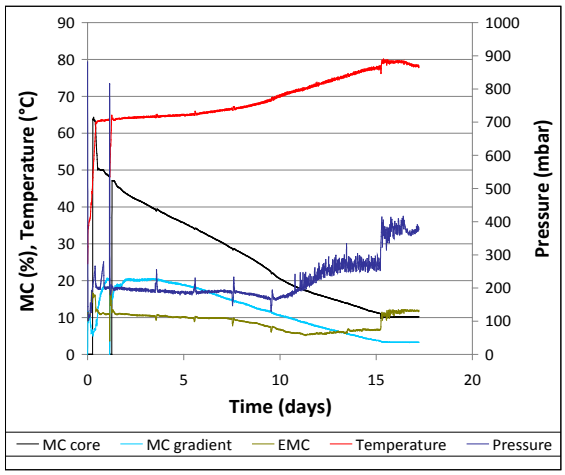

Figure 19. Vacuum drying chart – SPG2 trial

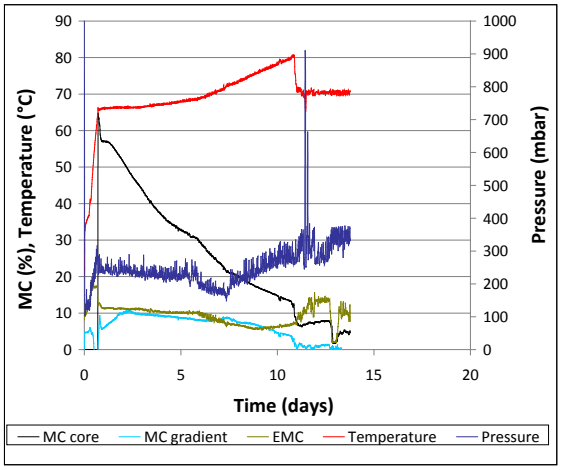

Figure 21. Vacuum drying chart – SPG4 trial

Summary – C. citriodora

A summary of the results for the *C. citriodora* trials is provided in Table 17, where unacceptable results are highlighted.

The total drying time for the **SPG1** vacuum drying trial was 14 days, 66% of the conventional kiln drying time from the green condition (21 days). The average final cross–sectional MC, MC gradient, drying stress, distortion, collapse, surface check, and end split results were all within permissible grade limits for the SPG1 vacuum trial. Similar results for the SPG1 conventional trial were obtained, with the exception of the final cross–sectional MC variation. The unacceptable final cross–sectional MC results for the SPG1 conventional trial were due to under–drying.

Due to a fan failure during the SPG1 vacuum drying trial, we repeated the same vacuum drying schedule for the **SPG2** vacuum drying trial. The total drying time for the SPG2 vacuum drying trial was 17.2 days (82% of the SPG1 conventional drying from green trial) and was longer than the previous trial due to over–drying. The total SPG2 conventional air-drying time was 144 days. Over–drying resulted in both vacuum and conventionally dried SPG2 boards achieving unacceptable final cross-sectional MC limits in accordance with *AS 2796:1999*; however the acceptable grade quality B was achieved for both SPG2 runs in accordance with the more recent *AS/NZS 4787:2001*. This seems to highlight a discrepancy between the standards. All other wood and dried quality properties were within permissible limits for the SPG2 vacuum drying trial, however only 8% of SPG2 conventionally dried boards achieved select grade for surface checking and unacceptable grade quality resulted for drying stress.

Due to favourable dried quality resulting from the first two vacuum trials, we increased the DBT throughout the schedule for the **SPG3** vacuum trial, with the aim of reducing the drying time. Also, the final equalisation EMC was increased to bring the final MC closer to the target (11%) and reduce drying stresses. The total drying time for the SPG3 vacuum trial was 12 days, 57% of the conventional kiln drying time from the green condition. Dried quality results for the SPG3 vacuum trial were all acceptable except for drying stress. However, the end-matched conventionally dried boards also achieved unacceptable drying stress quality results, suggesting this batch of *C. citriodora* was particularly prone to this form of drying defect. Additionally, under-drying resulted in unacceptable final cross-sectional MC grade quality for the conventional SPG3 trial.

For the **SPG4** vacuum trial, we chose the same schedule used for the SPG3 trial except we increased the equalisation time from 48 to 72 hours in an attempt to alleviate unacceptable drying stress recorded in the previous two trials. The total drying time for this trial was 13.6 days, 66% of the conventional drying time. For the vacuum trial all grade quality results were within acceptable limits. For the end-matched conventionally dried boards unacceptable twist and surface checking were recorded.

Overall, the results show vacuum drying *C.citriodora* was significantly faster, producing better dried quality, than for conventional kiln drying. We recommend using the SPG4 vacuum drying schedule for this species based on the dried quality outcomes.

Table 17. *C. citriodora* results summary

Species Trial ID. Drying method	Days drying [% of conventional kiln drying time]	Initial basic density (kg/m3) [stdev.]	Initial MC (%) [stdev.]	Final MC (%) average [stdev.] {grade}*	Final MC % select grade (%)**	MC gradient (%) [stdev.] {grade}*	Drying stress grade quality [stdev.] {grade}*	Distortion % in grade** [major type]	Collapse (% affected)	Surface check % select** [%check free]	Internal check % check free	End split grade*
C. citriodora												
1 (SPG1)												
vacuum	14.0 [66]	887.4 [34.4]	37.9 [3.8]	10.7 [1.4] {B}	90	1.0 [0.6] {A}	0.9 [0.2] {B}	99 [twist]	0	99 [93]	100	A
conventional (kiln)	21			**13.6 [1.0] {C}**	**66**	1.3 [0.5] {A}	0.6 [0.2] {B}	98 [twist]	0	**89 [84]**	100	A
significance (p)				<0.0001		<0.0001	<0.0001			0.56		0.063
5 (SPG2)												
vacuum	17.2 [82]	891.7 [44.3]	34.8 [5.5]	8.8 [0.7] {B}	**36**	0.7 [0.8] {A}	0.7 [0.3] {B}	94 [twist]	0	100 [96]	100	A
conventional (air)	159			9.5 [0.7] {B}	**84**	1.0 [0.5] {A}	**1.4 [0.3] {C}**	93 [twist]	0	**8 [3]**	100	A
significance (p)				<0.0001		<0.0001	<0.0001			<0.0001		<0.0001
9 (SPG3)												
vacuum	12.0 [57]	904.8 [42.2]	32.3 [4.8]	9.5 [0.9] {B}	**70**	1.4 [0.9] {B}	**1.5 [0.4] {C}**	98 [twist]	0	92 [85]	100	A
conventional (kiln)	21			**7.9 [0.7] {C}**	**9**	0.6 [0.7] {A}	**1.6 [0.3] {C}**	**86 [twist]**	0	93 [83]	100}	B
significance (p)				<0.0001		<0.0001	<0.0001			0.571		0.053
13 (SPG4)												
vacuum	13.8 [66]	852.2 [53.3]	37.3 [5.0]	10.2 [0.8] {B}	96	0.7 [0.7] {B}	0.5 [0.4] {B}	96 [twist]	0	93 [86]	100	A
conventional (kiln)	21			10.2 [0.7] {B}	95	-1.5 [0.8] {B}	**1.3 [0.4] {C}**	83 [twist]	0	**87 [72]**	100	B
significance (p)				0.056		<0.0001	<0.0001			0.019		0.014

* AS/NZS 4787:2001 Timber-Assessment of drying quality.

** AS 2796: 1999 Hardwood-Sawn and milled products.

4.1.2 *Eucalyptus marginata* - jarrah

Drying schedules

The vacuum kiln used for the study was supplied with a standard software package that includes a number of pre-set schedules for various species (predominantly American and European species) of varying thickness. Only two pre-set schedules pertaining to native Australian eucalypts exist (*Eucalyptus regnans* and *Eucalyptus globulus)*. The drying properties of these 'ash' type species are very different from those for *E. marginata*. For this reason, we judged existing vacuum drying schedules for Australian species unsuitable.

The schedules used for each trial are shown (Table 18) including for each MC change point, the dry bulb temperature (DBT), wet bulb depression (WBD) and equilibrium moisture content (EMC). The initial schedule chosen for vacuum drying trial JAR1 was the preset schedule provided for *Quercus alba* (white oak) and was chosen on the understanding (supported by Simpson and Verill, 1997) that in general, timbers of similar densities often have similar drying characteristics. The average dried density (12% MC) of mature *Q. alba* is 760 kg/m^3 (Lincoln 1991), which is similar to 820 kg/m^3 reported for mature *E. marginata* (http://www.dpi.qld.gov.au, 2008). Although presented as a conventional stepwise schedule, the dry and wet bulb temperatures were actually ramped between MC change points. A 48 hour equalisation phase was performed at the end of drying at an EMC of 11%. After approximately 11.5 days of drying, the average MC of the test boards had only fallen to 43% and we decided that the drying rate had become too slow. We changed the schedule to the values shown in brackets (Table 18) in association with Brunner-Hildebrand, the kiln manufacturer.

We developed the JAR2 vacuum drying schedule to reduce the unacceptable amount of surface checking resulting from the JAR1 vacuum trial. Changes to the schedule include higher EMCs from green to 50% MC, to slow down drying during the early surface check prone drying stage, and lower dry-bulb temperature thereafter and a higher final equilibrium MC (12% compared with 11%).

Similarly for the JAR3 vacuum trial the EMC was further increased during the early stages of drying up to 40% MC due to undesirable checking results from the JAR2 trial. Lower DBTs during the latter stages of drying and we employed a further increased equalisation EMC (13%) to reduce MC gradients and associated drying stresses after drying.

For the JAR4 vacuum trial we chose the same schedule used for the JAR3 trial except the equalisation time was increased from 48 to 72 hours. We made this change in an attempt to alleviate drying stress, which was not within acceptable limits for the JAR3 vacuum trial.

As is generally the case when drying Australian hardwoods, the material was dried 1-2% below the target average MC and then re-wet during the equalisation phase to reach the target MC to minimise MC gradients and associated residual drying stresses. The fact that re-wetting timber (sorption) leads to lower values of MC at the same EMC than drying timber (desorption) is known as sorption hysteresis (Siau, 1984). For this reason, we increased the equalisation EMC for the JAR2 and JAR3 trials by 1% MC between subsequent trials to bring the final average MC closer to the target 11% and reduce unacceptable stress levels encountered in the first two trials.

Gunns Timber (Manjimup, Western Australia) supplied material for all four trials. Commercial confidentiality prevents us from discussing details of their conventional drying schedules.

Table 18. Vacuum drying schedules - *Eucalyptus marginata*

Trial	JAR1			JAR2			JAR3			JAR4		
MC change points (%)	DBT (°C)	WBD (°C)	EMC (%)	DBT (°C)	WBD (°C)	EMC (%)	DBT (°C)	WBD (°C)	EMC (%)	DBT (°C)	WBD (°C)	EMC (%)
Heat-up	44	2.0	18.0	44	2.1	18.0	44	2.0	18.0	44	2.0	18.0
Green - 70	44	3.0	16.0	44	2.8	16.0	44	3.0	16.0	44	3.0	16.0
70 - 60	44	3.5	15.0	44	2.8	16.0	44	3.0	16.0	44	3.0	16.0
60 - 50	45	4.0	14.0	45	3.6	14.5	45	3.5	14.5	45	3.5	14.5
50 - 40	45 (54)	4.8	13.0	48	4.8	13.0	45	4.2	13.5	45	4.2	13.5
40 - 30	45 (59)	5.4	12.0	53	5.6	12.0	45	5.4	12.0	45	5.4	12.0
30 - 25	48 (64)	7.7 (6.5)	10 (11.0)	58	7.1	10.5	48	7.7	10.0	48	7.7	10.0
25 - 20	53 (69)	9.4 (9.0)	9.0	63	9.3	9.0	53	9.4	9.0	53	9.4	9.0
20 - 15	60 (73)	14 (13.0)	6.7 (7.0)	67	13.0	6.9	60	14.0	6.7	60	14.0	6.7
15 - final	67 (76)	13.8 (14.0)	6.9	70	13.0	6.9	67	13.8	6.9	67	13.8	6.9
Equalise (48 hrs)	70	4.8	11.0	70	4.8	12.0	70	4.0	13.0	70	4.0	13 (72 hrs)

Moisture content

The initial MC results are shown (Table 19). For each trial, initial MC populations were not normally distributed, likely because of high MC outliers (Figure 22). Multiple pairwise comparisons produced no significant differences between sample populations of any trial.

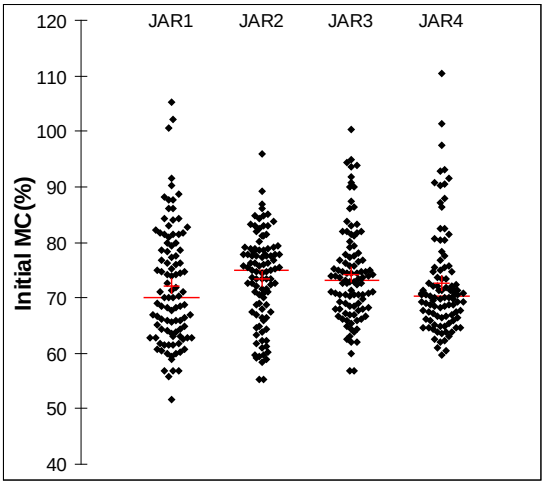

Figure 22. Scattergram of initial MC – *E. marginata*

Table 19. Initial MC results – *E. marginata*

	Initial MC (%)			
Trial	JAR1	JAR2	JAR3	JAR4
Average	72.0	73.5	74.2	72.5
Maximum	105.3	95.9	100.4	110.3
Minimum	51.5	55.4	56.7	59.6
Standard deviation	10.7	8.2	8.7	9.3

For each trial, we recorded significant differences between the final cross-sectional MC population means of end-matched conventional and vacuum trials (Figure 23 and Table 20). In accordance with both *AS/NZS 4787:2001* and *AS 2796:1999* trials JAR1 vacuum, JAR2 conventional and both JAR4 trials did not achieve acceptable grade quality in terms of average final cross-sectional MC. All other trials achieved acceptable grade quality. By observing the scattergrams and output results it can be surmised that the JAR2 conventional trial did not meet acceptable standards for final cross-sectional MC due to under-drying (average 14.4), and the JAR1 vacuum trial did not meet grade due to a large proportion of ‘wet’ boards occurring after drying. The ‘wet boards are evident in Figure 23 as the top thin section of the vacuum scattergram (i.e. boards vastly wetter than the average). The most likely cause of this phenomenon is due to ‘tension set’ caused by too harsh drying during early drying periods. This well known phenomena is commonly known as ‘case hardening’ (McMillen, 1963). It can be observed that by reducing the DBT and increasing the WBD between subsequent trials the number of ‘wet’ boards is reduced (and standard deviation) so that for the JAR3 vacuum trial the final cross-sectional MC spread is more uniformly distributed practically eliminating the under-dried boards.

We used the same vacuum drying schedule for trial JAR4 as for JAR3 except we added 24 hrs to the equalisation phase with the intention of improving drying stress quality (the only unacceptable drying defect for the JAR3 vacuum trial). Unfortunately, a PLC circuit board malfunction cut short the JAR4 trial; consequently, we cannot directly compare the results with the other trials. The result of this is evident by the high final MC for vacuum trial JAR4 (16.2 %) and subsequent failure to meet the standards.

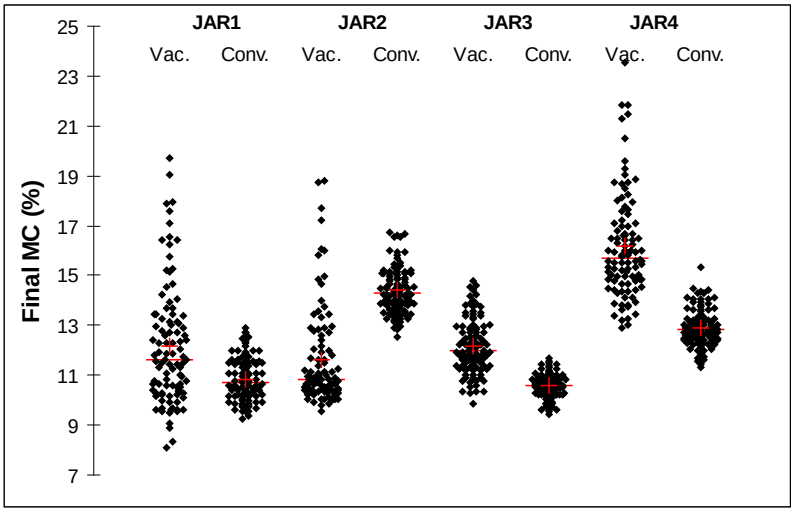

Figure 23. Scattergram of final MC – *E. marginata*

Table 20. Final MC results – *E. marginata*

	Final MC (%)							
	JAR1		JAR2		JAR3		JAR4	
	Vacuum	Conventional	Vacuum	Conventional	Vacuum	Conventional	Vacuum	Conventional
Average	12.2	10.9	11.6	14.4	12.2	10.6	16.2	12.9
Maximum	19.7	12.9	18.8	16.7	14.8	11.7	23.5	15.3
Minimum	8.1	9.3	9.6	12.5	9.9	9.5	12.9	11.3
Standard deviation	2.4	0.9	2.0	0.9	1.1	0.5	2.1	0.7
Significance (p)	< 0.0001		< 0.0001		< 0.0001		< 0.0001	
Grade quality (*AS/NZS 4787*)	D	B	B	D	B	B	Fail	C
% permissible (*AS 2796*)	83	100	91	41	94	100	12	89

Except for trial JAR4, we recorded significant differences between the final MC gradient means of end-matched conventional and vacuum trials (Figure 24 and Table 21). All trials achieved acceptable grade qualities (B or A) for final MC gradient except for vacuum trial JAR4. JAR1, JAR2 and JAR4 vacuum drying trials produced boards with unacceptably high MC gradients as observed in the scattergrams and higher standard deviations. As for the final average cross-sectional MC, we improved the MC gradient from vacuum drying trials JAR1 to JAR3 by progressively reducing the DBT, increasing the WBD, and increasing the final equalisation MC. Unfortunately, a PLC circuit board malfunction cut short the JAR4 trial; consequently, we cannot directly compare the results with the other trials.

The majority of MC gradient results for the JAR1 and JAR3 conventional trial were negative indicating that these boards were dried below the target MC and equalised for a period of time sufficient to rewet the board outer shell above that of the dried core. The conventionally dried equalisation phase could be shortened to target an average MC gradient of 0%, thus reducing the cost of the process.

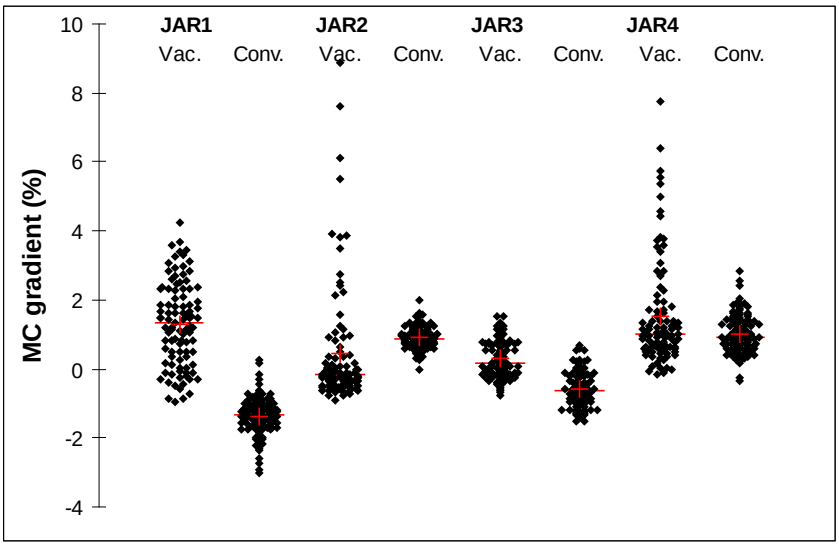

Figure 24. Scattergram of MC gradient – *E. marginata*

Table 21. MC gradient results – *E. marginata*

	Final MC gradient (%)							
	JAR1		JAR2		JAR3		JAR4	
	Vacuum	Conventional	Vacuum	Conventional	Vacuum	Conventional	Vacuum	Conventional
Average	1.3	-1.4	0.4	0.9	0.3	-0.6	1.0	0.9
Maximum	4.3	0.3	8.9	2.0	1.5	0.7	7.7	2.8
Minimum	-1.0	-3.0	-0.9	0.0	-0.8	-1.5	-0.2	-0.4
Standard deviation	1.2	0.6	1.7	0.3	0.5	0.5	1.5	0.6
Significance (p)	< 0.0001		0.0002		< 0.0001		0.106	
Grade quality (*AS/NZS 4787*)	B	A	B	A	A	A	D	A

Basic density

The basic density results are displayed in Figure 25 and Table 22. Multiple pairwise comparisons produced no significant differences between basic density populations of any trial. The average basic density recorded for each trial is similar to the value recorded by the Forest Products Commission Western Australia (http://www.fpc.wa.gov.au, 2009) of 670 kg/m^3 for mature native forest *E. marginata*.

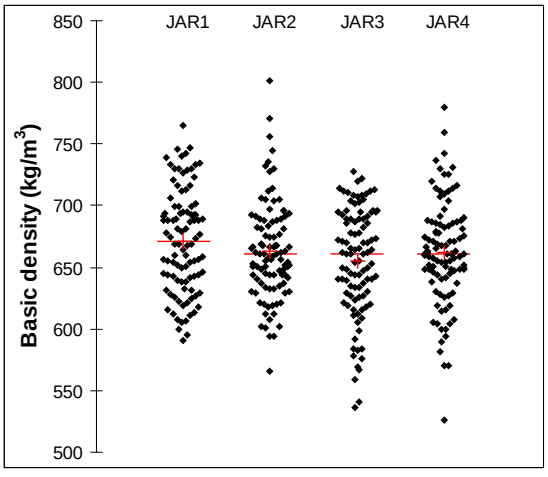

Figure 25. Scattergram of basic density – *E. marginata*

Table 22. Initial basic density results – *E. marginata*

	Basic density (kg/m^3)			
Trial	JAR1	JAR2	JAR3	JAR4
Average	671.5	663.0	654.6	661.8
Maximum	765.0	800.8	728.1	779.9
Minimum	590.2	565.4	536.2	525.8
Standard deviation	41.5	39.5	43.6	42.3

Distortion

We measured distortion on undressed boards before and after drying. For all trials, cupping was not included in the total percentage of boards within acceptable limits as all cupping was removed after dressing. Significant differences do not exist between conventional and vacuum end-matched trials for spring and bow of trial JAR1, cup of trial JAR2, spring, twist and cup of trial JAR3, and bow, twist and cup of trial JAR4. All other comparisons exhibited significant differences. Total distortion results were unacceptable (< 90%) after drying for JAR1 conventional and vacuum trials but was acceptable for all other trials. A significant reduction in distortion to within acceptable limits between vacuum trial JAR1 and subsequent vacuum trials can be attributed to doubling the stack weighting from 500 kg to 1000 kg between trials. For all trials, twist was the predominant type of distortion for boards failing to meet the standard.

Table 23. Distortion results after drying – *E. marginata*

		Distortion - % In grade									
Trial		Vacuum					Conventional				
		Spring	Bow	Twist	Cup	**Total**	Spring	Bow	Twist	Cup	**Total**
JAR1	Before drying	100	100	100	100	**100**	NA	NA	NA	NA	**NA**
	After drying	98	98	61	79	**61**	99	100	79	94	**79**
JAR2	Before drying	100	100	100	100	**100**	NA	NA	NA	NA	**NA**
	After drying	0	0	96	81	**96**	100	100	92	81	**92**
JAR3	Before drying	100	99	96	100	**95**	NA	NA	NA	NA	**NA**
	After drying	100	99	97	82	**96**	100	100	91	78	**91**
JAR4	Before drying	100	100	100	100	**100**	NA	NA	NA	NA	**NA**
	After drying	100	100	94	97	**94**	100	100	94	97	**94**

Table 24. Distortion grade results – *E.marginata*

		Distortion (mm)							
Trial		Vacuum				Conventional			
		Spring	Bow	Twist	Cup	Spring	Bow	Twist	Cup
JAR1	Average	3.7	3.4	6.3	0.6	3.6	2.6	4.0	0.2
	Maximum	15.0	16.0	28.0	5.5	17.0	9.0	22.0	4.0
	Minimum	0.0	0.0	0.0	0.0	0.0	0.0	0.0	0.0
	Standard deviation	2.9	3.2	5.8	1.2	2.6	2.1	4.0	0.7
	Significance (p)	0.826	0.121	0.002	0.0002				
JAR2	Average	3.6	2.9	2.2	0.9	4.8	4.3	3.6	0.7
	Maximum	11.0	8.0	10.0	5.5	15.0	19.0	24.0	3.0
	Minimum	0.0	0.0	0.0	0.0	0.0	0.0	0.0	0.0
	Standard deviation	2.2	1.7	1.9	1.1	2.8	2.7	3.6	0.8
	Significance (p)	0.0004	< 0.0001	< 0.0001	0.325				
JAR3	Average	3.5	2.8	2.4	0.6	4.0	3.9	3.1	0.9
	Maximum	10.0	12.0	28.0	5.0	13.0	14.0	16.0	3.0
	Minimum	0.0	0.0	0.0	0.0	0.0	0.0	0.0	0.0
	Standard deviation	2.2	2.0	3.1	1.0	2.9	3.0	3.1	0.9
	Significance (p)	0.286	0.002	0.074	0.028				
JAR4	Average	1.7	1.5	2.0	0.2	3.0	1.7	2.1	0.2
	Maximum	11.0	9.0	32.0	2.0	11.0	10.0	12.0	5.0
	Minimum	0.0	0.0	0.0	0.0	0.0	0.0	0.0	0.0
	Standard deviation	2.0	1.7	3.6	0.4	2.4	2.1	2.4	0.6
	Significance (p)	< 0.0001	0.688	0.274	0.243				

Surface and internal checking

Significant differences exist between the surface checking population means of all conventional and vacuum end-matched trials (Table 25). Unacceptable surface checking grade qualities resulted for the first two vacuum trials, JAR1 and JAR2 (Table 26). For the JAR3 and JAR4 vacuum trials acceptable surface checking grade quality resulted. We can attribute the improvement of surface check results for these vacuum these trials to reducing the DBT and increasing the WBD during the early stages of drying compared with previous trials.

Unfortunately, a PLC circuit board malfunction cut short the JAR4 trial; consequently, we cannot directly compare the results with the other trials.

All of the boards from each trial were free of internal checking.

Table 25. Surface checking results – *E. marginata*

	Surface checking (mm)							
	JAR1		JAR2		JAR3		JAR4	
	Vacuum	Conventional	Vacuum	Conventional	Vacuum	Conventional	Vacuum	Conventional
Average	43.1	19.4	71.4	21.0	14.6	8.2	44.0	6.1
Maximum	670.0	550.0	1900.0	1920.0	1000.0	573.0	1065.0	279.0
Minimum	0.0	0.0	0.0	0.0	0.0	0.0	0.0	0.0
Standard deviation	89.8	73.4	182.7	149.8	93.2	49.1	138.3	33.1
Significance (p)	< 0.0001		< 0.0001		0.0300		< 0.0001	

Table 26. Surface checking grade results – *E. marginataa*

	JAR1		JAR2		JAR3		JAR4	
Grade	Vacuum	Conventional	Vacuum	Conventional	Vacuum	Conventional	Vacuum	Conventional
Select (%)	89	94	83	97	97	99	93	100
Medium feature (%)	8	2	7	0	0	0	0	0
High feature (%)	3	3	10	3	3	1	7	0
Surface check free boards (%)	69	86	40	91	93	84	57	95
Internal check free boards (%)	100	100	100	100	100	100	100	100

End splits

Significant differences exists between the end split population means of JAR1 and JAR2 conventional and vacuum end-matched trials, but not for the JAR3 and JAR4 trials (Table 27). End splitting was more prevalent in the JAR1 conventionally dried boards (29% of boards affected), which achieved the unacceptable grade quality C. All other trials achieved acceptable grade quality A. Unfortunately, a PLC circuit board malfunction cut short the JAR4 trial; consequently, we cannot directly compare the results with the other trials.

It may be that due to extra internal overpressure caused by the vacuum itself, more end drying is present during vacuum drying compared to conventional methods. This theory is reinforced by the test board thermocouple results presented in section *4.3.4 Board temperature* of this report. The thermocouple results show noticeably lower temperatures at the board ends than the centres indicating a higher degree of free water at the ends of the boards. This would certainly reduce the level of shrinkage variation at the board ends and hence reduce the incidence and severity of end-splitting.

Table 27. End split results – *E. marginata*

	End splits (mm)							
	JAR1		JAR2		JAR3		JAR4	
	Vacuum	Conventional	Vacuum	Conventional	Vacuum	Conventional	Vacuum	Conventional
Average	3.9	9.4	0.0	3.0	1.9	1.7	1.0	1.2
Maximum	140.0	205.0	0.0	175.0	122.0	153.0	71.0	242.0
Minimum	0.0	0.0	0.0	0.0	0.0	0.0	0.0	0.0
Standard deviation	18.7	38.6	0.0	18.2	12.3	13.0	7.9	17.1
Significance (p)	0.003		0.008		0.774		0.955	
Grade quality (*AS/NZS 4787*)	A	C	A	A	A	A	A	A

Drying stress

Significant differences exist between the drying stress population means of JAR2 and JAR3 but not for the other conventional and vacuum end-matched trials (Table 28). Only the JAR3 conventional trial achieved an acceptable grade quality for drying stress. These results suggest improvements to the vacuum drying schedule, particularly the equalisation phase, are still required to reduce drying stress to within acceptable limits for this species. Unfortunately, a PLC circuit board malfunction cut short the JAR4 trial; consequently, we cannot directly compare the results with the other trials.

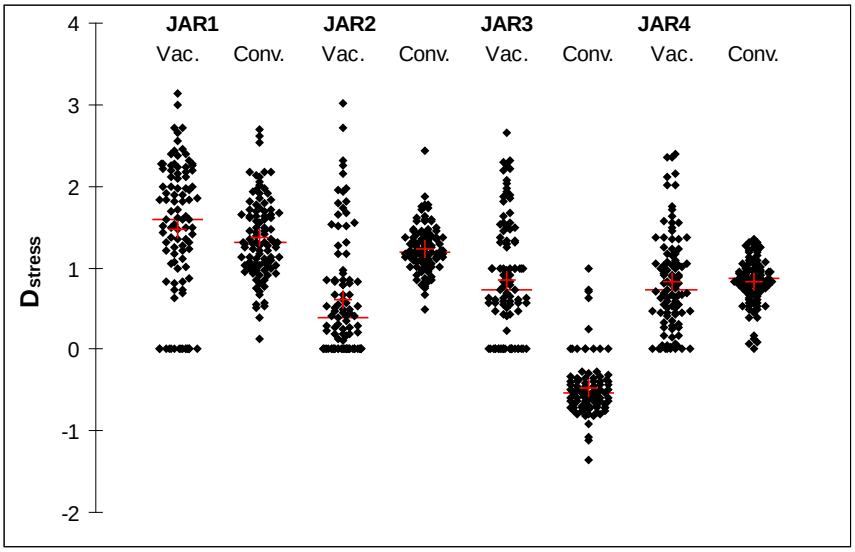

Figure 26. Scattergram of drying stress – *E. marginata*

Table 28. Drying stress results – *E. marginata*

	Drying stress (D_{stress})							
	JAR1		JAR2		JAR3		JAR4	
	Vacuum	Conventional	Vacuum	Conventional	Vacuum	Conventional	Vacuum	Conventional
Average	1.5	1.4	0.6	1.2	0.8	-0.5	0.8	0.8
Maximum	3.1	2.7	3.0	2.4	2.6	1.0	2.4	1.3
Minimum	0.0	0.1	0.0	0.5	0.0	-1.4	0.0	0.0
Standard deviation	0.8	0.5	0.7	0.3	0.7	0.4	0.6	0.3
Significance (p)	0.13		< 0.0001		< 0.0001		0.606	
Grade quality (*AS/NZS 4787*)	D	C	C	C	C	A	C	C

Collapse

No signs of collapse were present for any boards from any trial.

Sawn orientation

The majority of boards were a combination of back sawn and transitionally sawn (Table 29). Backsawing is the desired cutting pattern for this species as it usually provides a higher green off-saw (GOS) recovery than quartersawing, and better aesthetics because of growth ring orientation.

Table 29. Sawn orientation results – *E. marginata*

	Sawn orientation (%)			
	SPG1	SPG2	SPG3	SPG4
Quartersawn	9	2	3	2
Backsawn	41	71	73	78
Transitional	50	27	24	20

Gross shrinkage

Significant differences exist between the width and thickness gross shrinkage means for all trials suggesting that, in terms of shrinkage in the radial and tangential directions, *E. marginata* is not isotropic. The results are considerably higher than published tangential (7.4%) and radial (4.9%) shrinkages (http://www.dpi.qld.gov.au, 2008). The results may be somewhat skewed however, as the outlying high shrinkage samples correspond to those boards that were cupped. Unfortunately, a PLC circuit board malfunction cut short the JAR4 trial; consequently, we cannot directly compare the results with the other trials.

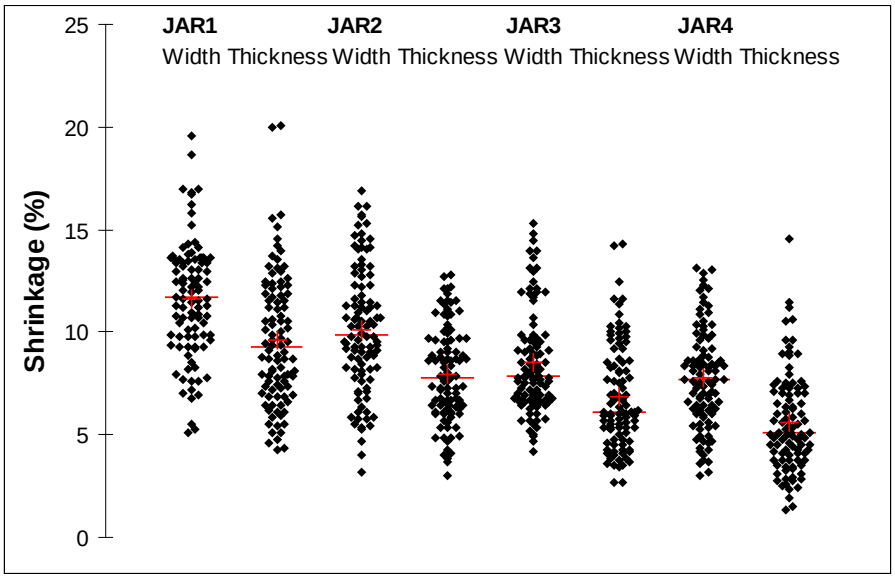

Figure 27. Scattergram of gross shrinkage – *E. marginata*

Table 30. Gross shrinkage results – *E. marginata*

	Gross shrinkage (mm)							
	JAR1		JAR2		JAR3		JAR4	
	Width	Thickness	Width	Thickness	Width	Thickness	Width	Thickness
Average	11.6	9.6	10.2	8.0	8.5	6.8	7.8	5.6
Maximum	19.6	20.1	16.9	12.8	15.3	14.3	13.1	14.5
Minimum	5.1	4.2	3.2	3.0	4.2	2.7	3.0	1.3
Standard deviation	2.8	3.2	3.1	2.3	2.5	2.5	2.4	2.4
Significance (p)	< 0.0001		< 0.0001		< 0.0001		< 0.0001	

Drying times and vacuum kiln output

For each conventional trial the total kiln drying time was 61 days. The total drying times, including equalisation for the vacuum trials JAR1, JAR2 ,JAR3 and JAR4 were 25.6, 19.5, 24.9 and 25.4 days, respectively (Figure 28 to Figure 31). Unfortunately, a PLC circuit board malfunction cut short the JAR4 trial; consequently, we cannot directly compare the results with the other trials.

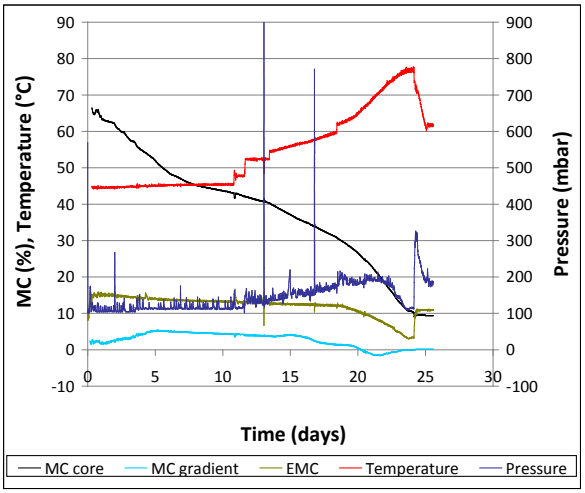

Figure 28. Vacuum drying chart – JAR1 trial

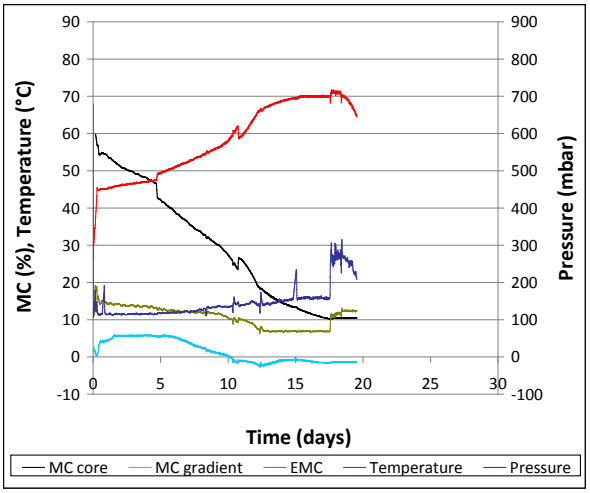

Figure 29. Vacuum drying chart – JAR2 trial

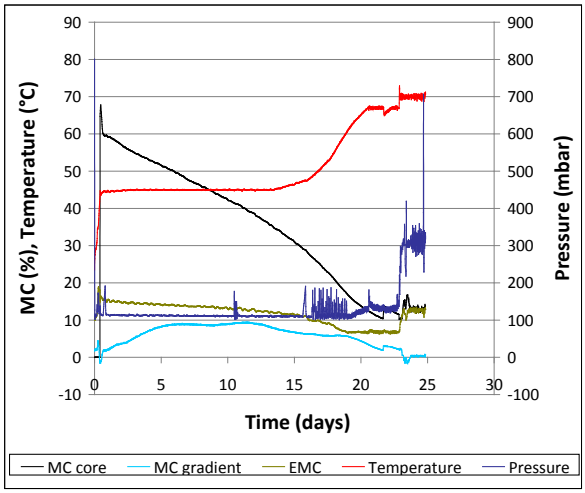

Figure 30. Vacuum drying chart – JAR3 trial

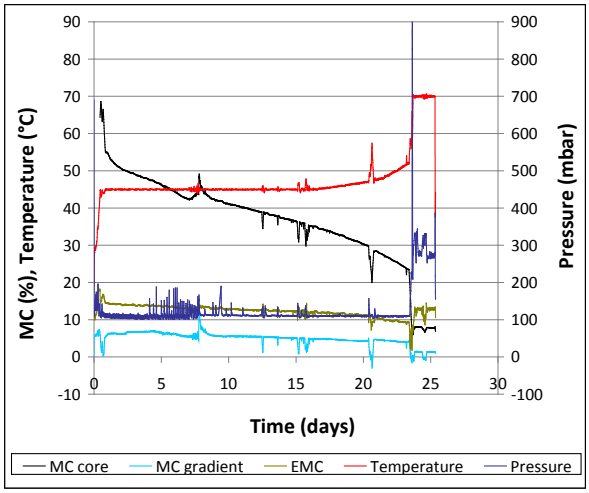

Figure 31. Vacuum drying chart – JAR4 trial

Summary – E. marginata

A summary of the results for the *E. marginata* trials is provided in Table 31where unacceptable results are highlighted.

The total drying time for the **JAR1** vacuum drying trial was 25.6 days, 42% of the conventional drying time from the green condition. For both vacuum and conventional JAR1 trials, we recorded unacceptable levels of twist distortion and drying stress. For both JAR1 trials, collapse internal checking and final MC gradient were within permissible limits. The final cross–sectional MC variation for the JAR1 vacuum trial was outside the permissible limits due to five under–dried 'wet' outlying boards, possibly caused by case-hardening. Unacceptable surface checking results were recorded for the JAR1 vacuum drying trial. Unacceptable end–splitting resulted from the JAR1 conventional trial.

Due to results from the first trial, we implemented a milder schedule for the **JAR2** vacuum drying trial. The total drying time for the JAR2 vacuum drying trial 19.5 days 32% of the conventional kiln drying time from the green condition. Schedule refinements resulted in acceptable final cross–sectional MC variation. Due to under-drying, the final cross-sectional MC results for the JAR2 conventional trial were unacceptable. Residual drying stress was improved between vacuum drying trials; but although still unacceptable, it was comparable to the conventional trial. We greatly reduced twist distortion to within acceptable limits for the JAR2 vacuum drying trial by doubling the concrete stack weighting between trials. For the JAR2 vacuum drying trial, surface checking results were still unacceptable but were acceptable for the JAR2 conventional trial.

Similar to the previous trial, the **JAR3** vacuum schedule was adjusted to give milder conditions. The total drying time for the JAR3 vacuum drying trial was 27.9 days, 41% of the conventional kiln drying time from the green condition. Apart from unacceptable drying stress (a problematic form of degrade even when conventionally dried) all other dried quality results were acceptable for the JAR3 vacuum trial. All dried quality results were acceptable for the JAR3 conventional trial.

For the **JAR4** vacuum trial we chose the same schedule used for the JAR3 trial except the equalisation time was increased from 48 to 72 hours in an attempt to alleviate drying stress. Unfortunately, a PLC circuit board malfunction cut short the JAR4 trial; consequently, we cannot directly compare the results with the other trials. Thus, the results of this trial are highlighted grey in Table 31.

Overall, the results show vacuum drying *E. marginata* was significantly faster producing the same dried quality as for conventional kiln drying. We recommend using the JAR4 vacuum drying schedule for this species based on the dried quality outcomes of trial JAR3 that used the same schedule but with a shorter equalisation period. We believe an extended equalisation period for this species should improve drying stress grade quality results. Results show that drying stress seems to be an endemic form of degrade for this species independent of drying method.

Table 31. *E. marginata* results summary

Species **Trial ID**. Drying method	Days drying [% of conventional kiln drying time]	Initial basic density (kg/m3) [stdev.]	Initial MC (%) [stdev.]	Final MC (%) average [stdev.] {grade}*	Final MC % select grade (%)**	MC gradient (%) [stdev.] {grade}*	Drying stress grade quality [stdev.] {grade}*	Distortion % in grade** [major type]	Collapse (% affected)	Surface check % select** [%check free]	Internal check % check free	End split grade*
E. marginata												
2 (JAR1)												
vacuum	25.6 [42]	667.8 [48.5]	72.0 [10.7]	**12.2 [2.4] {D}**	**83**	1.3 [1.2] {B}	**1.5 [0.8] {D}**	**61 [twist]**	0	**89 [69]**	100	A
conventional (kiln)	61			10.9 [0.9] {B}	100	-1.4 [0.6] {A}	**1.4 [0.5] {C}**	**79 [twist]**	0	94 [86]	100	**C**
significance (p)				<0.0001		<0.0001	0.13			<0.0001		0.0002
6 (JAR2)												
vacuum	19.5 [32]	663.0 [39.5]	73.5 [8.2]	11.6 [2.0] {B}	91	0.4 [1.7] {B}	**0.6 [0.7] {C}**	96 [twist]	0	**83 [40]**	100	A
conventional (kiln)	61			**14.4 [0.9] {D}**	**41**	0.9 [0.3] {A}	**1.2 [0.3] {C}**	92 [twist]	0	97 [91]	100	A
significance (p)				<0.0001		<0.0001	<0.0001			<0.0001		0.0008
10 (JAR3)												
vacuum	24.9 [41]	654.6 [43.6]	74.2 [8.7]	12.2 [1.1] {B}	94	0.3 [1.5] {A}	**0.8 [0.7] {C}**	96 [twist]	0	97 [93]	100	A
conventional (kiln)	61			10.6 [0.5] {B}	100	-0.6 [0.5] {A}	-0.5 [0.4] {A}	91 [twist]	0	99 [84]	100	A
significance (p)				<0.0001		<0.0001	<0.0001			0.03		0.05
14 (JAR4)												
vacuum	25.4 [42]	661.8 [42.3]	72.5 [9.3]	16.2 [2.1] {F}	12	1.0 [1.5] {D}	0.8 [0.6] {C}	94 [twist]	0	93 [57]	100	A
conventional (kiln)	61			**12.9 [0.7] {C}**	**89**	0.9 [0.6] {A}	**0.8 [0.3] {C}**	94 [twist]	0	100 [95]	100	A
significance (p)				<0.0001		0.106	0.606			<0.0001		0.955

* AS/NZS 4787:2001 Timber-Assessment of drying quality.

** AS 2796: 1999 Hardwood-Sawn and milled products.

4.1.3 *Eucalyptus pilularis* – blackbutt

Drying schedules

The vacuum kiln used for the study was supplied with a standard software package that includes a number of pre-set schedules for various species (predominantly American and European species) of varying thickness. Only two pre-set schedules pertaining to native Australian eucalypts exist (*Eucalyptus regnans* and *Eucalyptus globulus)*. The drying properties of these 'ash' type species are very different from those for *E. pilularis*. For this reason, we judged existing vacuum drying schedules for Australian species unsuitable.

The schedules used for each trial are shown (Table 32) including for each MC change point, the dry bulb temperature (DBT), wet bulb depression (WBD) and equilibrium moisture content (EMC). The initial schedule chosen for vacuum drying trial BBT1 was the preset schedule provided for *Quercus rubra* (red oak) and was chosen on the understanding (supported by Simpson and Verill, 1997) that in general, timbers of similar densities often have similar drying characteristics. The average dried density (12% MC) of mature *Q. rubra* is 890 kg/m^3 (Lincoln 1991), which is similar to 930 kg/m^3 reported for mature *E. pilularis* (http://www.fpc.wa.gov.au, 2009). Also, *Q. rubra* and *E. pilularis* are similarly constrained by surface checking as the primary drying defect. Although presented as a conventional stepwise schedule, the dry and wet bulb temperatures were actually ramped between MC change points. We performed a 48 hour equalisation phase at the end of drying at an 11% EMC.

We developed the BBT2 vacuum drying schedule to reduce the unacceptable amount of surface checking resulting from the BBT1 vacuum trial. Changes to the schedule include higher EMCs from green to 50% MC, to slow down drying during the early surface check prone drying stage. Additionally, we used a higher final equilibrium MC (12% compared with 11%) to improve residual drying stress resulting from the first vacuum trial.

Similarly, for the BBT3 and BBT4 vacuum trials, we increased the EMC further during the early stages of drying up to 30% MC due to undesirable checking resulting from the respective BBT2 and BBT3 vacuum trials.

Hurford Hardwood sawmill (Casino, New South Wales) supplied material for conventional trial BBT1 and Boral Timber (Murwillumbah) for conventional trials BBT2 and BBT3. **Due to time constraints, conventional trial BBT4 did not occur**. The conventionally dried end–matched boards of trial BBT1 were air dried from green to approximately 15% MC before final kiln drying. Conventional trials BBT2 and BBT3 were kiln dried from the green condition. Commercial confidentiality prevents details of the conventional drying schedule used by Hurford Hardwood and Boral Timber from being discussed.

Table 32. Vacuum drying schedules - *Eucalyptus pilularis*

Trial	BBT1			BBT2			BBT3			BBT4		
MC change points (%)	DBT (°C)	WBD (°C)	EMC (%)	DBT (°C)	WBD (°C)	EMC (%)	DBT (°C)	WBD (°C)	EMC (%)	DBT (°C)	WBD (°C)	EMC (%)
Heat-up	44	2.1	18.0	44	2.1	18.0	44	2.1	18.0	44	2.1	18.0
Green - 70	44	3.0	15.0	44	2.6	16.0	44	2.8	16.0	44	2.4	17.0
70 - 60	44	3.4	14.0	44	3.2	15.0	44	2.8	16.0	44	2.4	17.0
60 - 50	45	4.0	13.0	45	3.8	14.0	45	2.8	16.0	45	2.4	17.0
50 - 40	45	4.4	13.0	45	4.4	13.0	45	3.4	15.0	45	3.2	15.5
40 - 30	45	5.2	12.0	45	5.2	12.0	45	4.6	13.0	45	4.4	13.5
30 - 25	48	6.7	10.0	48	7.7	10.0	48	7.7	10.0	48	7.7	10.0
25 - 20	53	9.5	9.0	53	9.5	9.0	53	9.5	9.0	53	9.5	9.0
20 - 15	60	14.0	6.7	60	14.0	6.7	60	14.0	6.7	60	14.0	6.7
15 - final	67	13.0	6.9	67	13.0	6.9	67	13.0	6.9	67	13.0	6.9
Equalise (48 hrs)	70	6.5	11.0	67	5.4	12.0	67	5.4	12.0	67	5.4	12.0

Moisture content

The initial MC results are shown (Table 33). For each trial, initial MC populations were not normally distributed, likely because of high MC outliers (Figure 32). Multiple pairwise comparisons produced no significant differences between sample population trials BBT1 and BBT2, and BBT1 and BBT3. All other pairwise comparisons produced significant differences.

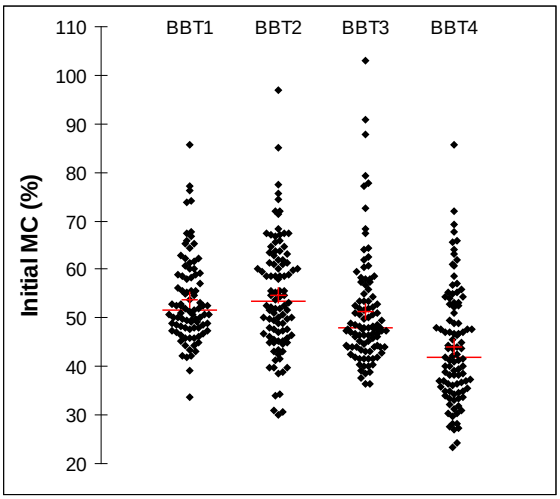

Figure 32. Scattergram of initial MC – *E. pilularis*

Table 33. Initial MC results – *E. pilularis*

	Initial MC (%)			
Trial	BBT1	BBT2	BBT3	BBT4
Average	53.8	54.6	51.3	44.2
Maximum	85.6	96.9	103.0	85.8
Minimum	33.8	30.1	36.3	23.4
Standard deviation	9.0	11.7	11.6	11.8

For trials BBT2 and BBT3, we recorded significant differences between the final cross-sectional MC population means of end-matched conventional and vacuum trials (Figure 23 and Table 20). No significant difference was recorded for the BBT1 trials. In accordance with both *AS/NZS 4787:2001* and *AS 2796:1999* BBT2 and BBT3 conventional trials did not achieve acceptable grade quality in terms of average final cross-sectional MC because of over-drying. All other trials achieved acceptable grade quality. It can be observed that by increasing the equalisation EMC from 11% to 12% between the first BBT1 vacuum trial and subsequent vacuum trials, the spread (standard deviation) of final cross-sectional MC was reduced. Personal communications with Hurford Hardwood management (Engwirda, 2009), reveal tougher limitations are imposed on final cross-sectional MC variation for *E. pilularis* than those specified by *AS 2796:1999* (Standards Australia 1999) and *AS/NZS 4787:2001* (Standards Australia 1999). This is particularly true for strip flooring where a final cross–sectional variation of ± 1% is imposed for a target final MC of 10.5%. With respect to these specifications, the variation of final cross–sectional MC for all trials except for the BBT1 conventional trial is unacceptable.

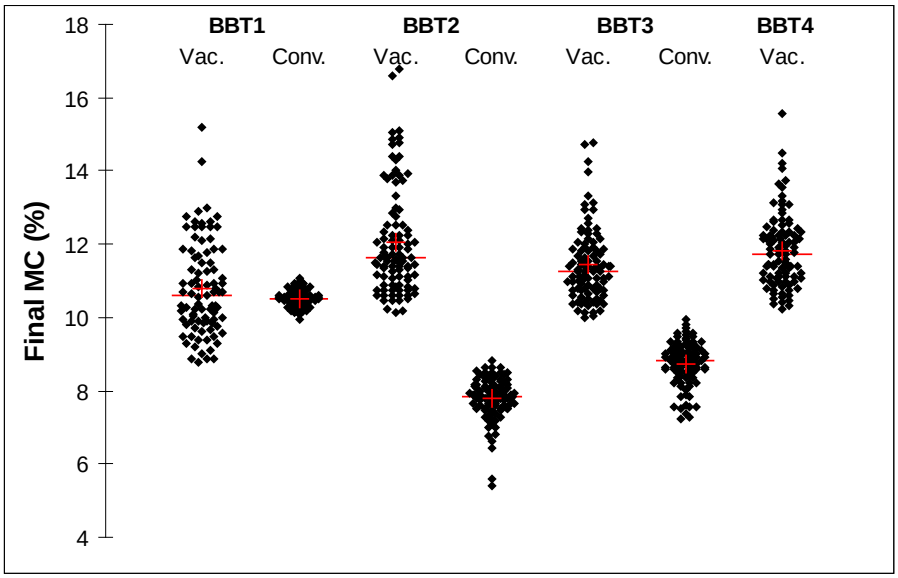

Figure 33. Scattergram of final MC – *E. pilularis*

Table 34. Final MC results – *E. pilularis*

	Final MC (%)						
	BBT1		BBT2		BBT3		BBT4
	Vacuum	Conventional	Vacuum	Conventional	Vacuum	Conventional	Vacuum
Average	10.8	10.5	12.0	7.8	11.4	8.7	11.8
Maximum	15.2	11.1	16.8	8.8	14.8	9.9	15.5
Minimum	8.8	10.0	10.2	5.4	10.0	7.2	10.2
Standard deviation	1.3	0.2	1.4	0.6	1.0	0.6	1.0
Significance (p)	0.1620		< 0.0001		< 0.0001		NA
Grade quality (*AS/NZS 4787*)	B	A	B	D	A	D	A
% permissible (*AS 2796*)	94	100	93	0	97	38	96

For each trial, we recorded significant differences between the final MC gradient means of end-matched conventional and vacuum trials (Figure 34 and Table 35). All trials achieved acceptable grade qualities (B or A) for final MC gradient. However, vacuum trials BBT1, BBT2 and BBT3 produced boards with high outlying MC gradients as observed via the scattergrams.

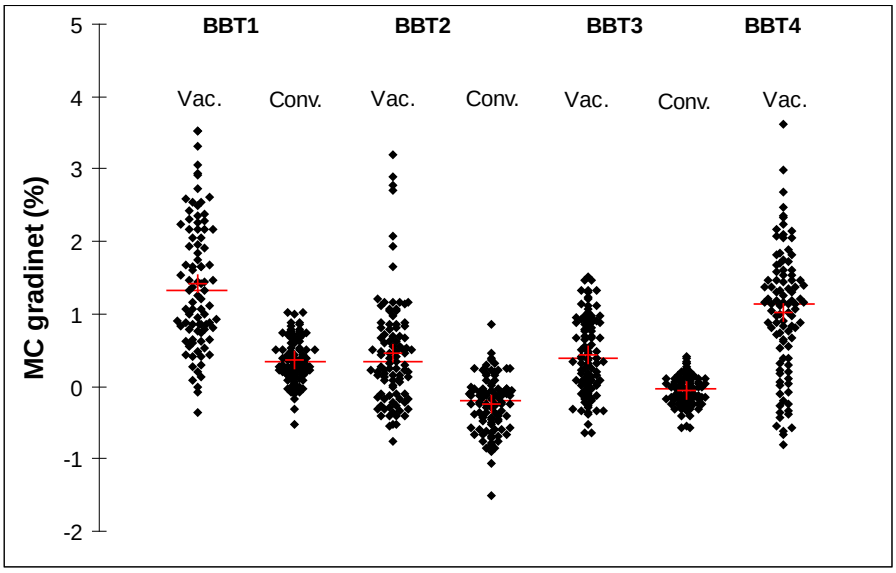

Figure 34. Scattergram of MC gradient – *E. pilularis*

Table 35. MC gradient results – *E.pilularis*

	Final MC gradient (%)						
	BBT1		BBT2		BBT3		BBT4
	Vacuum	Conventional	Vacuum	Conventional	Vacuum	Conventional	Vacuum
Average	1.4	0.4	0.5	-0.2	0.4	-0.1	1.0
Maximum	3.5	1.0	3.2	0.8	1.5	0.4	3.6
Minimum	-0.4	-0.5	-0.8	-1.5	-0.6	-0.6	-0.8
Standard deviation	0.9	0.3	0.7	0.4	0.5	0.2	0.9
Significance (p)	< 0.0001		< 0.0001		< 0.0001		NA
Grade quality (*AS/NZS 4787*)	B	A	A	A	A	A	A

Basic density

The basic density results are displayed in Figure 35 and Table 36. Multiple pairwise comparisons produced significant differences between basic density populations of trials BBT1 and BBT2 but not between any other trial. The average basic density recorded each trial is similar to the value recorded by (Bootle, 2004) of 710 kg/m^3 for mature native forest *E. pilularis*.

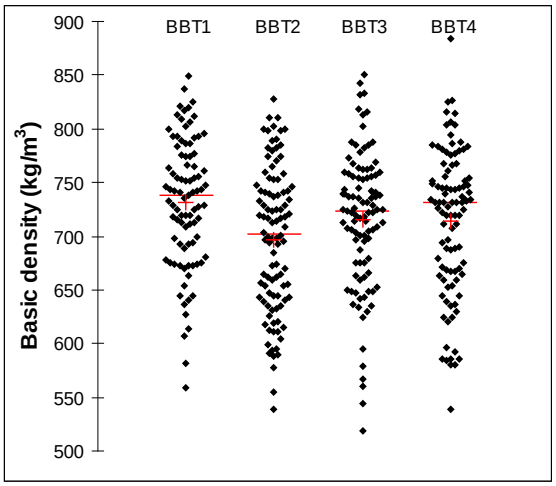

Figure 35. Scattergram of basic density – *E. pilularis*

Table 36. Initial basic density results – *E. pilularis*

	Basic density (kg/m^3)			
Trial	BBT1	BBT2	BBT3	BBT4
Average	731.2	696.6	715.5	713.6
Maximum	849.8	827.8	850.9	883.6
Minimum	558.2	538.6	518.5	539.2
Standard deviation	60.2	67.2	64.4	67.2

Distortion

We measured distortion on undressed boards before and after drying. For all trials, cupping was not included in the total percentage of boards within acceptable limits as all cupping was removed after dressing. Significant differences do not exist between conventional and vacuum end-matched trials for cup of trial BBT2 and spring and bow of trial BBT3. All other comparisons exhibited significant differences. All other comparisons exhibited significant differences. Total distortion results were unacceptable (< 90%) after drying for BBT1 vacuum trial but was acceptable for all other trials. A significant reduction in distortion to within acceptable limits between vacuum trial BBT1 and subsequent vacuum trials can be attributed to doubling the stack weighting from 500 kg to 1000 kg between trials. For all trials, twist was the predominant type of distortion for boards failing to meet the standard.

Table 37. Distortion results after drying – *E. pilularis*

		Distortion - % In grade									
Trial		Vacuum					Conventional				
		Spring	Bow	Twist	Cup	**Total**	Spring	Bow	Twist	Cup	**Total**
BBT1	Before drying	100	100	100	100	**100**	NA	NA	NA	NA	**NA**
	After drying	100	98	78	90	**78**	100	100	96	92	**96**
BBT2	Before drying	100	98	100	100	**98**	NA	NA	NA	NA	**NA**
	After drying	100	100	93	80	**93**	100	100	93	99	**93**
BBT3	Before drying	100	85	98	100	**83**	NA	NA	NA	NA	**NA**
	After drying	100	99	93	77	**92**	100	100	91	90	**91**
BBT4	Before drying	100	100	99	100	**99**					
	After drying	100	100	96	77	**96**					

Table 38. Distortion grade results – *E.pilularis*

		Distortion (mm)							
Trial		Vacuum				Conventional			
		Spring	Bow	Twist	Cup	Spring	Bow	Twist	Cup
BBT1	Average	2.7	1.9	3.5	0.3	3.5	2.8	2.1	0.4
	Maximum	10.0	15.0	15.0	4.0	11.0	9.0	17.0	4.0
	Minimum	0.0	0.0	0.0	0.0	0.0	0.0	0.0	0.0
	Standard deviation	2.1	2.9	3.8	0.8	2.4	2.2	2.6	0.8
	Significance (p)	0.011	0.001	0.004	0.011	NA	NA	NA	NA
BBT2	Average	2.4	3.3	2.3	0.6	3.7	4.2	3.6	0.3
	Maximum	12.0	9.0	12.0	5.0	11.0	15.0	25.0	4.0
	Minimum	0.0	0.0	0.0	0.0	0.0	1.0	0.0	0.0
	Standard deviation	2.2	2.1	2.4	1.2	2.6	2.7	3.7	0.6
	Significance (p)	0.0001	0.008	0.004	0.130	NA	NA	NA	NA
BBT3	Average	2.5	2.2	1.9	0.8	2.7	2.2	2.9	0.5
	Maximum	9.0	17.0	9.0	5.0	10.0	8.0	23.0	4.0
	Minimum	0.0	0.0	0.0	0.0	0.0	0.0	0.0	0.0
	Standard deviation	2.1	2.2	2.1	1.1	2.3	2.0	3.4	0.8
	Significance (p)	0.529	0.925	0.003	0.029	NA	NA	NA	NA
BBT4	Average	2.3	2.0	1.7	1.1				
	Maximum	11.0	11.0	10.0	9.0				
	Minimum	0.0	0.0	0.0	0.0				
	Standard deviation	2.3	1.9	2.0	1.6				
	Significance (p)	NA	NA	NA	NA				

Surface and internal checking

Significant differences exist between the surface checking population means of the BBT1 and BBT3conventional and vacuum end-matched trials (Table 39). This was not the case for the BBT2 trial indicating comparable results. Unacceptable surface checking grade quality resulted for all trials. The BBT3 vacuum trial produced the best grade quality results (82% select, 70% check free) compared with all other trials. This can be attributed to schedule

manipulation between vacuum drying trials, where the WBD was increased during the early stages of drying, thus creating a milder schedule. Except for the BBT2 trial, vacuum drying trials produced a higher percentage of select boards than conventional trials for surface checking.

Surface checking generally occurs during the early stages of drying when MC gradients and surface tension are at their highest (McMillen, 1963). For future vacuum drying *E. pilularis* trials, we need to reconsider early vacuum drying schedule conditions to reduce the severity of surface checking within acceptable grade quality.

Internal checking was present in boards for all vacuum and conventional trials. Unacceptable internal check grade quality resulted for the BBT1 vacuum, BBT2 vacuum and conventional and the BBT3 conventional trials. Again, we can attribute the improvement of internal checking to within acceptable limits for the BBT3 and BBT4 vacuum trials to using a milder schedule.

Table 39. Surface checking results – *E. pilularis*

	Surface checking (mm)						
	BBT1		BBT2		BBT3		BBT4
	Vacuum	Conventional	Vacuum	Conventional	Vacuum	Conventional	Vacuum
Average	119	627	119	627	148	1181	85
Maximum	1260	1900	1260	1900	1370	1900	1061
Minimum	0	0	0	0	0	0	0
Standard deviation	224	662	224	662	320	770	204
Significance (p)	< 0.0001		0.250		< 0.0001		NA

Table 40. Surface checking grade results – *E. pilularis*

	BBT1		BBT2		BBT3		BBT4
Grade	Vacuum	Conventional	Vacuum	Conventional	Vacuum	Conventional	Vacuum
Select (%)	79	33	54	62	82	35	78
Medium feature (%)	2	0	0	0	0	0	0
High feature (%)	19	67	46	38	18	65	22
Surface check free boards (%)	51	17	39	51	70	17	65
Internal check free boards (%)	87	93	84	79	93	88	98

End splits

Significant differences exist between the end split population means of all conventional and vacuum end-matched trials (Table 41). End splitting was more prevalent in the conventionally dried boards, which achieved the unacceptable grade quality D. All vacuum trials achieved acceptable grade quality A.

It may be that due to extra internal overpressure caused by the vacuum itself, more end drying is present during vacuum drying compared to conventional methods. This theory is reinforced by the test board thermocouple results presented in section *4.3.4 Board temperature* of this report. The thermocouple results show noticeably lower temperatures at the board ends than the centres indicating a higher degree of free water at the ends of the boards. This would certainly reduce the level of shrinkage variation at the board ends and hence reduce the incidence and severity of end-splitting.

Table 41. End split results – *E. pilularis*

	End splits (mm)						
	BBT1		BBT2		BBT3		BBT4
	Vacuum	Conventional	Vacuum	Conventional	Vacuum	Conventional	Vacuum
Average	2.1	28.5	10.1	49.8	1.3	34.3	2.4
Maximum	125.0	600.0	1070.0	615.0	110.0	270.0	480.0
Minimum	0.0	0.0	0.0	0.0	0.0	0.0	0.0
Standard deviation	13.3	84.8	83.6	67.7	9.5	50.6	34.1
Significance (p)	< 0.0001		< 0.0001		< 0.0001		NA
Grade quality (*AS/NZS 4787*)	A	D	A	D	A	D	A

Drying stress

Significant differences exist between the drying stress population means of all trials (Table 42). Both vacuum BBT1 and vacuum BBT2 drying trials achieved unacceptable grade quality results for drying stress (quality C). All other trials achieved acceptable grade quality B or better. Using a milder schedule (higher early WBD) and a higher final equalisation EMC, the BBT3 and BBT4 vacuum trials achieved the acceptable grade quality for drying stress, comparable to the conventional drying trials.

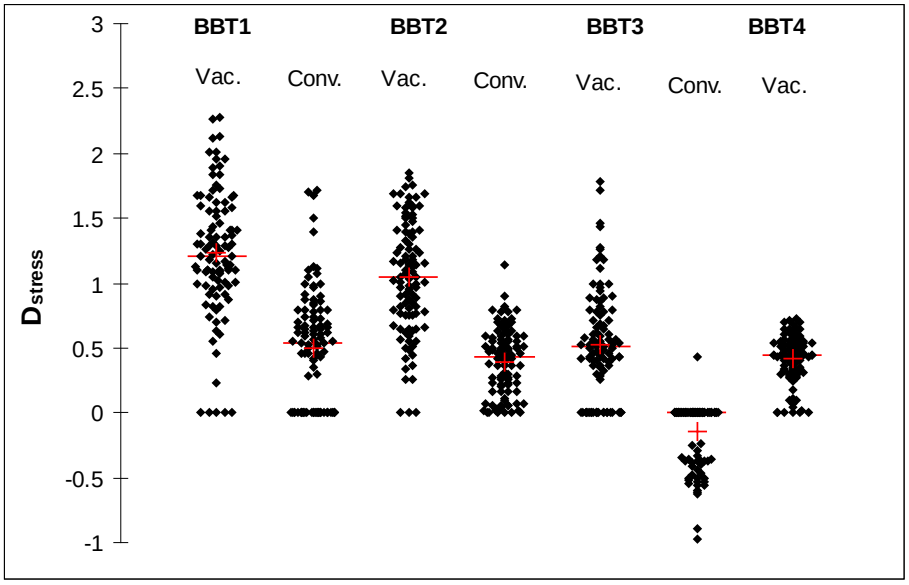

Figure 36. Scattergram of drying stress – *E. pilularis*

Table 42. Drying stress results – *E. pilularis*

	Drying stress (D_{stress})						
	BBT1		BBT2		BBT3		BBT4
	Vacuum	Conventional	Vacuum	Conventional	Vacuum	Conventional	Vacuum
Average	1.2	0.4	1.0	0.4	0.5	-0.1	0.4
Maximum	2.1	1.1	1.8	1.1	1.8	0.4	0.7
Minimum	0.0	0.0	0.0	0.0	0.0	-1.0	0.0
Standard deviation	0.4	0.4	0.4	0.3	0.4	0.2	0.2
Significance (p)	< 0.0001		< 0.0001		< 0.0001		NA
Grade quality (*AS/NZS 4787*)	C	B	C	B	B	A	B

Collapse

No signs of collapse were present for any boards from any trial.

Sawn orientation

The majority of boards were a combination of back sawn and transitionally sawn (Table 43). Backsawing is the desired cutting pattern for this species as it usually provides a higher green off-saw (GOS) recovery than quartersawing, and better aesthetics because of growth ring orientation.

Table 43. Sawn orientation results – *E. pilularis*

	Sawn orientation (%)			
	BBT1	BBT2	BBT3	BBT4
Quartersawn	12	7	1	24
Backsawn	58	67	46	40
Transitional	30	26	53	36

Gross shrinkage

Significant differences exist between the width and thickness gross shrinkage means for all trials suggesting that, in terms of shrinkage in the tangential and radial directions, *E. pilularis* is not isotropic. The results are higher than published tangential (7.3%) and radial (4.3%) shrinkages (http://www.dpi.qld.gov.au, 2008). The results may be somewhat skewed however, as the outlying high shrinkage samples correspond to those boards that were cupped.

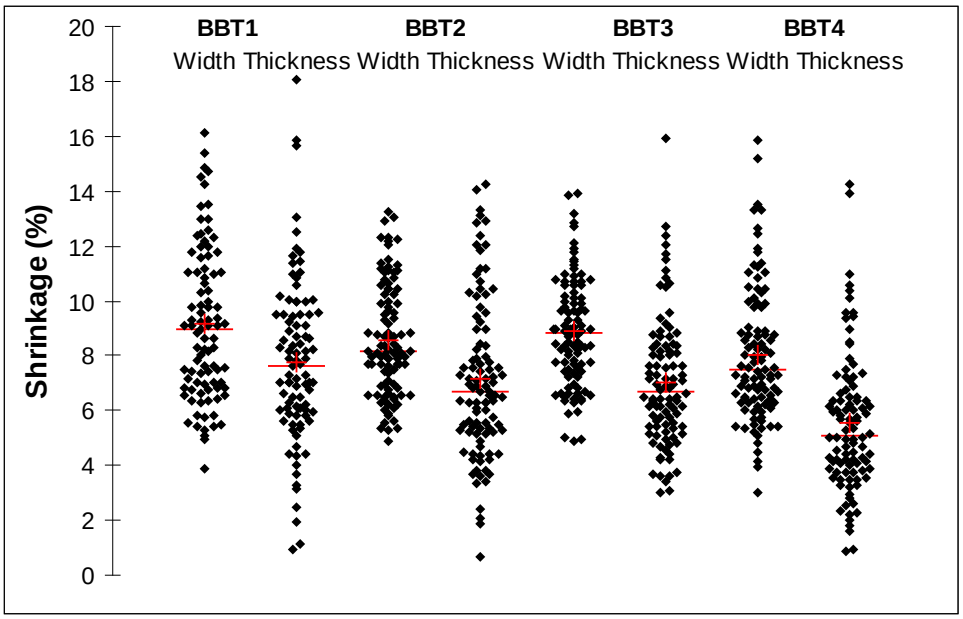

Figure 37. Scattergram of gross shrinkage – *E. pilularis*

Table 44. Gross shrinkage results – *E. pilularis*

	Gross shrinkage (mm)							
	BBT1		BBT2		BBT3		BBT4	
	Width	Thickness	Width	Thickness	Width	Thickness	Width	Thickness
Average	9.1	7.8	8.6	7.1	8.9	7.1	8.0	5.5
Maximum	16.2	18.0	13.3	14.3	13.9	15.9	15.9	14.3
Minimum	3.9	1.0	4.9	0.7	4.9	3.0	3.0	0.9
Standard deviation	2.8	3.0	2.0	2.9	2.0	2.4	2.5	2.5
Significance (p)	< 0.0001		0.0370		< 0.0001		< 0.0001	

Drying times and vacuum kiln output

For conventional trial BBT1, the total kiln drying time was 144 days as it was pre-air dried before final kiln drying. The remaining conventional trials were kiln dried from green, whereby the total drying time was 58 days.

As evident from the Figure 38 MC core curve, the drying rate after the fifth day of the vacuum drying trial BBT1 was compromised due to a kiln fan/variable speed drive (VSD) failure, whereby practically no drying occurred until approximately day 20 when the VSD was repaired. Through observation of the slope of the MC core curve, we estimate that the drying time should have been in the order of 25 days. The indicative conventional drying time from the green condition is 58 days for this species (Pearn, 2007). The total drying times, including equalisation for the vacuum trials BBT1to BBT4 were 25.0, 21.6, 27.9 and 24.8 days, respectively.

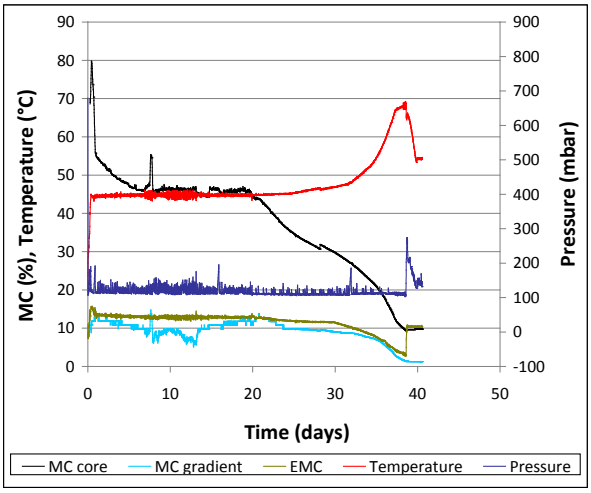

Figure 38. Vacuum drying chart – BBT1 trial

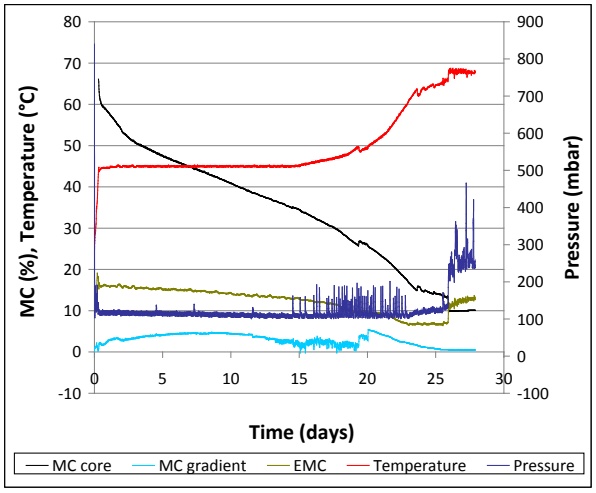

Figure 40. Vacuum drying chart – BBT3 trial

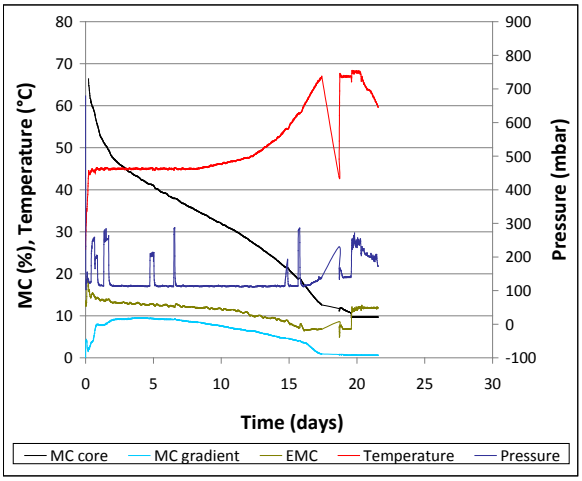

Figure 39. Vacuum drying chart – BBT2 trial

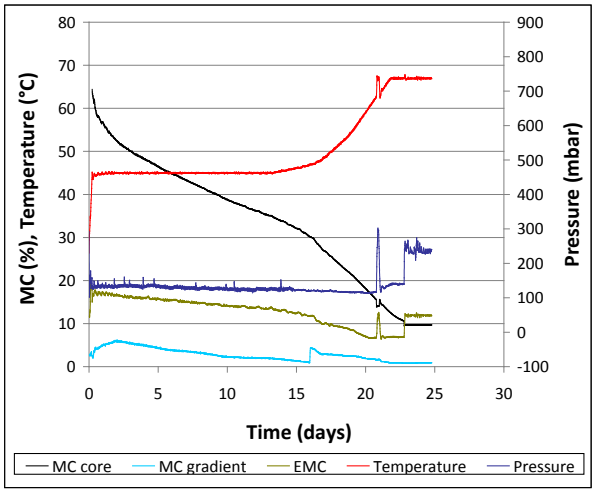

Figure 41. Vacuum drying chart – BBT4 trial

Summary – E. pilularis

A summary of the results for the *E. pilularis* trials are provided in Table 45 where unacceptable results are highlighted.

The total drying time for the **BBT1** vacuum drying was 25 days, 43% of reported (Pearn, 2007) conventional drying time from the green condition. The combined air/kiln drying time for the conventional trial was 144 days. Final cross–sectional MC, MC gradient, and collapse were within acceptable limits, according to the appropriate standards, for both the BBT1 vacuum and conventional drying trials. However, personal communications with Hurford Hardwood management (Engwirda, 2009), reveal tougher limitations are imposed on final cross-sectional MC variation for *E. pilularis* than those specified by *AS 2796:1999* (Standards Australia 1999) and *AS/NZS 4787:2001* (Standards Australia 1999). This is particularly true for strip flooring where a final cross–sectional variation of ± 1% is imposed for a target final MC of 10.5%. Therefore, the variation of final cross–sectional MC for the BBT1 vacuum trial is considered unacceptable by Hurford Hardwood. Using the same limitations, the BBT1 conventional trial final MC variation was acceptable. Drying stress results for the BBT1 vacuum trial were outside the acceptable limitations Surface checking results were not within acceptable limits for either the vacuum or conventional drying trials. Only 33% of the conventionally dried boards made select grade for surface checking compared with 78% for the vacuum drying trial. Internal checking was not within permissible limits for the BBT1 vacuum drying .Unacceptable end–splitting resulted from the BBT1 conventional trial Unacceptable twist distortion was recorded for the BBT1 vacuum drying trial. Unacceptable end splitting resulted from the BBT1 conventional trial.

For the second **BBT2** vacuum drying trial the drying schedule was adjusted to provide milder humidity conditions The total drying time for the BBT2 vacuum drying trial was 21.5 days, 37% of the conventional drying time (58 days) from the green condition. Final cross–sectional MC, MC gradient, collapse, and internal checking were within acceptable limits, according to the appropriate standards, for the BBT2 vacuum drying trial. Drying stress results for the BBT2 vacuum trial were still outside the acceptable limitations indicating again, surface checking results were not within acceptable limits for the vacuum trial Surface checking was also outside acceptable limits for the conventional BBT2 trial, so the results are comparable. Comparable results were also obtained for internal checking where unacceptable results were obtained for both trials. Twist distortion was greatly reduced to within acceptable limits for the BBT2 vacuum drying trial by doubling the concrete stack weighting between trials.

An even milder schedule was used for the **BBT3** vacuum where the total drying time for the BBT3 vacuum drying trial was 27.9 days, 48% of the conventional drying time (58 days) from the green condition. At the stage of writing this report the BBT3 conventional trial was still drying. Drying stress and internal check dried quality were improved to within acceptable limits for the BBT3 vacuum trial compared to previous trials due to careful schedule manipulation. All other BBT3 vacuum trial dried quality parameters were within acceptable limits except surface checking where 82% of boards made select grade. However, this is higher than any previous BBT vacuum or conventional drying trial to date.

For the **BBT4** vacuum trial we increased the EMC further during the early stages of drying up to 30% MC due to undesirable checking resulting from the BBT3 vacuum trial. **Due to time constraints, conventional trial BBT4 did not occur**. The total drying time for the BBT4 vacuum drying trial was 24.8 days, 43% of the previous conventional drying time (58 days) from the green

condition. Apart from unacceptable surface checking (a problematic form of degrade even when conventionally dried) all other dried quality results were acceptable for the BBT4 vacuum trial.

Overall, the results show vacuum drying *E.pilularis* was significantly faster producing the same dried quality as for conventional kiln drying. We recommend using the BBT4 vacuum drying schedule for this species based on the dried quality outcomes of this trial We believe a milder initial vacuum drying schedule for this species should improve surface checking grade quality results. Results show that drying surface checking seems to be an endemic form of degrade for this species independent of drying method.

Table 45. *E. pilularis* results summary

Species Trial ID. Drying method	Days drying [% of conventional kiln drying time]	Initial basic density (kg/m3) [stdev.]	Initial MC (%) [stdev.]	Final MC (%) average [stdev.] {grade}*	Final MC % select grade (%)**	MC gradient (%) [stdev.] {grade}*	Drying stress grade quality [stdev.] {grade}*	Distortion % in grade** [major type]	Collapse (% affected)	Surface check % select** [%check free]	Internal check % check free	End split grade*
E. pilularis												
3 (BBT1)												
vacuum	25 [43]†	731.2 [60.2]	53.8 [9.0]	10.8 [1.3] {B}	94	1.4 [0.9] {B}	**1.2 [0.4] {C}**	**78 [twist]**	0	**79 [51]**	**87**	A
conventional (air)	144			10.5 [0.2] {A}	100	0.4 [0.3] {A}	0.4 [0.4] {B}	96 [twist]	0	**33 [17]**	93	**D**
significance (p)				<0.0001		<0.0001				<0.0001		<0.0001
7 (BBT2)												
vacuum	21.5 [37]†	696.6 [67.2]	54.6 [11.7]	12.0 [1.4] {B}	93	0.5 [0.7] {A}	**1.0 [0.4] {C}**	93 [twist]	0	**54 [39]**	**84**	A
conventional (kiln)	58			**7.8 [0.6] {D}**	**0**	-0.2 [0.4] {A}	0.4 [0.3] {B}	93 [twist]		**62 [51]**	**79**	**D**
significance (p)				<0.0001		<0.0001	<0.0001			0.25		<0.0001
11 (BBT3)												
vacuum	27.9 [48]†	715.5 [64.4]	51.3 [11.6]	11.4 [1.0] {A}	97	0.4 [0.5] {A}	0.5 [0.4] {B}	92 [twist]	0	**82 [70]**	92	A
conventional (kiln)	58			**8.7 [0.6] {D}**	**38**	-0.1 [0.2] {A}	-0.1 [0.2] {A}	91 [twist]		**35 [17]**	**88**	**D**
significance (p)				<0.0001		<0.0001	<0.0001			<0.0001		<0.0001
15 (BBT4)												
vacuum	24.8 [43]†	713.6 [11.8]	44.2 [11.8]	11.8 [1] {A}	96	1.0 [0.9] {A}	0.4 [0.2] {A}	96 [twist]	0	**78 [65]**	98	A
conventional (kiln)	Incomplete											

* AS/NZS 4787:2001 Timber-Assessment of drying quality.

** AS 2796: 1999 Hardwood-Sawn and milled products.

† Based on indicative conventional drying time of 58 days from green (Pearn 2007).

4.1.4 *Eucalyptus obliqua* - messmate

Drying schedules

The vacuum kiln used for the study was supplied with a standard software package that includes a number of pre-set schedules for various species (predominantly American and European species) of varying thickness. Only two pre-set schedules pertaining to native Australian eucalypts exist (*Eucalyptus regnans* and *Eucalyptus globulus).*

The schedules used for each trial are shown (Table 46) including for each MC change point, the dry bulb temperature (DBT), wet bulb depression (WBD) and equilibrium moisture content (EMC). The initial schedule chosen for vacuum drying trial MES1 was the preset schedule provided for *E. globulus* and was chosen because *E. globulus* and *E. obliqua* share the same recommended quartersawn conventional drying schedule (Rozsa and Mills, 1997). They also have similar drying defect limitations, particularly surface and internal checking, and collapse. Although presented as a conventional stepwise schedule, the dry and wet bulb temperatures were actually ramped between MC change points. A 48-hour equalisation phase was performed at the end of drying at a 12% EMC.

We developed the MES2 vacuum drying schedule to reduce the unacceptable amount of internal checking resulting from the MES1 vacuum trial. Changes to the schedule include higher initial relative humidities down to 30% MC.

Due to favourable dried quality resulting from the MES2 vacuum trial, we increased the DBT during the latter stages of the MES3 schedule, from 30% MC to final dry, to increase the drying rate and improve overall drying time.

Unfortunately, although instructed to completely wrap these boards block packed with impermeable plastic after sawing, the MES3 pack was presented unwrapped and exposed to the weather before tagging. The pack had been exposed for approximately 3-4 weeks during December/January; Tasmanian summer. As these boards were partially dried before testing, the results of this trial have been compromised and do not represent a complete drying trial and thus cannot directly be compared with other trials. For this reason, we repeated the MES3 vacuum drying schedule for the MES4 vacuum trial.

Integrated Tree Cropping (ITC) Timber (Huonville, Tasmania) (now Gunns Timber) supplied material for conventional trials MES1 and MES2, and Gunns Timber (Launceston, Tasmania – sourced from Huonville) for conventional trial MES3. The conventionally dried end–matched boards of trial MES1 were air dried from green to approximately 15% MC before final kiln drying. Material for the conventional MES2 and MES3 were kiln dried from the green condition. Commercial confidentiality prevents us discussing the details of the conventional drying schedules used by these mills.

Table 46. Vacuum drying schedules – *E. obliqua*

Trial	MES1			MES2			MES3 and MES4		
MC change points (%)	DBT (°C)	WBD (°C)	EMC (%)	DBT (°C)	WBD (°C)	EMC (%)	DBT (°C)	WBD (°C)	EMC (%)
Heat-up	44	2.4	18.0	44	2.4	18.0	44	2.4	18.0
Green - 70	44	2.6	16.0	44	2.8	16.0	44	2.8	16.0
70 - 60	44	3.2	15.0	44	2.8	16.0	44	2.8	16.0
60 - 50	45	3.8	14.0	45	3.4	15.0	45	3.4	15.0
50 - 40	45	4.4	13.0	45	4.8	13.5	45	4.8	13.5
40 - 30	45	5.2	12.0	45	5.0	12.5	45	5.0	12.5
30 - 25	48	6.7	10.0	48	7.1	10.0	58	7.5	10.0
25 - 20	53	9.5	9.0	53	9.5	9.0	64	10.0	8.4
20 - 15	60	14.0	6.7	60	14.0	6.7	72	16.0	6.1
15 - final	67	13.0	6.9	67	13.0	6.9	80	13.0	6.9
Equalise (48 hrs)	67	5.4	12.0	67	5.4	12.0	72	5.5	12.5

Moisture content

The initial MC results are shown (Table 47). Multiple pairwise comparisons produced significant differences between sample populations of all trials indicating a high variability in initial MC for this species. The average MC for trial MES3 is almost half of the other two trials (Table 47). As the MES3 vacuum boards were partially dried before testing the results cannot be directly compared with other trials.

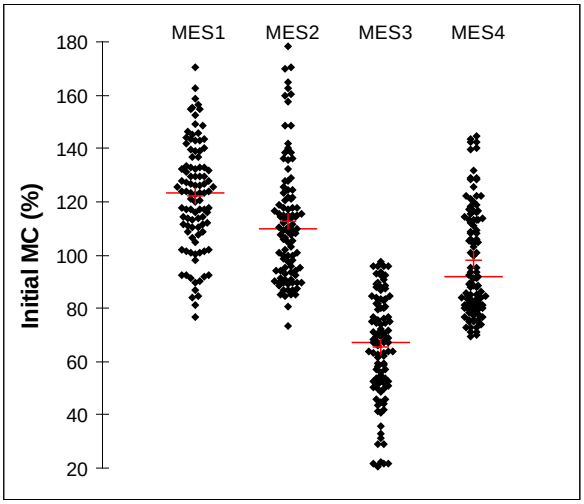

Figure 42. Scattergram of initial MC – *E. obliqua*

Table 47. Initial MC results – *E. obliqua*

	Initial MC (%)			
Trial	MES1	MES2	MES3	MES4
Average	122.0	112.5	65.3	98.0
Maximum	170.7	178.3	97.7	144.4
Minimum	76.5	73.2	20.5	69.2
Standard deviation	20.0	22.7	19.8	20.5

Except for trial MES2, we recorded significant differences between the final cross-sectional MC population means of end-matched conventional and vacuum trials (Figure 43 and Table 48). In accordance with both *AS/NZS 4787:2001* and *AS 2796:1999* all trial achieved acceptable grade quality in terms of average final cross-sectional MC. Vacuum trial MES2 and conventional trial MES 4 resulted in some outlying boards with higher than normal final cross-sectional MC. As the MES3 vacuum boards were partially dried before testing the results cannot be directly compared with other trials.

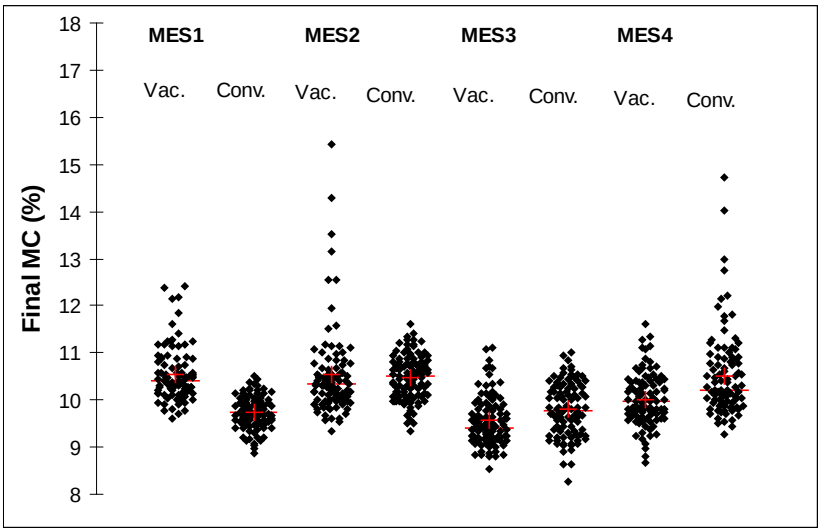

Figure 43. Scattergram of final MC – *E. obliqua*

Table 48. Final MC results – *E. obliqua*

	Final MC (%)							
	MES1		MES2		MES3		MES4	
	Vacuum	Conventional	Vacuum	Conventional	Vacuum	Conventional	Vacuum	Conventional
Average	10.5	9.7	10.5	10.5	9.6	9.8	10.0	10.5
Maximum	12.4	10.5	15.4	11.6	11.1	11.0	11.6	14.7
Minimum	9.6	8.9	9.3	9.4	8.5	8.3	8.7	9.3
Standard deviation	0.6	0.3	0.9	0.5	0.5	0.6	0.6	0.9
Significance (p)	< 0.0001		0.725		0.0040		< 0.0001	
Grade quality (*AS/NZS 4787*)	A	A	B	B	B	B	B	B
% permissible (*AS 2796*)	100	98	98	100	91	96	98	99

For each trial, we recorded significant differences between the final MC gradient means of end-matched conventional and vacuum trials (Figure 44 and Table 49). All trials achieved acceptable grade qualities (A) for final MC gradient. As the MES3 vacuum boards were partially dried before testing the results cannot be directly compared with other trials.

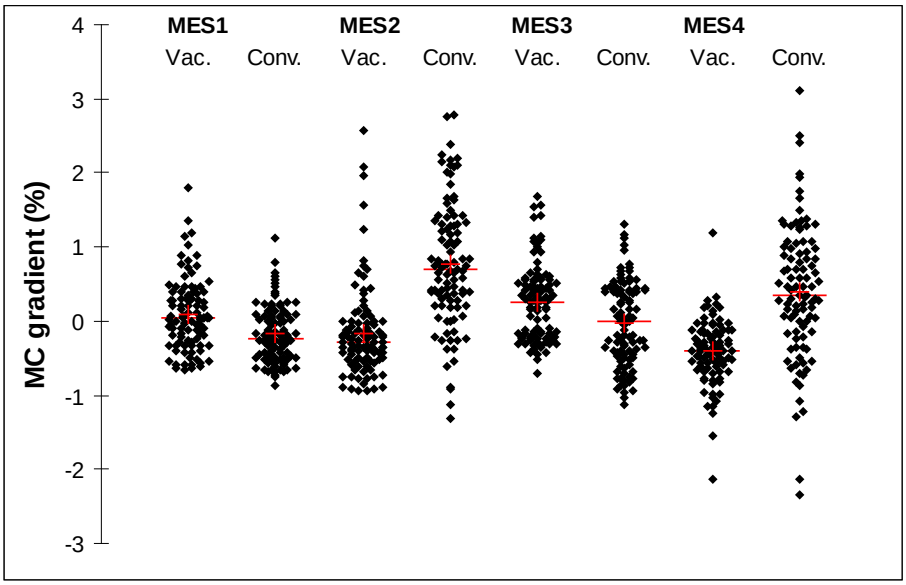

Figure 44. Scattergram of MC gradient – *E. obliqua*

Table 49. MC gradient results – *E.obliqua*

	Final MC gradient (%)							
	MES1		MES2		MES3		MES4	
	Vacuum	Conventional	Vacuum	Conventional	Vacuum	Conventional	Vacuum	Conventional
Average	0.1	-0.2	-0.2	0.8	0.3	0.0	-0.4	0.4
Maximum	1.8	1.1	2.6	2.8	1.7	1.3	1.2	3.1
Minimum	-0.7	-0.9	-0.9	-1.3	-0.7	-1.1	-2.1	-2.3
Standard deviation	0.5	0.4	0.6	0.8	0.5	0.6	0.4	0.9
Significance (p)	< 0.0001		< 0.0001		0.0002		< 0.0001	
Grade quality (*AS/NZS 4787*)	A	A	A	A	A	A	A	A

Basic density

The basic density results are displayed in Figure 45 and Table 50. Multiple pairwise comparisons produced no significant differences between basic density populations of trials MES1 and MES2, and MES3 and MES4. The average basic density recorded for each trial is considerably lower than the value reported by (Bootle, 2004) of 630 kg/m^3 for mature native forest *E. obliqua*. As the MES3 vacuum boards were partially dried before testing the basic density results for this trial may be erroneous as some of the sections tested were not fully saturated and cannot be directly compared with other trials.

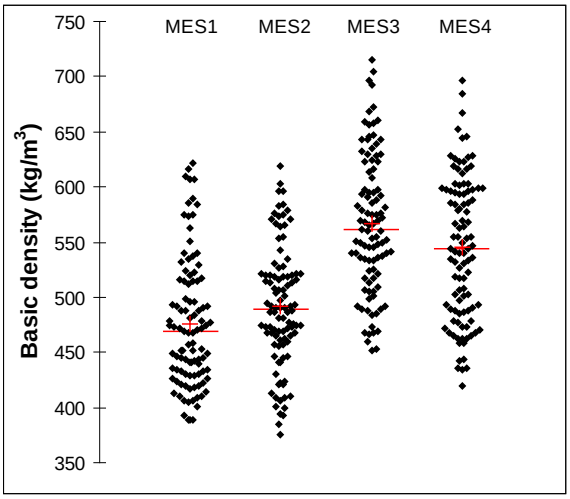

Figure 45. Scattergram of basic density – *E. obliqua*

Table 50. Initial basic density results – *E. obliqua*

	Basic density (kg/m^3)			
Trial	MES1	MES2	MES3	MES4
Average	476.1	491.2	569.5	544.7
Maximum	621.1	618.5	829.9	696.2
Minimum	388.2	375.5	451.3	419.2
Standard deviation	58.7	54.6	67.7	64.1

Distortion

We measured distortion on undressed boards before and after drying. For all trials, cupping was not included in the total percentage of boards within acceptable limits as all cupping was removed after dressing. Significant differences do not exist between conventional and vacuum end-matched trials for spring and bow of trials MES2 andMES3, and spring and twist for trial MES4. All other comparisons exhibited significant differences. Total distortion results were acceptable after drying for all trials. As the MES3 vacuum boards were partially dried before testing the results cannot be directly compared with other trials.

Table 51. Distortion results after drying – *E. obliqua*

		Distortion - % In grade									
Trial		Vacuum					Conventional				
		Spring	Bow	Twist	Cup	**Total**	Spring	Bow	Twist	Cup	**Total**
MES1	Before drying	100	100	100	100	**100**	NA	NA	NA	NA	**NA**
	After drying	99	100	97	100	**96**	100	100	100	100	**96**
MES2	Before drying	100	100	100	100	**100**	NA	NA	NA	NA	**NA**
	After drying	98	100	99	100	**97**	98	99	100	98	**97**
MES3	Before drying	100	100	100	100	**100**	NA	NA	NA	NA	**NA**
	After drying	100	100	99	100	**99**	99	100	97	100	**96**
MES4	Before drying	100	100	100	100	**100**	NA	NA	NA	NA	**NA**
	After drying	99	100	95	100	**95**	100	100	97	98	**97**

Table 52. Distortion grade results – *E.obliqua*

		Distortion (mm)							
Trial		Vacuum				Conventional			
		Spring	Bow	Twist	Cup	Spring	Bow	Twist	Cup
MES1	Average	2.3	2.0	1.7	0.2	3.9	2.9	2.3	0.3
	Maximum	14.0	7.0	6.0	1.0	21.0	15.0	8.0	2.0
	Minimum	0.0	0.0	0.0	0.0	0.0	0.0	0.0	0.0
	Standard deviation	2.2	1.7	1.7	0.4	3.4	2.6	1.8	0.6
	Significance (p)	< 0.0001	0.009	0.014	NA	NA	NA	NA	NA
MES2	Average	3.8	2.5	1.6	0.3	4.2	2.3	1.1	0.1
	Maximum	21.0	9.0	6.0	1.2	24.0	30.0	5.0	2.0
	Minimum	0.0	0.0	0.0	0.0	0.0	0.0	0.0	0.0
	Standard deviation	3.2	1.6	1.6	0.4	3.6	3.2	1.3	0.4
	Significance (p)	0.327	0.021	0.033	NA	NA	NA	NA	NA
MES3	Average	2.4	2.5	1.6	0.4	3.2	2.3	1.2	0.1
	Maximum	9.0	7.0	10.0	1.3	14.0	11.0	12.0	2.0
	Minimum	0.0	0.0	0.0	0.0	0.0	0.0	0.0	0.0
	Standard deviation	2.4	1.5	1.5	0.5	2.9	2.5	1.9	0.3
	Significance (p)	0.105	0.157	0.003	NA	NA	NA	NA	NA
MES4	Average	3.7	3.6	2.0	1.0	3.6	2.1	1.7	0.2
	Maximum	25.0	10.0	10.0	4.0	11.0	7.0	7.0	2.0
	Minimum	0.0	0.0	0.0	0.0	0.0	0.0	0.0	0.0
	Standard deviation	3.6	2.4	2.1	0.9	2.6	1.4	1.7	0.4
	Significance (p)	0.632	< 0.0001	0.537	NA	NA	NA	NA	NA

Surface and internal checking

Significant differences exist between the surface checking population means of MES2 and MES3 conventional and vacuum end-matched trials (Table 53). Unacceptable surface checking grade qualities resulted for conventional trial MES2 and both MES3 trials (Table 54). As the MES3 vacuum boards were partially dried before testing the results cannot be directly compared with other trials. The remaining vacuum trials all achieved acceptable surface checking results.

Internal checking was present in boards for all vacuum and conventional trials. Unacceptable internal check grade quality resulted for both MES1 trials and MES2 vacuum trial. The milder

schedule used for vacuum trial MES2 compared with vacuum trial MES1, greatly improved the number of boards free of internal checks (89% cf. 78%) to a level comparable with the conventionally dried boards of the MES1 trial (88%). Further schedule manipulations reduced the incidence of surface checking to within acceptable limits for the final MES4 vacuum trial.

Table 53. Surface checking results – *E. obliqua*

	Surface checking (mm)							
	MES1		MES2		MES3		MES4	
	Vacuum	Conventional	Vacuum	Conventional	Vacuum	Conventional	Vacuum	Conventional
Average	14.4	33.7	26.2	84.2	41.2	148.9	7.0	5.9
Maximum	1070.0	2719.0	1400.0	1900.0	810.0	1900.0	600.0	452.0
Minimum	0.0	0.0	0.0	0.0	0.0	0.0	0.0	0.0
Standard deviation	104.7	247.4	157.6	292.8	138.9	438.3	56.8	45.8
Significance (p)	0.075		0.009		0.031		0.859	

Table 54. Surface checking grade results – *E.obliqua*

	MES1		MES2		MES3		MES4	
Grade	Vacuum	Conventional	Vacuum	Conventional	Vacuum	Conventional	Vacuum	Conventional
Select (%)	97	95	96	84	91	78	98	98
Medium feature (%)	0	0	0	0	1	0	0	0
High feature (%)	3	5	4	16	8	21	2	2
Surface check free boards (%)	96	94	94	71	80	72	98	94
Internal check free boards (%)	78	88	89	96	95	85	96	97

End splits

Significant differences exist between the end split population means of all conventional and vacuum end-matched trials, except the MES4 trials (Table 55). End splitting was more prevalent in the MES1-3 conventionally dried boards, failing to meet even the lowest grade quality E. As the MES3 vacuum boards were partially dried before testing the results cannot be directly compared with other trials. It may be that due to extra internal overpressure caused by the vacuum itself, more end drying is present during vacuum drying compared to conventional methods. This theory is reinforced by the test board thermocouple results presented in section section*4.3.4 Board temperature* of this report. The thermocouple results show noticeably lower temperatures at the board ends than the centres indicating a higher degree of free water at the ends of the boards. This would certainly reduce the level of shrinkage at the board ends and hence reduce the incidence and severity of end-splitting.

Table 55. End split results – *E.obliqua*

	End splits (mm)							
	MES1		MES2		MES3		MES4	
	Vacuum	Conventional	Vacuum	Conventional	Vacuum	Conventional	Vacuum	Conventional
	6.6	53.7	20.5	77.9	0.0	61.9	6.4	0.3
Maximum	300.0	980.0	1082.0	989.0	0.0	947.0	390.0	50.0
Minimum	0.0	0.0	0.0	0.0	0.0	0.0	0.0	0.0
Standard deviation	39.2	147.7	107.4	151.5	0.0	136.8	40.0	3.6
Significance (p)	< 0.0001		< 0.0001		< 0.0001		0..932	
Grade quality (*AS/NZS 4787*)	A	Fail	A	Fail	A	Fail	A	A

Drying stress

Significant differences exist between the drying stress population means of MES1 and MES4 but not for the other conventional and vacuum end-matched trials (Table 56). All trials achieved acceptable grade quality B results for drying stress, except for conventional trial MES4. As the MES3 vacuum boards were partially dried before testing the results cannot be directly compared with other trials.

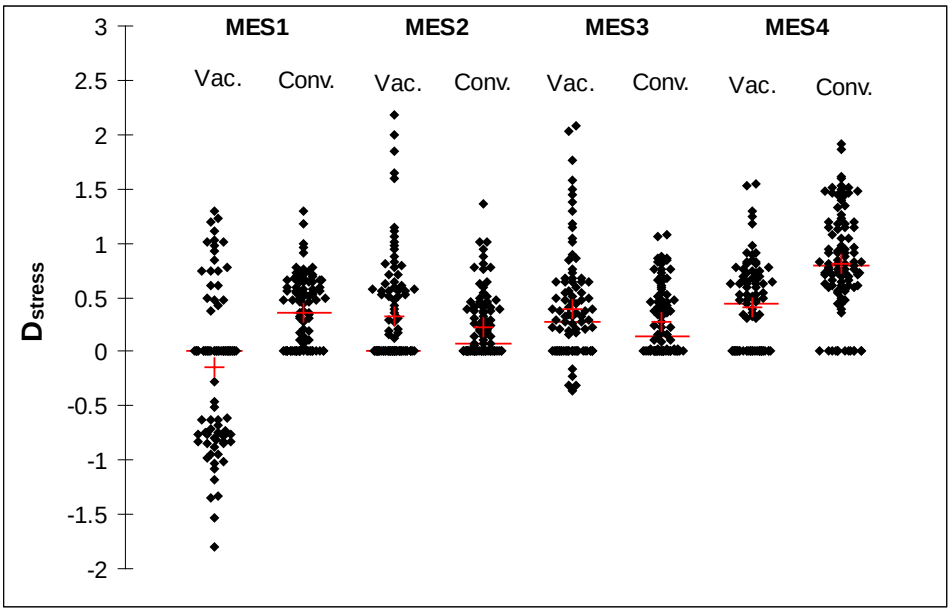

Figure 46. Scattergram of drying stress – *E. obliqua*

Table 56. Drying stress results – *E. obliqua*

	Drying stress (D_{stress})							
	MES1		MES2		MES3		MES4	
	Vacuum	Conventional	Vacuum	Conventional	Vacuum	Conventional	Vacuum	Conventional
Average	-0.1	0.4	0.3	0.2	0.4	0.3	0.4	0.8
Maximum	1.3	1.3	2.2	1.4	2.1	1.1	1.6	1.9
Minimum	-1.8	0.0	0.0	0.0	-0.4	0.0	0.0	0.0
Standard deviation	0.7	0.3	0.5	0.3	0.5	0.3	0.4	0.5
Significance (p)	< 0.0001		0.375		0.077		< 0.0001	
Grade quality (*AS/NZS 4787*)	B	B	B	B	B	B	B	C

Collapse

Varying amounts of collapse were present for all boards in each vacuum drying trial before reconditioning. After reconditioning, drying and surface dressing the vacuum dried sample boards, 50% of the non-reconditioned sample boards for trials MES1 and MES 2, and 40% for trial MES3 and MES4, were affected by miss after dressing due to excessive collapse. Miss affected zero percent of the reconditioned boards after dressing. These results indicate vacuum dried collapsed boards can be successfully reconditioned using standard industry practice.

After drying, cross–sections from all 100 sample boards were scanned for further quantification of collapse recovery between reconditioned and non-reconditioned boards. Plate 21 shows a representative sample of scanned cross sections of the non-reconditioned (two left columns) and reconditioned boards (two right columns). The effect of collapse recovery on the reconditioned boards is visually evident.

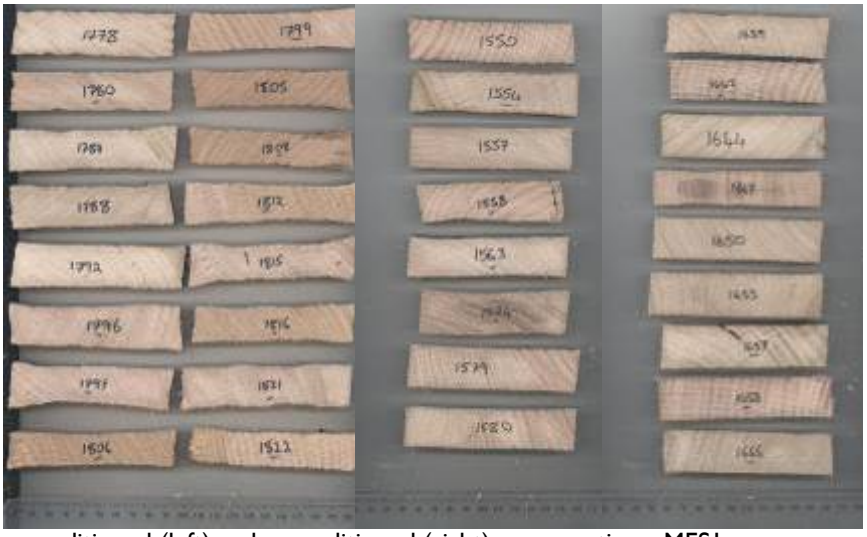

Plate 21. Non-reconditioned (left) and reconditioned (right) cross sections–MES1

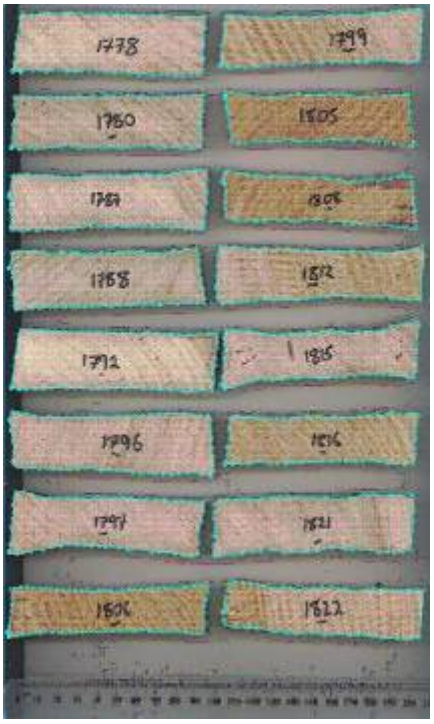

Plate 22. Example of *MeshPore* contour generation

We accurately determined the surface area of each cross section using *MeshPore* (Perré, 2005b), an image analysis software package developed to characterise the morphology and produce finite element meshes of wood anatomy. Using *MeshPore*, cross–section edge contours could be rapidly generated (Plate 22), and the surface area automatically calculated. The comparative cross-sectional area results between reconditioned (A_r) and non-reconditioned samples (A_{nr}) before and after vacuum drying, and the ratio of cross sectional area of dried reconditioned and non-reconditioned samples to the original green cross sectional area (A_g) for all vacuum trials are presented in Figure 47 and Table 57. Significant differences do not exist between the cross–sectional surface area of reconditioned and non–reconditioned samples before drying for each vacuum trial. However, significant differences between the means of vacuum dried reconditioned and non–reconditioned samples and dry/green ratios exist for each trial, as evident from the scattergrams. The results show a significant increase in the average cross–sectional area between dry non–reconditioned and reconditioned samples and corresponding dry/green cross–sectional area ratios. We propose

that the normalised ratio of dry/green surface area has potential to be used as a quantitative and comparative method (between/within species and treatments) to characterise collapse and the effectiveness of the reconditioning process.

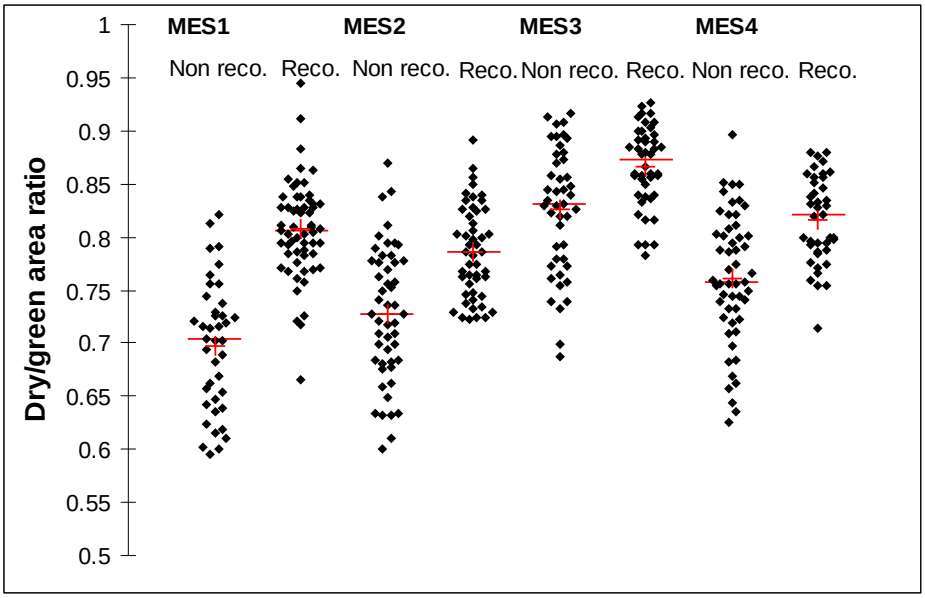

Figure 47. Ratio of dry versus green non-reconditioned and reconditioned cross-sectional area – *E. obliqua*

Table 57. Reconditioned and non-reconditioned cross-sectional area results – *E. obliqua*

	Green area (cm^2)		Dry area (cm^2)		Dry/green area ratio	
	A_g		A_{nr}	A_r	A_{nr}/A_g	A_r/A_g
	non-reco.	reco.	non-reco.	reco.	non-reco.	reco.
MES1						
Average	33.09	33.43	23.06	26.96	0.70	0.81
Stdev.	1.56	1.21	2.04	1.64	0.061	0.046
Sig. (p)	0.15		< 0.0001		< 0.0001	
MES2						
Average	33.26	33.55	24.21	26.36	0.73	0.79
Stdev.	1.30	1.95	2.34	1.77	0.063	0.044
Sig. (p)	0.85		< 0.0001		< 0.0001	
MES3						
Average	33.40	33.24	27.57	28.77	0.83	0.87
Stdev.	1.17	1.53	2.13	1.44	0.059	0.038
Sig. (p)	0.717		0.002		< 0.0001	
MES4						
Average	26.46	26.03	20.11	21.08	0.75	0.81
Stdev.	1.09	1.35	2.00	1.77	0.120	0.048
Sig. (p)	0.242		0.016		< 0.0001	

Sawn orientation

The majority of boards were a combination of quartersawn and transitionally sawn (Table 29). Quartersawing is the desired cutting pattern for this species as it generally produces boards with less surface checking and collapse induced degrade than backsawing.

Table 58. Sawn orientation results – *E. obliqua*

	Sawn orientation (%)			
	MES1	MES2	MES3	MES4
Quartersawn	50	62	50	48
Backsawn	5	0	1	0
Transitional	45	38	49	52

Gross shrinkage

Width and thickness vacuum drying gross shrinkage results, split into non-reconditioned (n-r) and reconditioned (r) groups, are presented in Figure 48 and Table 59. Significant differences exist between the width and thickness gross shrinkage means of reconditioned and non–reconditioned samples for each trial ($p<0.0001$). The reduction of gross shrinkage (width and thickness) for the reconditioned samples is due to collapse recovery. The results are higher than published tangential (8.9%) and radial (4.4%) shrinkages (Bootle, 2004) due to the presence of collapse shrinkage. As the MES3 vacuum boards were partially dried before testing the results can not directly be compared with other trials. This is evident from the lower shrinkage values recorded for this trial, as slower pre-drying usually causes less collapse to occur.

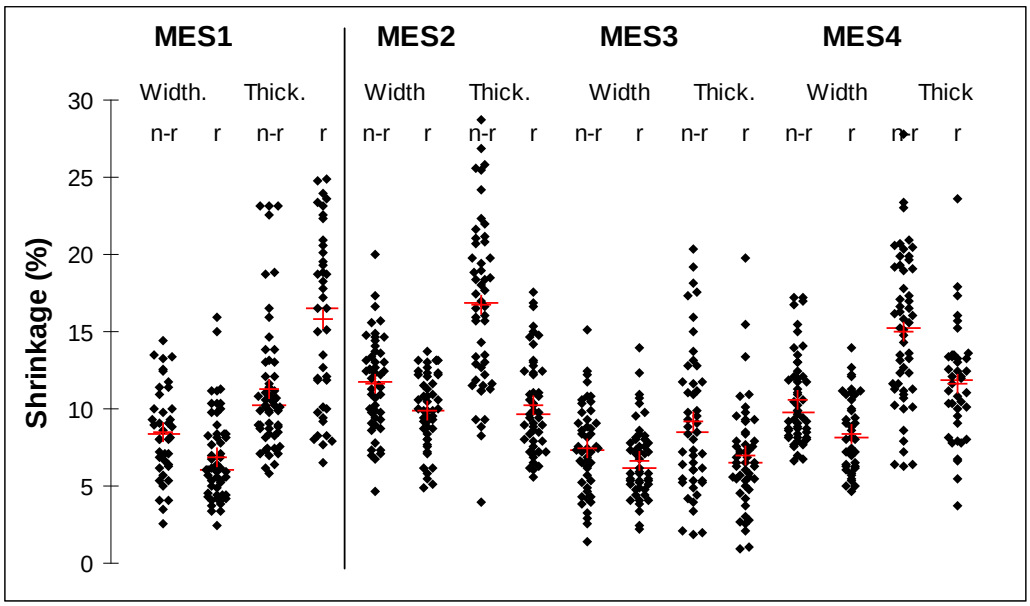

Figure 48. Scattergram of gross shrinkage – *E. obliqua*

Table 59. Gross shrinkage results – *E. obliqua*

		Gross shrinkage (mm)			
Trial		Not reconditioned		Reconditioned	
		Width	Thickness	Width	Thickness
MES1	Average	8.5	15.8	7.0	11.6
	Maximum	14.4	24.9	16.0	23.2
	Minimum	2.5	6.5	2.4	5.8
	Standard deviation	3.0	5.7	2.8	4.6
MES2	Average	11.6	16.7	9.9	10.3
	Maximum	20.0	28.7	13.7	17.5
	Minimum	4.6	3.9	4.9	5.6
	Standard deviation	3.1	5.4	2.4	3.1
MES3	Average	7.4	9.1	6.7	6.9
	Maximum	15.1	20.3	14.0	19.8
	Minimum	1.4	1.8	2.2	1.0
	Standard deviation	2.8	4.6	2.4	3.5
MES4	Average	10.6	15.0	8.4	11.6
	Maximum	17.2	27.8	13.9	23.6
	Minimum	6.6	6.3	4.6	3.7
	Standard deviation	2.8	4.8	2.4	3.6

Drying times and vacuum kiln output

Conventional drying time for this species from the green condition is reported to take approximately 59 days (Innes *et al.*, 2008). The total drying times, including equalisation for the vacuum trials MES1, MES2, MES3 and MES4 were 36.3, 37.0, 38.4 and 36.7 days, respectively (Figure 49 to Figure 52). As the MES3 vacuum boards were partially dried before testing the results cannot be directly compared with other trials. Electrical interference caused the distorted output presented for trial MES4 in Figure 52. We have since remedied this.

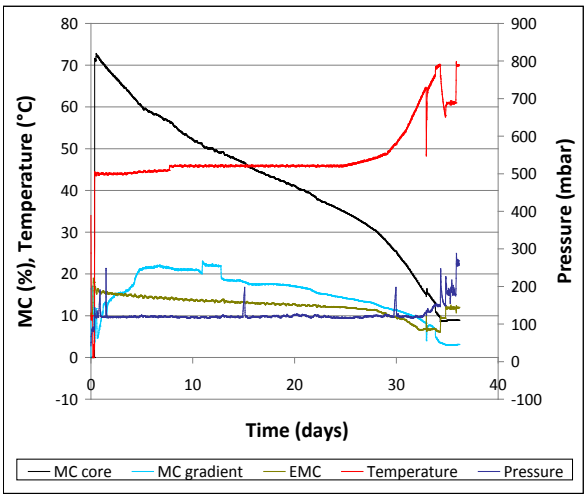

Figure 49. Vacuum drying chart – MES1 trial

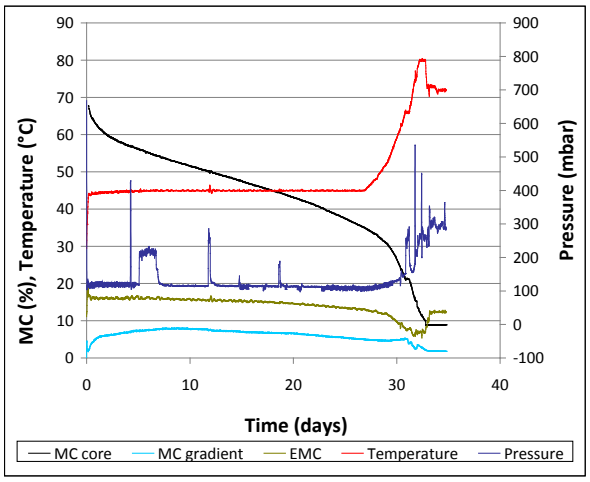

Figure 51. Vacuum drying chart – MES3 trial

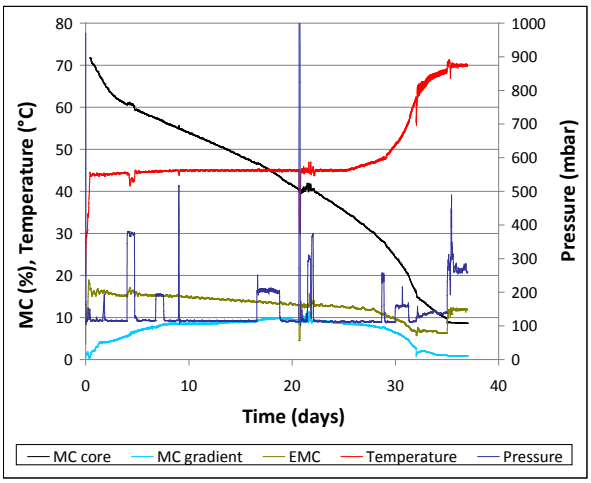

Figure 50. Vacuum drying chart – MES2 trial

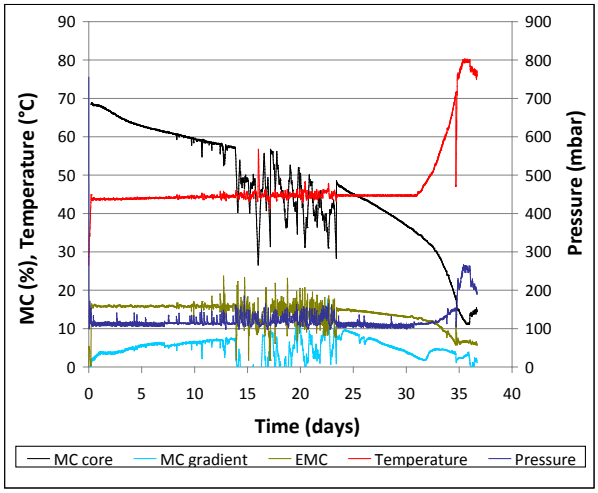

Figure 52. Vacuum drying chart – MES4 trial

Summary – E. obliqua

A summary of the results for the *E. obliqua* trials is provided in Table 60 where unacceptable results are highlighted.

The total drying time for the **MES1** vacuum drying trial was 36.3 days, 61% of reported conventional drying time from the green condition. Final cross–sectional MC variation, MC gradient, residual drying stress, distortion, and surface checking were within acceptable limits, for both the MES 1 conventional and vacuum drying trials. An unacceptable number of MES1 vacuum and conventionally dried boards contained internal checking. *E. obliqua* is particularly prone to this type of degrade. Unacceptable end–splitting resulted from the MES1 conventional trial which failed to make the lowest quality grade, but was minimal for the MES1 vacuum drying trial.

We used a milder schedule for the second **MES2** vacuum drying trial in an attempt to alleviate internal checking. The total drying time for the MES2 vacuum drying trial was 39 days, 63% of reported conventional drying time from the green condition. Final cross–sectional MC, MC gradient, residual drying stress, distortion, and surface checking were within acceptable limits for the MES2 vacuum drying trial. Internal checking results for the MES2 vacuum trial were still outside the acceptable limitations, but were an improvement on the first MES1 vacuum drying trial. For the MES2 conventional trial, all forms of degrade were within acceptable limits except for surface checking and end-splitting.

As material provided for the **MES3** trials were partially air-dried through exposure prior to testing the results are considered to be compromised and cannot be compared with previous trials. Although the results are presented in this report they are not discussed in this summary.

Due to favourable dried quality resulting from the MES2 vacuum trial, we increased the DBT during the latter stages of the **MES4** schedule, from 30% MC to final dry, to increase the drying rate and improve overall drying time. The total drying time for the MES4 vacuum drying trial was 36.7 days, 62% of reported conventional drying time. For the MES4 vacuum drying trial all forms of degrade were within acceptable limits. For the corresponding conventional trial, all forms of degrade were acceptable except for drying stress.

Collapse was present for all vacuum dried boards before reconditioning. No noticeable collapse was present on the MES1 conventional trial boards as they had been reconditioned by the sawmill prior to analysis. Using *MeshPore*, we generated cross–section edge contours and calculated the surface area. The results show a significant increase in the average cross–sectional area between dry non–reconditioned and reconditioned samples and corresponding dry/green cross–sectional area ratios. Successful recovery of collapse after reconditioning was evident as 100% of reconditioned boards, when dressed to a thickness of 19 mm, were free of collapse-induced ‘miss’. Between 40 and 50% of non–reconditioned boards were free of collapse-induced ‘miss’ or ‘skip’ after dressing for all trials. The author proposes that the normalised ratio of dry/green surface area has potential to be used as a quantitative and comparative method (between/within species and treatments) to characterise collapse and the effectiveness of the reconditioning process.

Overall, the results show vacuum drying *E. obliqua* was significantly faster producing the same or better dried quality than for conventional kiln drying. We recommend using the MES4 vacuum drying schedule for this species based on the dried quality outcomes and drying time.

Table 60. *E. obliqua* results summary

Species Trial ID. Drying method	Days drying [% of conventional kiln drying time]	Initial basic density (kg/m3) [stdev.]	Initial MC (%) [stdev.]	Final MC (%) average [stdev.] {grade}*	Final MC % select grade (%)**	MC gradient (%) [stdev.] {grade}*	Drying stress grade quality [stdev.] {grade}*	Distortion % in grade** [major type]	Collapse (% affected)	Surface check % select** [%check free]	Internal check % check free	End split grade*	Indication of Economic viability
E. obliqua													
4 (MES1)													
vacuum	36.3 [61]††	476.1 [58.7]	122.0 [20.0]	10.5 [0.6] {A}	100	0.1 [0.5] {B}	-0.1 [0.7] {B}	96 [twist]	100‡	97 [96]	**78**	A	viable
conventional (air)	380			9.7 [0.3] {A}	99	-0.2 [0.4] {A}	0.4 [0.3] {B}	96 [twist]	------	95 [94]	**88**	**FAIL**	
significance (p)				<0.0001		<0.0001	<0.0001			0.075		<0.0001	
8 (MES2)													
vacuum	37 [63]	491.2 [54.6]	112.5 [22.7]	10.5 [0.9] {B}	98	-0.2 [0.6] {A}	0.3 [0.5] {B}	97 [twist]	100‡	96 [94]	**89**	A	viable
conventional (kiln)	59			10.5 [0.5] {B}	100	0.8 [0.8] {A}	0.2 [0.3] {B}	97 [twist]	------	**84 [71]**	96	**FAIL**	
significance (p)				0.725		<0.0001	0.375			0.009		<0.0001	
12 (MES3)													
vacuum	34.8 [59]	569.5 [67.7]	65.3 [19.8]	9.6 [0.5] {B}	91	0.3 [0.5] {A}	0.4 [0.3] {B}	99 [twist]	100‡	91 [80]	95	A	NA
conventional (kiln)	59			9.8 [0.6] {B}	96	0.0 [0.6] {A}	0.3 [0.3] {B}	96 [twist]	------	78 [72]	85	FAIL	
significance (p)				0.004		0.0002	0.077			0.031		<0.0001	
16 (MES4)													
vacuum	36.7 [62]	544.7 [64.1]	98.0 [20.5]	10.0 [0.6] {B}	98	-0.4 [0.4] {A}	0.4 [0.4] {B}	95 [twist]	100‡	98 [98]	96	A	?
conventional (kiln)	59			10.5 [0.9] {B}	99	0.4 [0.9] {A}	**0.8 [0.5] {C}**	97 [twist]	------	98 [94]	97	A	
significance (p)				<0.0001		<0.0001	<0.0001			0.859		0.932	

* AS/NZS 4787:2001 Timber-Assessment of drying quality.

** AS 2796: 1999 Hardwood-Sawn and milled products.

† † Based on indicitive conventional drying time of 59 days from green (Innes *et al* . 2008).

‡ Approximately half of the boards were reconditioned. 50% of nonreconditioned boards affected by collapse miss when dressed to 19 mm. 0% of reconditioned boards affected by collapse miss.

4.2 Applied drying - Economic model

We performed three (3) case studies to examine the economic viability of vacuum drying compared to conventional drying for each species. The different case studies relate to three different sized operations, namely: small, medium and large relating to wood capacities of 10, 35 and 50 m^3, respectively. For each of the case studies, we used the same constant input values shown in Table 61. The justification for these values is provided in section *3.2.2 Inputs*.

Table 61. Constant input values used for each case study

Constant input	Conventional drying	Vacuum drying
project life (yrs)	20	20
interest rate (%)	7	7
wood value ($)	426	426
Electrical cost ($/kWh)	0.2	0.2
Heat cost ($/MJ)	0.05	0.05
Thermal loss (%)	65	30
Average fan load (kW)	2	1.5
Vacuum pump rating (kW)	NA	3
Vacuum pump usage (%)	NA	20
Condensor fan rating (kW)	NA	11
Condensor fan usage (%)	NA	25
Operational year (days)	328	328

The species specific, and drying condition data used in the case studies for each species are the same values generated from the best quality and fastest drying outcome applied drying trials. For each species this related to the last or fourth drying trial conducted. Kiln related data was provided by the project collaborator, Brunner-Hildebrand. The kiln costs do not take into account the cost of the heat plant or installation of the kilns. Installation values are assumed the same for installing the same sized kiln, either vacuum or conventional.

The results of the case studies are shown in Table 62 where non-viable vacuum drying (loss) is highlighted. From the drying trials, the reduction in vacuum drying time compared to conventional for *C. citriodora* and *E. obliqua* was similar at 66 and 62% respectively. For *E.marginata* and *E. pilularis* the reduction was also similar at 43 and 41% respectively. Results of the case studies indicate that in terms of the cost/m^3, for the small and medium sized operations, vacuum drying of *C. citriodora* and *E.obliqua* is not economically viable. However, for both species vacuum drying is economically viable (2.7 % gain for *C. citriodora* and 1.3 % for *E.obliqua*) for the large operation, primarily due to a reduction in the capital growth of larger capacity vacuum drying kilns.

For all sized operations, vacuum drying was found to be economically viable for *E.marginata* and *E. pilularis*. We encountered the same trend for each species where economic viability in terms of gain (%) increased with increasing operation size. For these two species, at the largest operation size tested (case study 3) the gain results indicate an increase of 15.7 and 18.9 % respectively for *E. marginata* and *E. pilularis* when comparing vacuum drying to conventional.

Results indicate that for small and medium sized operations, for vacuum drying to be economically viable, the vacuum drying time needs to be less than approximately 60% of the conventional drying time.

Table 62. *Economic case study viability results*

			Input variables									Output variables		
Case study No.	Species	Kiln type	Kiln capacity (m^3)	Kiln capital ($)	No. Kilns	No. Fans	Kiln drying time (hrs)	Max. Temp. (°C)	Initial MC (%)	Final MC (%)	Basic density (kg/m^3)	Throughput (m^3/Yr)	Cost ($/$m^3$)	Gain/Loss (%)
1. Small scale -same volume kiln	*C. citriodora*	Conventional	10	47000	1	2	504	75	37.3	10.2	852	156.2	109.84	**-22.1**
		Vacuum	10	134000	1	4	336	75	37.3	10.2	852	234.29	134.11	
	E. marginata	Conventional	10	47000	1	2	1464	67	74.2	12.2	662	53.77	252.44	4.5
		Vacuum	10	134000	1	4	622	67	74.2	10.6	662	126.56	240.97	
	E. pilularis	Conventional	10	47000	1	2	1392	67	51.3	8.7	715	56.55	223.92	5.3
		Vacuum	10	134000	1	4	595	67	51.3	11.8	715	132.3	211.99	
	E. obliqua	Conventional	10	47000	1	2	1416	75	98	10	545	55.59	261.86	**-23.0**
		Vacuum	10	134000	1	4	881	75	98	10.5	545	89.35	322.2	
2. Medium scale - same volume kiln	*C. citriodora*	Conventional	35	60000	1	3	504	75	37.3	10.2	852	546.67	77.24	**-5.0**
		Vacuum	35	241000	1	6	336	75	37.3	10.2	852	820	81.09	
	E. marginata	Conventional	35	60000	1	3	1464	67	74.2	12.2	662	188.2	157.74	9.5
		Vacuum	35	241000	1	6	622	67	74.2	10.6	662	442.96	142.82	
	E. pilularis	Conventional	35	60000	1	3	1392	67	51.3	8.7	715	197.93	133.9	11.8
		Vacuum	35	241000	1	6	595	67	51.3	11.8	715	463.06	118.1	
	E. obliqua	Conventional	35	60000	1	3	1416	75	98	10	545	194.58	170.28	**-7.6**
		Vacuum	35	241000	1	6	881	75	98	10.5	545	312.74	183.18	
3. Large scale -same volume kiln	*C. citriodora*	Conventional	50	74000	1	4	504	75	37.3	10.2	852	780.95	75.34	2.7
		Vacuum	50	281000	1	7	336	75	37.3	10.2	852	1171.43	73.28	
	E. marginata	Conventional	50	74000	1	4	1464	67	74.2	12.2	662	268.85	152.23	15.7
		Vacuum	50	281000	1	7	622	67	74.2	10.6	662	632.8	128.37	
	E. pilularis	Conventional	50	74000	1	4	1392	67	51.3	8.7	715	282.76	128.64	18.9
		Vacuum	50	281000	1	7	595	67	51.3	11.8	715	661.51	104.29	
	E. obliqua	Conventional	50	74000	1	4	1416	75	98	10	545	227.97	164.93	1.3
		Vacuum	50	281000	1	7	881	75	98	10.5	545	446.77	162.73	

4.3 Drying modelling - Measurement of kiln conditions and wood drying properties

As the specialised instrumentation outputs were used for modelling purposes, and due to the large number of outputs over the 16 vacuum trials, only an example of each device output is provided.

4.3.1 Shrinkage and flying wood

An example of the strain gauge output for the JAR10 vacuum trial test and flying wood boards is presented in Figure 53. Classical shrinkage curves are presented for the test boards and flying wood board. The strain gauge pairs for the two test boards can be seen to follow similar shrinkage paths. The curves for the flying wood board show stress reversal as expected.

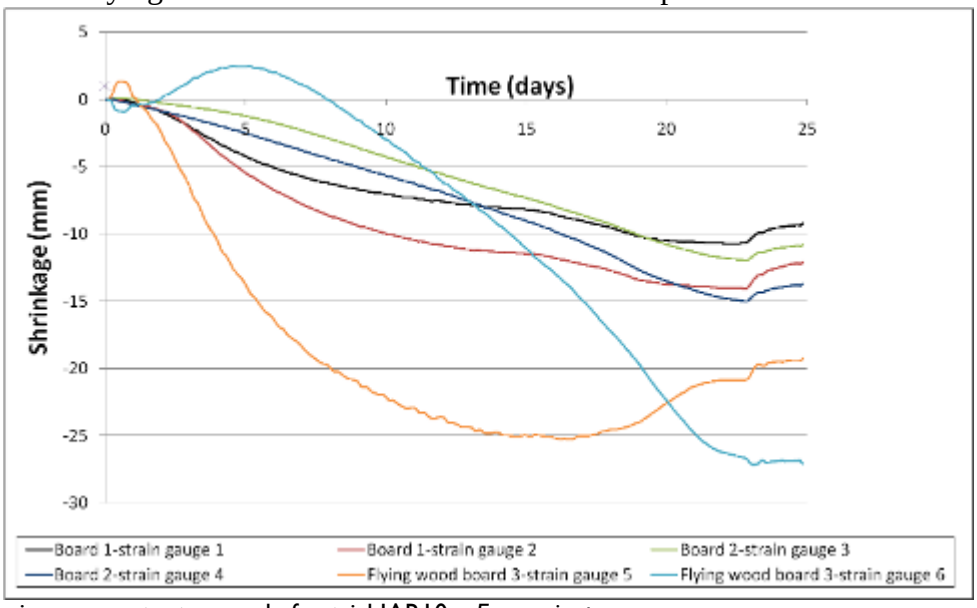

Figure 53. Strain gauge output example for trial JAR10 – *E. marginata*

4.3.2 Load/moisture content

An example of the load cell output for the BBT11 vacuum trial test and flying wood boards is presented in Figure 54. The curves follow the expected reduction due to drying, however there appears to be some noise in the output signal which may be electrical or caused by vibration of the boards due to airflow. Further analysis involved smoothing these curves using the 'sliding window' algorithm in Matlab. Once smoothed we converted the curve output from mass to MC. These curves were used for model verification and comparisons as detailed in section *4.5 Drying modelling* - Vacuum drying modelling.

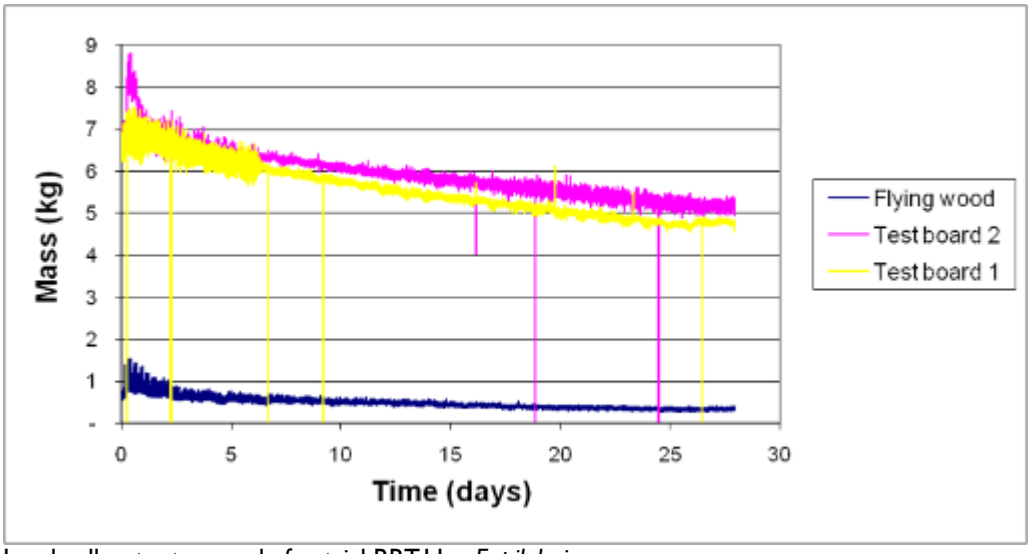

Figure 54. Load cell output example for trial BBT11 – *E. pilularis*

4.3.3 Airflow

An example of measured airflow results from the anemometers for trial MES1, is shown in Figure 55. As the airflow was reversed every 30 minutes, the airflow measurements are represented as markers. This allows us to observe the predominant airflow measurements as coloured bands. For each anemometer, we can observe two bands: the upper band represents air entering the anemometer side of the stack and the lower represents air exiting the opposite side. As the kiln only consists of one fan, anemometer 1 was consistently placed on the fan side of the stack and anemometer 2 on the non–fan side.

A common trend between trials was lower airflow measured on the air outlet side of the stack than that measured on the air inlet side. This common phenomenon occurs due to a drop of pressure across the stack, friction effects and the removal of water from the material, and thus necessitates frequent fan reversals to obtain even drying across the stack. The obvious difference between the airflows measured in these trials compared to conventional drying is the magnitude. Transferring the necessary heat of evaporation to the stack is the bottleneck in convective vacuum drying of wood. Therefore, higher gas/steam velocities are required to compensate for the lower gas density and to obtain similar heat and mass transfer characteristics as under normal pressure. According to Malmquist and Noack (1960), the required velocity of the drying medium to achieve an acceptable heat transfer in a superheated steam atmosphere has to be about four times higher than normal when reducing the pressure conditions from 1033 mbar to 200 mbar. The prescribed airflow to dry these species conventionally is between 1 and 2 m/s. The maximum airflows recorded during the vacuum trials range between approximately 4.5 and 9 m/s.

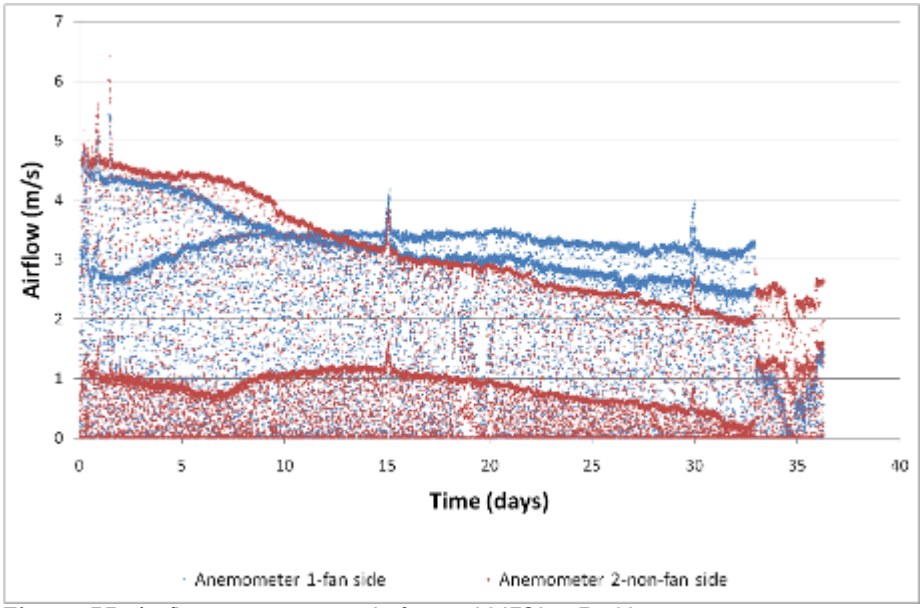

Figure 55. Airflow output example for trial MES1 – *E. obliqua*

4.3.4 Board temperature

An example of measured thermocouple output is provided in Figure 56. The kiln temperature and EMC conditions are also shown, as the internal board temperature is dependent on both properties. It is interesting that in most cases the end temperature was noticeably lower than the 1/2 and 1/3 depth temperatures, suggesting that the ends of the boards were wetter than the centre. This seems to indicate a high degree of end drying when under vacuum and requires further investigation.

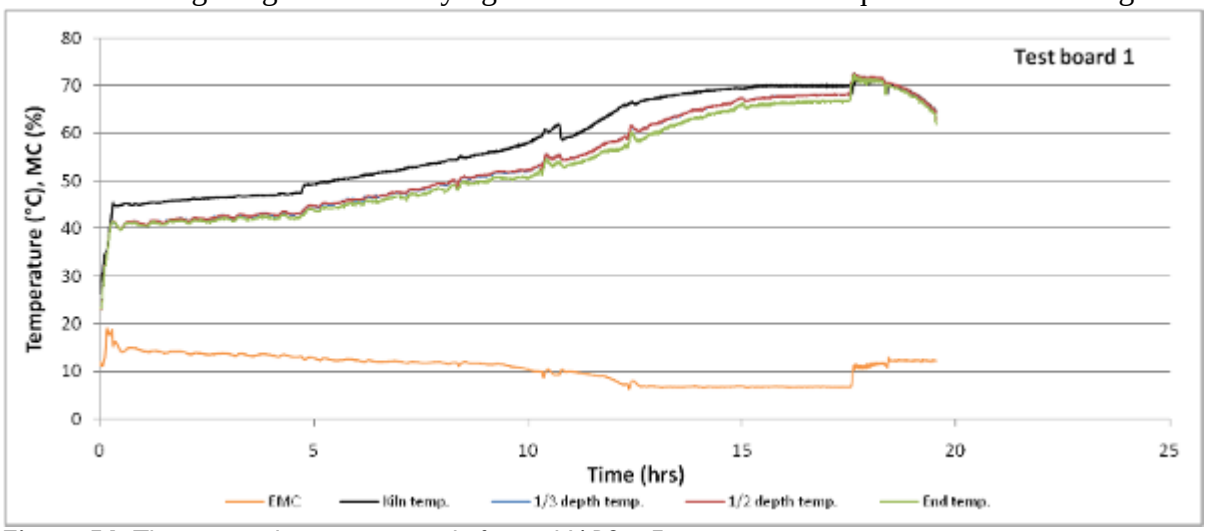

Figure 56. Thermocouple output example for trial JAR2 – *E. marginata*

4.4 Drying modelling - Measurement of essential wood properties

4.4.1 Wood density and initial MC

The wood density and initial MC values used in the drying model are derived from the kiln drying trials described in section *4.1 Applied drying* – Experimental drying trials.

4.4.2 Fibre porosity

Plate 23 to Plate 26 show the ESEM images captured for each species at 700X magnification. We cropped the ESEM images taken at this magnification to contain only wood fibre cells excluding ray parenchyma and vessel cells, for fibre porosity measurements using *Meshpore*.

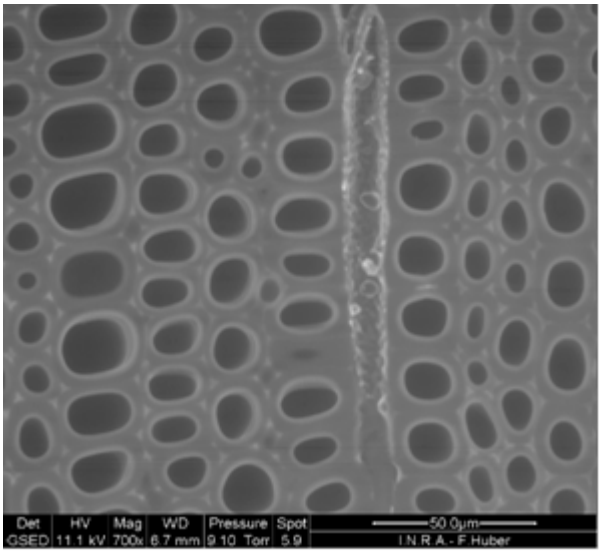

Plate 23. *E. obliqua* ESEM fibre image (700 X mag.)

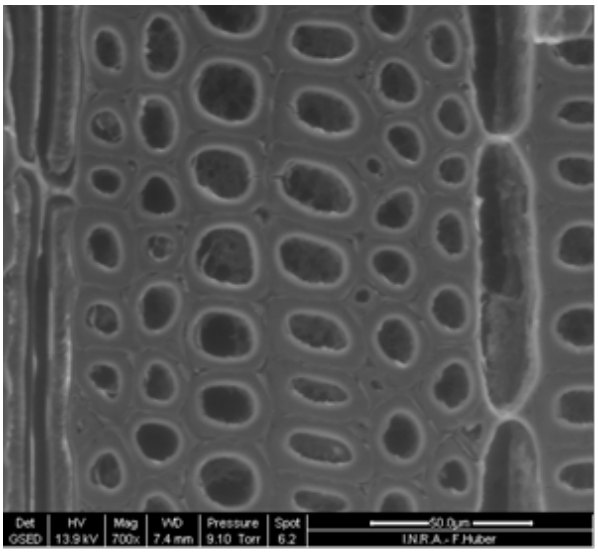

Plate 24. *E. marginata* ESEM fibre image (700 X mag.)

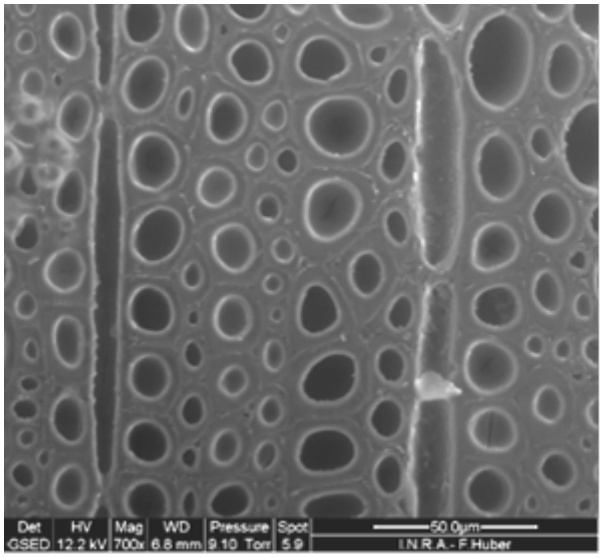

Plate 25. *E. pilularis* ESEM fibre image (700 X mag.)

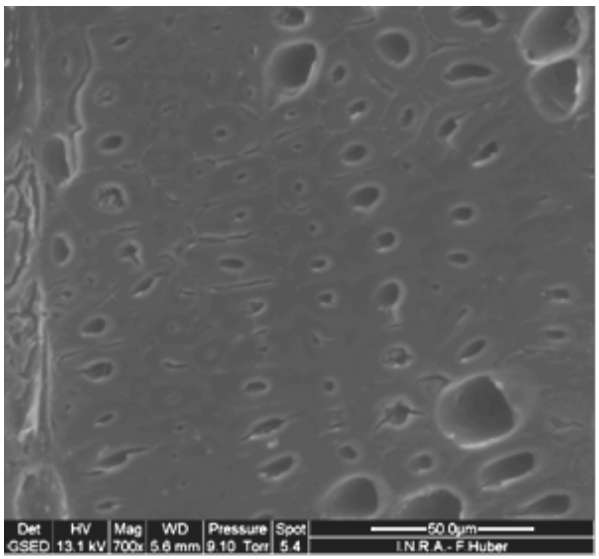

Plate 26. *C. citriodora* ESEM fibre image (700 X mag.)

A clear difference in fibre porosity, size, wall thickness and orientation is evident between species. For instance *Corymbia citriodora* is made up of fibres with very thick cell walls, and hence low porosity or lumen/wood tissue ratio, compared with *Eucalyptus obliqua* whose fibres have large lumens and thin cell walls. The cropped images were loaded into the *Meshpore* software and contours of the cell lumens were automatically generated for fibre porosity determination.

Table 63 contains the fibre porosities and, measured, and calculated densities for each species sample. We measured distinct fibre porosity between species, as can be visually observed from ESEM images. Calculated density values were higher than the basic density values measured because the density calculation uses the published oven dry density of wood tissue and other voids were not taken into consideration such as vessels. Additionally, intra-wall voids could also contribute to a lesser extent. However, a strong correlation was observed between measured and calculated density (R^2 = 0.973) as shown in Figure 57.

Table 63 Average fibre porosity, measured and calculated density for each species

Species	Measured basic density (kg/m^3)	Calc density - fibre (kg/m^3)	Fibre porosity
E. obliqua	489.0	945	0.37
E. marginata	635.9	1110	0.26
E. pilularis	674.0	1080	0.28
C. citriodora	921.0	1395	0.07

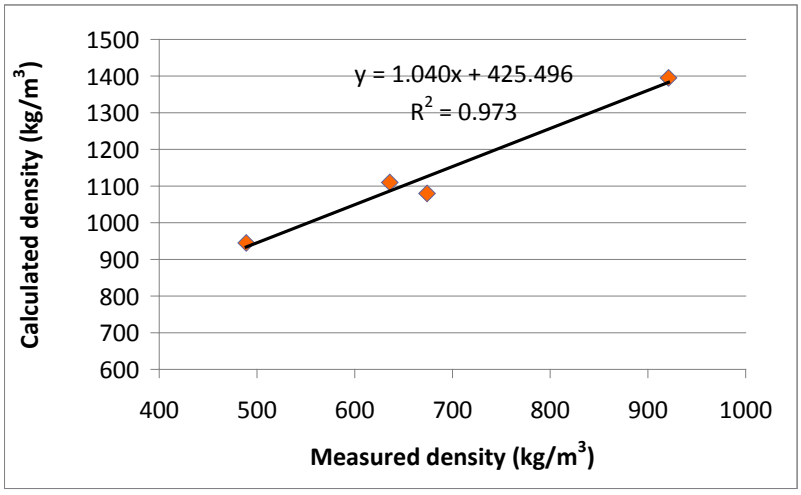

Figure 57. Calculated versus basic density correlation

4.4.3 Gas permeability

The average permeability results measured for each species in the longitudinal, radial and tangential directions are given in Table 64. The results highlight the dramatic anisotropy ratios of these species and the vast difference between species. As stated by Perré (2007a), "wood has dramatic anisotropy ratios: the longitudinal permeability can be 1000 times greater than the transverse permeability for softwoods, and more than 10^6 for hardwoods". This is certainly the case for the species measured where the longitudinal to transverse anisotropy ratio was in the order of 10^7 for some species. No permeability values were measured for *C. citriodora* in the radial direction as, even after 24 hours, no noticeable measurement could be made indicating this species is highly impermeable in this direction (>10^{-23} m^2). *C. citriodora* was the lowest permeability species measured, with the permeability order of the other species changing depending on wood direction.

After extensive literature review, very little work measuring gas permeability in all three directions has been conducted. For comparative purposes, Table 64 includes permeability data for the softwood *Pinus taeda* (Milota *et al.*, 1995) and the hardwood *Quercus falcata* (Perré, 2007a). The gas permeability data for *Quercus falcata* was the lowest gas permeability for a hardwood species this author could find. The four species measured in this report were still at least a factor of 10 less permeable than the lowest published figure, demonstrating the high impermeability of Australian hardwoods.

Table 64. L-R-T average permeability results for each species

	Species	*E. obliqua*	*E. marginata*	*E. pilularis*	*C. citriodora*	*Pinus taeda* (Milota,1995)	*Quercus falcata* (Perré,2007)
Longitudinal	Diameter (mm)	19.3	19.6	19.6	19.7		
	Length (mm)	17.6	17.3	16.8	17.0		
	Permeability (m^2)	5.55E-14	6.74E-14	3.50E-14	7.65E-17	1.01E-05	6.90E-13
Radial	Diameter (mm)	74.4	73.9	74.6	74.3		
	Length (mm)	7.8	7.9	7.8	7.9		
	Permeability (m2)	8.60E-18	4.68E-20	1.44E-20	N/A	2.00E-07	N/A
Tangential	Diameter (mm)	74.5	74.1	74.2	74.1		
	Length (mm)	8.0	8.0	7.8	8.0		
	Permeability (m2)	2.95E-19	4.41E-16	1.70E-20	3.44E-21	7.30E-08	N/A
Anisotropy ratios	L/R	6400	1440000	2440000	N/A	50	110000
	L/T	189000	150.0	2060000	22000	140	143000
	R/T	29.2	0.0001	0.846	N/A	2.74	1.3

4.4.4 Bound water diffusion

Figure 58 to Figure 61 show the evolution of mass loss per unit volume over time of radial, tangential and longitudinal disc samples for each species. As radial and tangential sample diameters were much larger than those in the longitudinal direction, and because the samples were of slight varying thickness the mass loss was 'normalised' by dividing by the mass loss per unit volume. Both figures show two distinctive groups of curves, one of small slopes and one of extensive bigger slopes. The big slope represents fluxes of water vapour in the longitudinal direction, and the small slopes through the radial and tangential directions.

The vapour flux in all directions is markedly lower for *C. citriodora* than for *E. obliqua*, with the other species falling in between. This may be attributed to the vast anatomical and chemical differences between these species. We specifically chose these species for this research based on their highly diverse wood property, chemistry, anatomical and drying capabilities.

Table 65 contains the measured diffusion coefficient results in the radial, tangential and longitudinal directions for each species. Average values are shown along with the direction ratios. Because three samples were used per species direction (labelled R1..R3, T1..T3 and L1.. L3 for the radial, tangential and longitudinal directions, respectively), standard deviation values are not included.

C. citriodora diffusion coefficients were much lower in all directions compared with the other species, where *E. obliqua* was the highest. The R/T ratio of diffusion coefficient for *C. citriodora* was approximately 1:1 indicating low diffusion isotropy in this plane. This is evident in many other wood property ratios measured for this species in this report, such as

shrinkage and permeability. The converse is true for the other species where relatively higher isotropy has been encountered for the same parameters compared with *C. citriodora*. Again this is reflective of other wood properties measured for these species.

The ratio of longitudinal diffusion to both radial and tangential directions is much greater for *E. obliqua* than *C. citriodora*, indicating *E. obliqua's* greater propensity for drying in the longitudinal direction which may be advantageous during vacuum drying. Further work is planned to test this hypothesis by simulating drying in the longitudinal direction using *Transpore 2-D*.

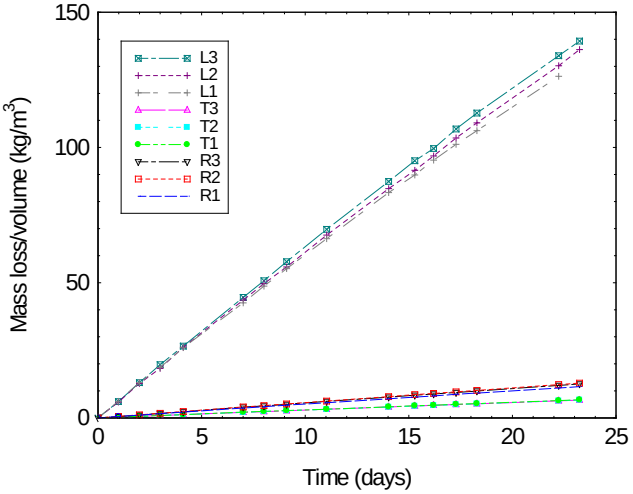

Figure 58. Evolution of bound water flux per unit volume with time in the R, T and L directions for *E. obliqua*

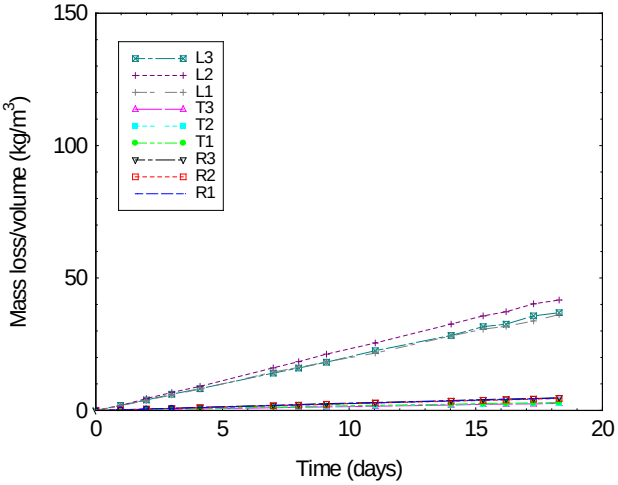

Figure 60. Evolution of bound water flux per unit volume with time in the R, T and L directions for *E.pilularis*

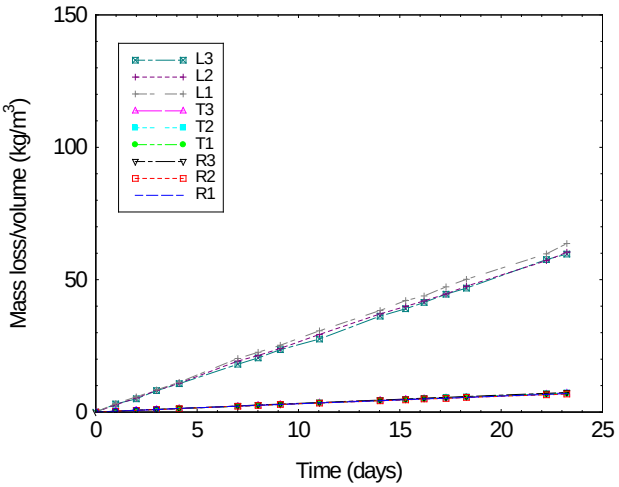

Figure 59. Evolution of bound water flux per unit volume with time in the R, T and L directions for *E. marginata*

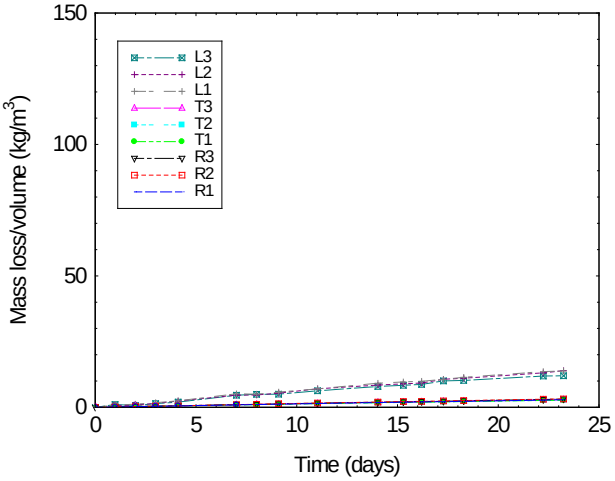

Figure 61. Evolution of bound water flux per unit volume with time in the R, T and L directions for *C. citriodora*

Table 65. Measured diffusion coefficient values and ratios in the R, T and L directions, for *C. citriodora* and *E. obliqua*

		E. obliqua			*E. marginata*			*E. pilularis*			*C. citriodora*		
Direction	Sample	D_b (m^2/s)	Average	Ratios	D_b (m^2/s)	Average	Ratios	D_b (m^2/s)	Average	Ratios	D_b (m^2/s)	Average	Ratios
Radial	1	6.56E-11		R/T	2.54E-11		R/T	2.76678E-11		R/T	1.54E-11		R/T
	2	7.34E-11	7.05E-11	1.74	2.57E-11	2.58E-11	0.68	2.51635E-11	2.67E-11	1.61	1.31E-11	1.43E-11	0.99
	3	7.24E-11			2.63E-11			2.73334E-11			1.44E-11		
Tangential	1	4.22E-11		L/T	3.69E-11		L/T	1.78046E-11		L/T	1.35E-11		L/T
	2	3.97E-11	4.05E-11	25.36	3.81E-11	3.77E-11	7.19	1.63278E-11	1.66E-11	14.18	1.42E-11	1.44E-11	4.17
	3	3.97E-11			3.82E-11			1.56768E-11			1.56E-11		
Longitudinal	1	9.55E-10		L/R	2.81E-10		L/R	2.20932E-10		L/R	6.39E-11		L/R
	2	1.04E-09	1.03E-09	14.59	2.72E-10	2.71E-10	10.50	2.63111E-10	2.35E-10	8.81	6.26E-11	6.02E-11	4.21
	3	1.09E-09			2.60E-10			2.22006E-10			5.40E-11		

4.4.5 Shrinkage

For each shrinkage sample, we generated plots of shrinkage, MC and dew point temperature as a function of time and shrinkage as a function of MC. A typical output of the experimental data is shown in Figure 62 collected for a micro-sample of *Eucalyptus pilularis*. For the first drying cycle, at high relative humidity, very little shrinkage occurs in both the radial and tangential directions, as the samples surface remains above FSP. The sample reaches equilibrium, as shown by the plateau of shrinkage and moisture content, before the shrinkage rate gently increases with decreasing humidity (represented by the dew point temperature). The MC steadily decreases during this period. At the end of the plateau we increase the relative humidity, where the sample picks up moisture and swells. Even though equilibrium is not fully attained, either through desorption or adsorption, a hysteresis effect is apparent, as the MC is less in adsorption than desorption.

The same data can be plotted as a shrinkage versus MC curve as shown in Figure 63. Note that the data defines a very accurate curve during the test period as the adsorption/desorption shrinkage closely follows the same curve (low MC tail of the graph). This lack of hysteresis evident in shrinkage versus MC curves compared to the hysteresis evident in the shrinkage and MC versus time curves is consistent with published data (Perré, 2007b). Observation of the curve distinguishes two different phases: the removal of free water with minimal shrinkage starting above the fibre saturation point, and a noticeable shrinkage phase, denoting the removal of bound water with a linear relationship with MC.

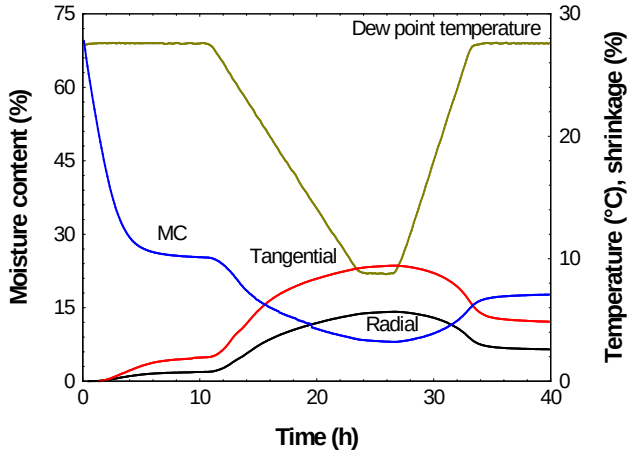

Figure 62. Typical experimental data (MC, tangential and radial shrinkage, and dew point temperature versus time) collected with a *Eucalyptus pilularis* micro-sample.

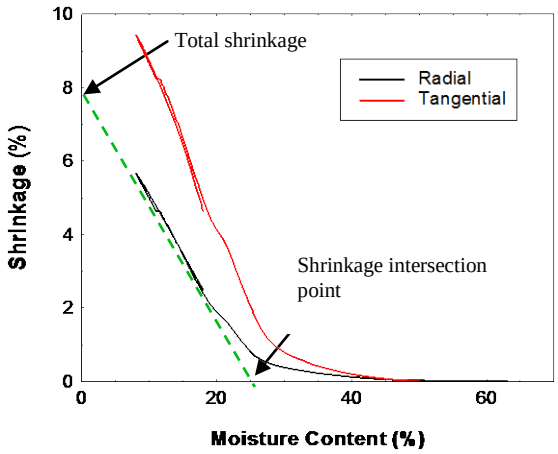

Figure 63. Typical experimental data expressed as shrinkage (radial and tangential) versus MC with a *Eucalyptus pilularis* micro-sample

Similar plots resulted for all species, except original 1 mm thick micro-samples of *E. obliqua*, which showed abnormal shrinkage occurring at high MC due to cell collapse during free water removal (Figure 64). *E obliqua* is a renowned collapse prone species (Bootle, 2004). The radial and tangential shrinkage begins very soon after drying commences and increases abnormally down to 20-40 % MC. At this point the collapse shrinkage slows down as the sample reaches the bound water domain. In the domain of bound water, normal shrinkage takes place (< 20 % MC). Only this part of the shrinkage is recovered when the sample re-absorbs water. The *E. obliqua* collapse results observed are consistent with results observed by Perré (2007b) for *E. gundal* (*E. gunnii x dalrympleana*).

This author theorised that it may be possible to avoid collapse shrinkage during shrinkage tests for this species by cutting thinner R-T sections in the longitudinal direction. Dadswell (1972), observed the range of fibre length of *E. obliqua* is between 1.04-1.27 mm Thus, by reducing the dimension of samples to less than 0.6 mm thickness, the majority of wood fibres will be severed. A cut fibre will not collapse as tension of the cell wall will not be set up if the ends of the fibres are not whole (Redman, 2001).

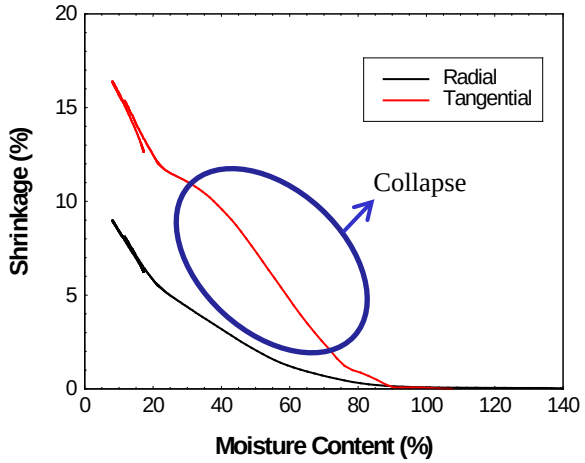

Figure 64. Excessive shrinkage caused by collapse Tangential and radial shrinkage versus MC – *E. obliqua* original 1 mm thick sample

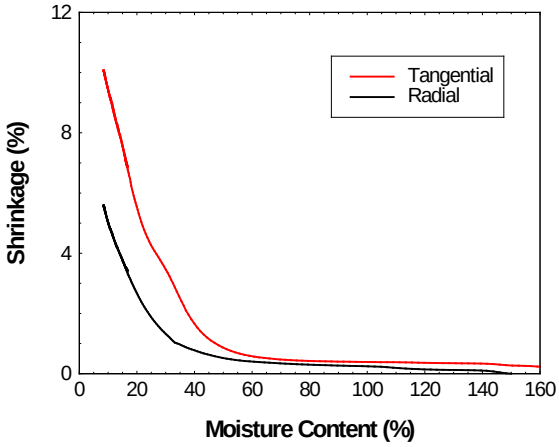

Figure 66. Tangential and radial shrinkage versus MC – *E. obliqua* 1 mm thick sample

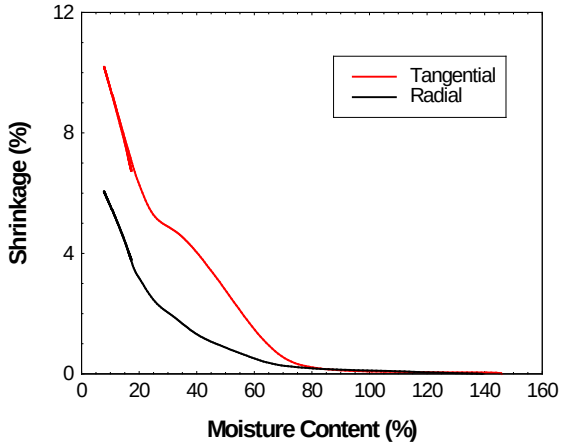

Figure 65. Tangential and radial shrinkage versus MC – *E. obliqua* 2 mm thick sample

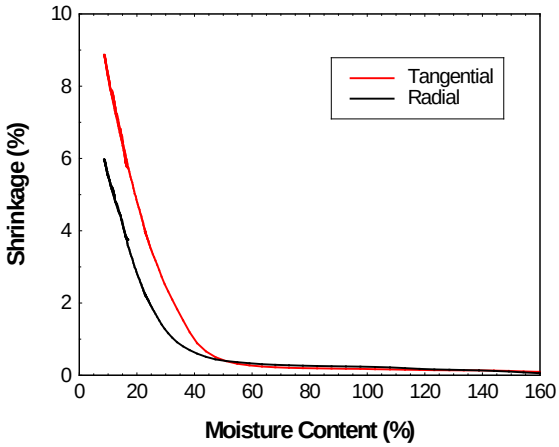

Figure 67. Tangential and radial shrinkage versus MC – *E.* 0.5 mm thick sample

To test this theory, 2, 1 and 0.5 mm thick R-T sections were prepared and retested. The results can be observed in Figure 65 to Figure 67. By observation, collapse shrinkage during testing is reduced with decreasing sample thickness so that no obvious collapse shrinkage is present for the 0.5 mm sample.

The shrinkage intersection point (also referred to as the fibre saturation point) and total shrinkage can be calculated from the shrinkage versus MC curve by subtending the linear portion of the curve, in the bound water/shrinkage phase, until it intersects the x and y axis (Figure 63). We calculated the shrinkage at 12 %, a common published quantification of shrinkage, from the equation of the subtended line. Calculations occurred on the 1 mm thick samples for species *C. citriodora*, *E. marginata* and *E. pilularis*, and to avoid collapse shrinkage, on the 0.5 mm *E. obliqua* samples.

Table 66 provides the total shrinkage, intersection point and shrinkage at 12% for each species. Published intersection point and 12% MC shrinkage values are also included, where the published intersection point data is from Budgen (1981) and the shrinkage values at 12 % MC are from Bootle (2005). No published intersection point values were available for *Eucalyptus marginata* or *Eucalyptus obliqua*. Radial and tangential shrinkage curves for all species can be observed in Figure 68 and Figure 69.

Measured intersection point, total shrinkage and 12% MC shrinkage are consistent within species providing good repeatability. Published intersection point and 12% MC shrinkage values are consistent with measured data. Shrinkage values vary greatly between the tangential and radial directions as expected. Moreover, shrinkage values between species differ due to variations in physical and chemical properties. This seems particularly true for *C. citriodora* where the R/T shrinkage ratio at 12% MC is almost 1:1, significantly different from other species. Thus, in terms of shrinkage this species is more isotropic compared with the others tested.

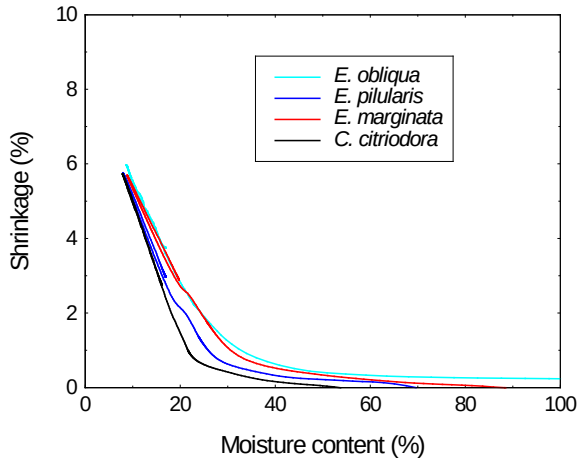

Figure 68. Radial shrinkage versus MC – all species

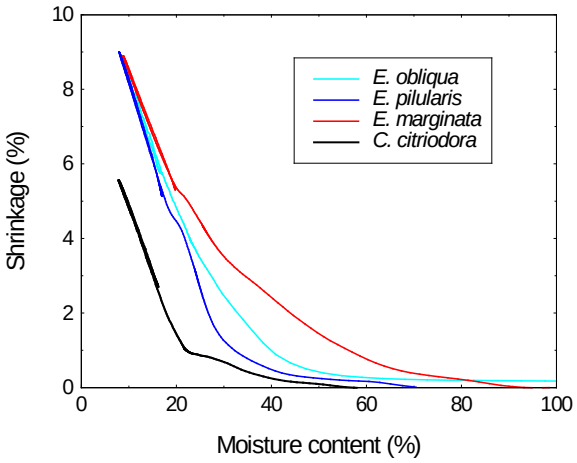

Figure 69. Tangential shrinkage versus MC – all species

Table 66. Shrinkage data measured and published per species (IP: intersection point (%) (Budgen 1981), Total shrinkage and shrinkage at 12 % MC (Bootle 2005))

		Intersection point (%)				Total shrinkage (%)		Shrinkage at 12 % MC					
		Measured		Published				Measured			Published		
Sample #	Species	R	T	R	T	R	T	R	T	R/T	R	T	R/T
1	*C. citriodora*	23.2	27.5	21.4	24.5	8.6	7.2	4.2	4.1	1.02	4.5	6.0	0.75
2	*C. citriodora*	23.4	23.7			8.7	8.1	4.2	4.0	1.06			
1	*E. marginata*	28.3	33.9	-	-	8.3	12.2	4.8	7.9	0.60	5.0	7.5	0.67
2	*E. marginata*	28.6	38.1			8.0	12.9	4.7	8.9	0.53			
1	*E. pilularis*	24.6	26.7	25.1	31.2	8.5	14.3	4.4	7.9	0.55	4.0	7.0	0.57
2	*E. pilularis*	24.4	29.2			8.6	12.4	4.4	7.3	0.60			
1	*E. obliqua*	28.0	31.3	-	-	9.041	12.31	5.2	7.6	0.68	3.5	6.5	0.54
2	*E. obliqua*	28.1	33.5			8.036	11.7	4.6	7.5	0.61			

By observing the MC versus RH sorption/desorption curves for each species, the hysteresis phenomenon is evident (Figure 70). The curves differ for each species due to different anatomical and chemical make up. The reducing RH/MC part of the curve (top part) is the desorption curve and is more applicable to wood drying which is a desorption process. Using data from this part of the curve, the desorption isotherm was calculated for each species by solving equation (**53**) using Matlab. Constants C1 and C2 were generated and are presented in Table 67.

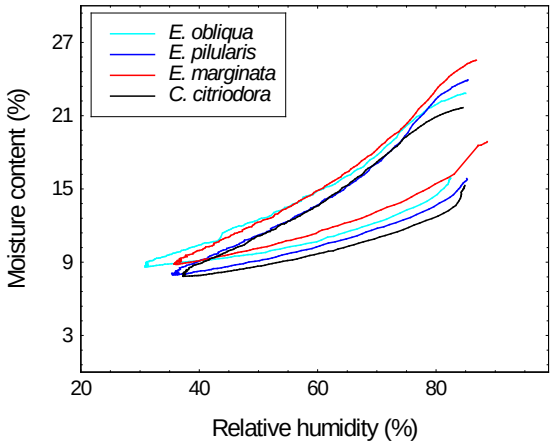

Figure 70. MC versus RH curves for each species showing sorption hysteresis

Table 67. Sorption isotherm equation solutions

	Sorption isotherm constants	
Species	*C1*	*C2*
E. obliqua	0.808	2.2796
E. marginata	0.9716	0.8401
E.pilularis	1.1847	0.7211
C. citriodora	1.0047	0.9076

4.5 Drying modelling - Vacuum drying modelling

At the time of running model simulations, not all vacuum drying trials were completed. For model validation, one vacuum drying trial was chosen per species. We chose the trial that, to date, had produced the best-dried quality outcome in the quickest drying time (most optimised). The vacuum drying trials chosen were the *E. obliqu*a trial MES8, *C. citriodora* trial SPG9, *E. marginata* trial JAR10 and *E. pilularis* trial BBT11.

4.5.1 Input parameters

The static (scalar) input simulation parameters are presented in Table 68. Most input parameters have been measured as part of this project and are reported here in sections *4.1 Applied drying* – Experimental drying trials and *4.3 Drying modelling - Measurement of kiln conditions and* wood drying properties. We have calculated some parameters via theory as discussed in section *3.5 Drying modelling* - Vacuum drying modelling. The liquid phase absolute permeabilities were calculated the same as measured gas phase absolute permeabilites, due to the lack of pit aspiration in hardwoods. We presumed the initial wood temperature based on average Queensland climatic conditions prior to drying.

Table 68. Measured and calculated model input static wood property and drying condition data

Static Wood Properties and Drying Conditions	*Corymbia citriodora* (spotted gum)	Eucalyptus marginata (jarrah)	*Eucalyptus pilularis* (blabkbutt)	*Eucalyptus obliqua* (messmate)	Measured ✓ Calculated ×
Wood density	859 kg m^3	695	833	576	✓
Porosity	0.07	0.26	0.28	0.37	✓
Radial direction Absolute Permeabilities					
Gas phase	1.0×10^{-22} m^2	4.9×10^{-20} m^2	1.4×10^{-20} m^2	8.6×10^{-18} m^2	✓
Liquid phase	1.0×10^{-22} m^2	4.9×10^{-20} m^2	1.4×10^{-20} m^2	8.6×10^{-18} m^2	×
Tangential direction Absolute permeabilites					
Gas phase	3.4×10^{-21} m^2	4.4×10^{-16} m^2	1.7×10^{-20} m^2	2.9×10^{-19} m^2	✓
Liquid phase	3.4×10^{-21} m^2	4.4×10^{-16} m^2	1.7×10^{-20} m^2	2.9×10^{-19} m^2	×
Initial moisture content	31.9 %	62.1%	51.1%	84.9 %	✓
Fibre saturation point	23.3 %	24.5%	24.5%	31.4 %	✓
Initial temperature	25 °C	25 °C	25 °C	25 °C	×
Wood cross-section	100 mm x 28 mm	113 mm x 31 mm	113 mm x 28 mm	110 mm x 30 mm	✓
Direction	Width (T) x Thickness (R)	Width (T) x Thickness (R)	Width (T) x Thickness (R)	Width (R) x Thickness (T)	
Sorption isotherm parameters (equation 22)	C1 = 1.0047 C2 = 0.9076	C1 = 0.9716 C2 = 0.8401	C1 = 1.1847 C2 = 0.7211	C1 = 0.808 C2 = 2.2796	✓

Dynamic drying condition and wood property data, expressed as equations and associated polynomial parameters are shown in Table 69. We derived these equations by fitting curves to measured kiln and wood property data using *TableCurve 2-D* curve fitting software. We measured wood properties from single board samples during kiln drying trials where global kiln drying conditions were also measured. Drying trials and associated wood property measurements are detailed previously in this report.

Table 69. Dynamic model input drying condition and wood property equations and parameters

Species		Equation (x = time (days))	Equation parameters										
			a	b	c	d	e	f	g	h	i	j	k
Corymbia citriodora (spotted gum)	*Kiln Drying Conditions (y)*												
	Kiln dry-bulb temperature (°C)	$y = (a+cx+ex^2+gx^3+ix^4)/(1+bx+dx^2+fx^3+hx^4+jx^5)$	25.09824	1.050118	175.7577	-13.11334	-942.8711	25.64237	1686.637	-1.759628	-96.41856	0.00939	
	Kiln wet-bulb termperature (°C)	$y = (a+cx+ex^2+gx^3+ix^4+kx^5)/(1+bx+dx^2+fx^3+hx^4+jx^5)$	24.10899	-1.946256	2.446867	2.480538	16.63163	2.134097	186.7808	-0.437323	-36.75123	0.022864	1.989112
	Kiln pressure (mbar)	$y = (a+cx+ex^2+gx^3+ix^4+kx^5)/(1+bx+dx^2+fx^3+hx^4+jx^5)$	72.0981	-0.336344	96.36251	-1.488453	-311.5401	3.155001	437.9089	-0.977339	-128.7287	0.083329	10.78346
	Vapour pressure (mbar)	$y = (a+bx^{0.5}+cx+dx^{1.5}+ex^2+fx^{2.5}+gx^3+hx^{3.5}+ix^4+jx^{4.5}+kx^5)$	9.291708	734.1874	-7577.285	29998.4	-57435.44	62529.5	-41624.61	17303.38	-4390.019	622.497	-37.83447
	Air velocity (m s^{-1})	$y = (a+cx+ex^2+gx^3+ix^4+kx^5)/(1+bx+dx^2+fx^3+hx^4+jx^5)$	3.430585	-2.789865	-9.835245	3.049291	11.4533	-0.724218	-2.273578	0.149094	0.355187	-0.009667	-0.021258
	Measured wood properties (y)												
	Moisture content (%)	$y = (a+cx+ex^2+gx^3+ix^4+kx^5)/(1+bx+dx^2+fx^3+hx^4+jx^5)$	31.80614	28.49166	840.0826	-33.69939	-898.1737	36.94318	996.4027	-2.050704	-114.6033	0.179011	5.265619
	Core temperature (°C)	$y = (a+cx+ex^2+gx^3+ix^4)/(1+bx+dx^2+fx^3+hx^4+jx^5)$	19.73979	-1.0289	83.06063	-4.447864	-470.0424	15.39768	1046.283	-0.800037	-48.7236	-0.006134	
	1/3 thickness temperature (°C)	$y = (a+cx+ex^2+gx^3+ix^4)/(1+bx+dx^2+fx^3+hx^4+jx^5)$	19.46381	-0.977005	86.03428	-4.700255	-484.8206	16.01669	1082.206	-0.879266	-52.83295	-0.004908	
	End temperature (°C)	$y = (a+cx+ex^2+gx^3+ix^4)/(1+bx+dx^2+fx^3+hx^4+jx^5)$	19.40364	-1.843058	53.78382	-2.239272	-369.3902	11.1985	792.8363	-0.722616	-52.35535	-0.008219	
Eucalyptus marginata (jarrah)	*Kiln Drying Conditions (y)*												
	Kiln dry-bulb temperature (°C)	$y = (a+c^{0.5}x+ex+gx^{1.5}+ix^2)/(1+bx^{0.5}+dx+fx^{1.5}+hx^2+jx^{2.5})$	24.98261	-2.162479	-50.09957	2.82762	84.94561	-1.127095	-32.67566	0.161873	3.593319	-0.006482	
	Kiln wet-bulb termperature (°C)	$y = (a+c^{0.5}x+ex+gx^{1.5}+ix^2)/(1+bx^{0.5}+dx+fx^{1.5}+hx^2)$	18.70169	-1.987647	-41.70276	3.713938	130.4141	-1.387433	-52.36977	0.145114	5.652007		
	Kiln pressure (mbar)	$y = (a+cx+ex^2+gx^3)/(1+bx+dx^2+fx^3)$	801.1691	412.2433	67964.77	1506.816	160194.6	-56.76526	-5748.158				
	Vapour pressure (mbar)	$y = (a+c^{0.5}x+ex+gx^{1.5}+ix^2)/(1+bx^{0.5}+dx+fx^{1.5}+hx^2)$	13.86692	-2.442183	-52.47841	3.611502	148.8812	-1.284182	-59.51057	0.131855	6.448573		
	Air velocity (m s^{-1})	$y = (a+bx+cx^2+dx^3+ex^4+fx^5+gx^6+hx^7+ix^8+jx^9+kx^{10})$	2.378729	1.908323	-1.59325	0.654172	-0.156185	0.022924	-0.002135	0.000127	-4.63E-06	9.51E-08	-8.41E-10
	Measured wood properties (y)												
	Moisture content (%)	$y = (a+c^{0.5}x+ex+gx^{1.5}+ix^2+kx^{2.5})/(1+bx^{0.5}+dx+fx^{1.5}+hx^2+jx^{2.5})$	63.92859	-0.03847	-29.30539	1.235045	198.1811	0.453928	-87.11208	-0.385634	12.64633	0.073612	-0.343617
	Core temperature (°C)	$y = (a+c^{0.5}x+ex+gx^{1.5}+ix^2)/(1+bx^{0.5}+dx+fx^{1.5}+hx^2+jx^{2.5})$	20.29554	-2.492598	-51.82349	3.34581	91.78403	-1.335406	-35.07264	0.193227	3.819816	-0.008032	
	1/3 thickness temperature (°C)	$y = (a+c^{0.5}x+ex+gx^{1.5}+ix^2)/(1+bx^{0.5}+dx+fx^{1.5}+hx^2+jx^{2.5})$	20.35059	-2.410237	-48.64503	3.128427	83.19301	-1.248507	-31.72462	0.182967	3.461281	-0.007872	
	End temperature (°C)	$y = (a+c^{0.5}x+ex+gx^{1.5}+ix^2)/(1+bx^{0.5}+dx+fx^{1.5}+hx^2+jx^{2.5})$	21.44466	-2.405978	-51.38488	3.035166	82.31327	-1.196646	-30.92135	0.173356	3.347669	-0.007307	
Eucalyptus pilularis (blackbutt)	*Kiln Drying Conditions (y)*												
	Kiln dry-bulb temperature (°C)	$y = (a+bx^{0.5}+cx+dx^{1.5}+ex^2+fx^{2.5}+gx^3+hx^{3.5}+ix^4+jx^{4.5}+kx^5)$	21.05758	13.30673	152.2667	-331.9183	307.6886	-155.0254	44.49284	-6.818755	0.37742	0.025953	-0.003153
	Kiln wet-bulb termperature (°C)	$y = (a+bx^{0.5}+cx+dx^{1.5}+ex^2+fx^{2.5}+gx^3+hx^{3.5}+ix^4+jx^{4.5})$	16.15641	-1.905191	201.0087	-389.146	347.0033	-175.4021	53.21503	-9.605924	0.951297	-0.039785	
	Kiln pressure (mbar)	$y = (a+c^{0.5}x+ex+gx^{1.5}+ix^2+kx^{2.5})/(1+bx^{0.5}+dx+fx^{1.5}+hx^2+jx^{2.5})$	839.991	-8.177421	12372.89	575.2753	45762.35	-202.9122	-12942.22	-8.184022	-3217.716	5.906387	864.4798
	Vapour pressure (mbar)	$y = (a+bx^{0.5}+cx+dx^{1.5}+ex^2+fx^{2.5}+gx^3+hx^{3.5}+ix^4+jx^{4.5}+kx^5)$	9.128715	-57.66021	714.3979	-1404.159	1335.73	-737.0472	250.8548	-53.20044	6.802226	-0.474981	0.013692
	Air velocity (m s^{-1})	$y = (a+bx^{0.5}+cx+dx^{1.5}+ex^2+fx^{2.5}+gx^3+hx^{3.5}+ix^4+jx^{4.5}+kx^5)$	0.845786	12.90853	-37.63956	56.49159	-49.91481	27.71855	-9.937955	2.292074	-0.32757	0.026332	-0.000908
	Measured wood properties (y)												
	Moisture content (%)	$y = (a+cx+ex^2+gx^3+ix^4+kx^5)/(1+bx+dx^2+fx^3+hx^4+jx^5)$	45.97011	-1.319588	12.28071	3.357489	53.76897	-3.411007	-115.7957	1.347183	61.24097	0.005839	-1.545558
	Core temperature (°C)	$y = (a+bx^{0.5}+cx+dx^{1.5}+ex^2+fx^{2.5}+gx^3+hx^{3.5}+ix^4+jx^{4.5}+kx^5)$	15.13088	-0.24611	208.9832	-410.1061	366.1623	-182.6865	53.44872	-8.865936	0.698079	-0.004702	-0.001829
	1/3 thickness temperature (°C)	$y = (a+bx^{0.5}+cx+dx^{1.5}+ex^2+fx^{2.5}+gx^3+hx^{3.5}+ix^4+jx^{4.5}+kx^5)$	15.27078	0.265127	208.696	-413.0716	372.1457	-187.8926	55.97127	-9.593253	0.822149	-0.016266	-0.001375
	End temperature (°C)	$y = (a+c^{0.5}x+ex+gx^{1.5}+ix^2+kx^{2.5})/(1+bx^{0.5}+dx+fx^{1.5}+hx^2+jx^{2.5})$	23.20409	-4.90975	-133.9207	11.98187	410.3478	-12.84521	-496.0257	-0.935833	-48.31736	7.634354	325.9037
Eucalyptus obliqua (messmate)	*Kiln Drying Conditions (y)*												
	Kiln dry-bulb temperature (°C)	$y = (a+cx+ex^2+gx^3+ix^4+kx^5)/(1+bx+dx^2+fx^3+hx^4+jx^5)$	21.47429	1.745346	106.8552	0.222473	-1.564722	0.185306	9.793311	-0.012064	-0.612716	0.000191	0.009712
	Kiln wet-bulb termperature (°C)	$y = (a+bx^{0.5}+cx+dx^{1.5}+ex^2+fx^{2.5}+gx^3+hx^{3.5}+ix^4+jx^{4.5}+kx^5)$	9.389815	62.96826	-58.88654	73.61364	-94.45603	72.77886	-32.49599	8.636393	-1.352226	0.115275	-0.004128
	Kiln pressure (mbar)	$y = (a+cx+ex^2+gx^3+ix^4)/(1+bx+dx^2+fx^3+hx^4)$	968.4289	64.32669	-379.3608	439.0992	64716.55	703.9622	77553.55	-19.82232	-2167.794		
	Vapour pressure (mbar)	$y = (a+bx^{0.5}+cx+dx^{1.5}+ex^2+fx^{2.5}+gx^3+hx^{3.5}+ix^4+jx^{4.5}+kx^5)$	5.704617	2.930675	220.143	-304.7634	165.8306	-31.71577	-6.737982	4.710827	-0.993972	0.097387	-0.003748
	Air velocity (m s^{-1})	$y = (a+bx^{0.5}+cx+dx^{1.5}+ex^2+fx^{2.5}+gx^3+hx^{3.5}+ix^4+jx^{4.5}+kx^5)$	-0.329015	6.056036	0.105299	-5.694899	4.888553	-2.295708	0.755026	-0.180409	0.028826	-0.002653	0.000104
	Measured wood properties (y)												
	Moisture content (%)	$y = (a+cx+ex^2+gx^3+ix^4+kx^5)/(1+bx+dx^2+fx^3+hx^4+jx^5)$	83.61987	-0.332453	-27.52798	0.061815	4.363248	-0.007955	-0.490151	0.00052	0.034693	-3.81E-06	-0.000612
	Core temperature (°C)	$y = (a+bx^{0.5}+cx+dx^{1.5}+ex^2+fx^{2.5}+gx^3+hx^{3.5}+ix^4+jx^{4.5}+kx^5)$	19.63436	-48.68867	271.4879	-395.8346	289.4552	-122.624	31.45223	-4.826372	0.40935	-0.015044	3.57E-05
	1/3 thickness temperature (°C)	$y = (a+bx^{0.5}+cx+dx^{1.5}+ex^2+fx^{2.5}+gx^3+hx^{3.5}+ix^4+jx^{4.5}+kx^5)$	19.05202	-45.41257	263.9339	-386.259	281.9648	-118.5271	29.84978	-4.402655	0.339555	-0.008674	-0.000209
	End temperature (°C)	$y = (a+bx^{0.5}+cx+dx^{1.5}+ex^2+fx^{2.5}+gx^3+hx^{3.5}+ix^4+jx^{4.5}+kx^5)$	21.43497	-46.60472	242.7319	-334.966	227.0317	-85.32288	17.60166	-1.588135	-0.053979	0.021981	-0.001229

4.5.2 Simulations

Mesh generation

We conducted drying simulations using symmetrical, structured, triangular meshes (Figure 71). For each species we used actual board dimensions to generate the mesh circumferential geometry.

To provide rapid throughput when optimising the vacuum drying schedules, the code was run on the Queensland University of Technology (QUT) High Performance Computer (HPC) system. The model was optimised to enable efficient simulations via funds obtained from QCIF. The Matlab code has been optimised/ ported by the HPC group at QUT to ensure peak performance on the HPC system. Code profiling identified a core function (the finite volume wood physics function) that when recoded in a high level language to take advantage of the Intel Compiler led to approximately a 15-fold speedup in computation time.

We performed simulations using an Intel Dual Core T7300 processor using Matlab version 2008a. CPU convergence (completion) times for each species after optimisation are shown in Table 70. Simulation convergences are considered fast for this type of modelling, where simulations converged within at most a short number of minutes.

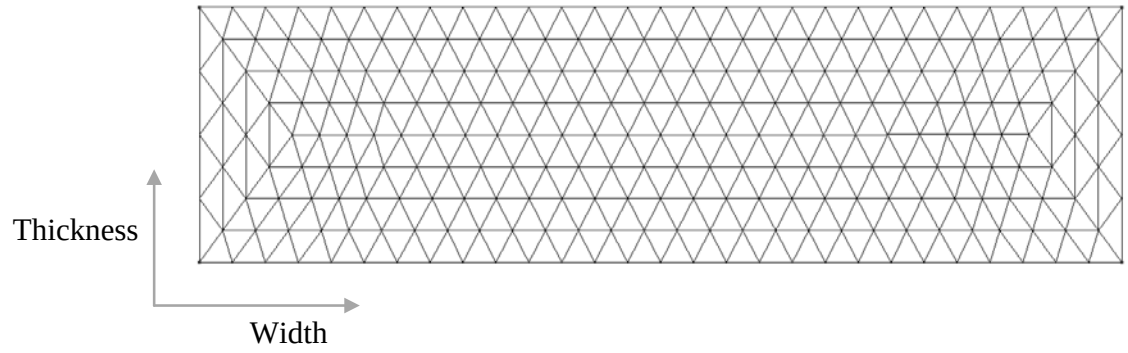

Figure 71. 516 element symmetrical, triangular, structured mesh used for simulations.

Table 70. CPU convergence times (after optimisation)

Species	CPU convergence time (s)
C. citriodora	39
E. marginata	242
E. pilularis	58
E. obliqua	146

Vacuum drying simulation results

Due to the large number of simulation outputs and similar results achieved between species, the model optimisation discussed below uses *C. citriodora* as an example for visual representation. A summary of important model outputs (figures and tables) is provided for all species towards the end of this section.

An example of the moisture content (MC), pressure and temperature field's visual simulations computed using *Transpore-2D* at 0, 16, 50, 100 and 225 hours is shown for *C. citriodora* (spotted gum) in Figure 72. As permeability values measured for each species are very low, drying is predominately driven by diffusion, hence the steep moisture gradients set-up during drying. The pressure gradient for *C. citriodora* was more pronounced than the other species as

C. citriodora is dried at much higher temperatures and has the lowest permeability and diffusivity.

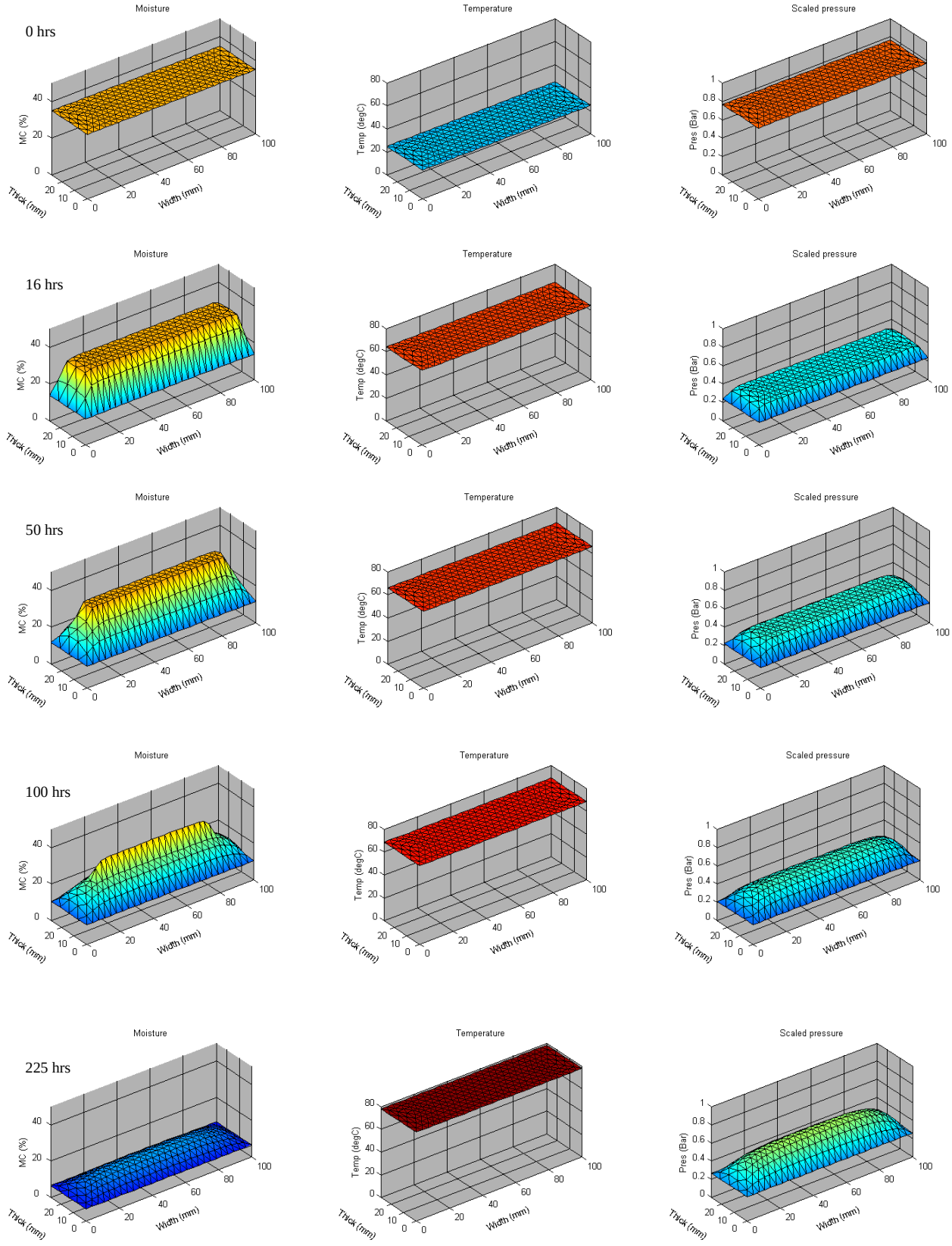

Figure 72. Transpore 2-D moisture content, temperature and pressure fields calculated at 0, 16, 50, 100 and 225 hrs for *C. citriodora*

Figure 73 shows a simulation result example for *C. citriodora*, using the input parameters provided in Table 68 and Table 69. For initial simulations, we used calculated diffusion coefficients for each species (equations (59) to (63)), because we had not yet measured diffusion coefficients we can observe that the simulated MC core results approach the final target MC much earlier than for the experimental results. Additionally, it appears that a rapid drop in simulated core MC is evident during the early stage of drying, up to approximately 16 hours, which is not replicated by experimental results. It can be observed from the simulated MC fields that, after 16 hours, a steep moisture gradient has been achieved affecting the first few millimetres into the thickness of the boards (Figure 73).

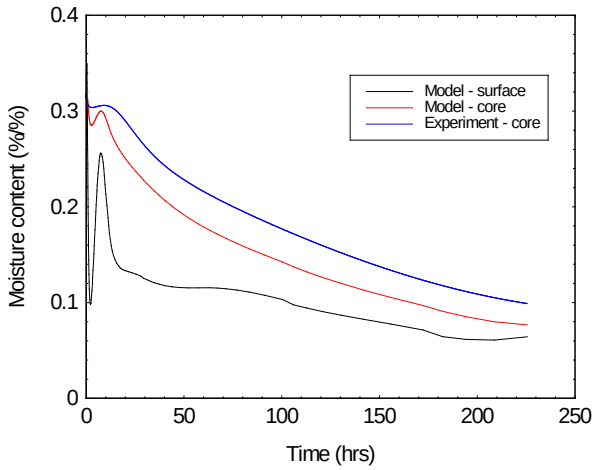

Figure 73. Transpore 2-D moisture content simulation results for *C. citriodora* using theoretical diffusion coefficient and unadjusted MC

It was postulated, that the experimental boards may already have suffered a level of surface drying during the sawing, transportation, grading and kiln stacking processes, thus not entering the kiln in a saturated condition (at least at the surface). We confirmed this from the most recent *C. citriodora* drying trial (SPG3), where, just prior to the boards entering the kiln, a sample board section was sliced into approximately 1 mm sections through the thickness and MC gradient measured, the results of which are shown in Figure 74. Figure 75 shows the simulated MC gradient for *C. citriodora* after 16 hours drying. After this period, the simulated MC gradient is similar to that shown in Figure 74.

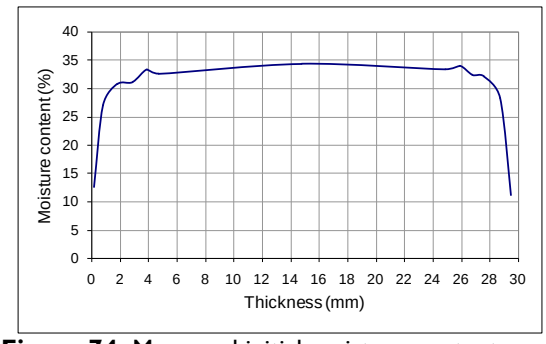

Figure 74. Measured initial moisture content gradient of spotted gum sample board immediately prior to vacuum kiln drying

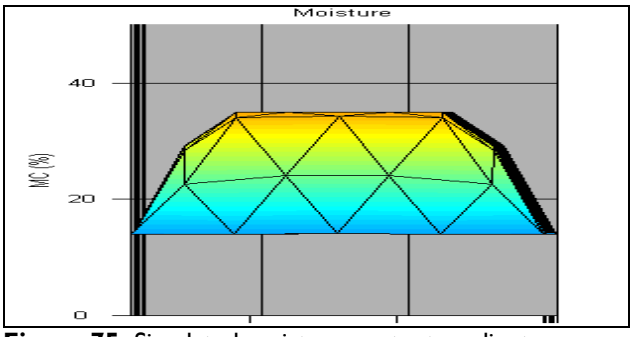

Figure 75. Simulated moisture content gradient for *C. citriodora after* 16 hours drying

To allow for this discrepancy, the initial MC for each species was increased for the second round of simulations, so that after 16 hours, the simulated and experimental core MC values were the same. Although not shown here, the final simulated core MC values for each species still approached the target final MC earlier than the experimental result. After testing the

sensitivity of all the drying 'driving force' parameters (porosity, permeability etc.) we concluded that the **diffusion coefficient** was by far the most sensitive in regards to the moisture content and pressure simulated outputs.

This conclusion led to the comparison of the measured diffusion coefficients with those calculated during the simulations. We did this by calculating the radial and tangential diffusion coefficients under the same temperature and humidity conditions that we measured diffusion coefficients. Table 71 shows the measured and calculated diffusion coefficient results and measured/calculated ratios for each species. Due to differing cutting patterns for each species only the radial diffusion coefficients for *C. citriodora*, *E. marginata*, and *E. pilularis* and tangential coefficients for *E. obliqua* were analysed, where the direction for each species pertains to perpendicular drying to the wide board face; the predominant drying direction. The results indicate that, except for *E. pilularis* a discrepancy exists between the measured and calculated diffusion coefficients, where the measured values are approximately 50 to 70% lower than the calculated values depending on the species. The reason for this discrepancy requires further investigation, however personal communication with Perrè (2010) suggests that extractive content could be a significant factor.

Table 71. Measured and calculated diffusion coefficient results under the same environmental conditions

	Diffusion Coefficient (m^2/s)		
	Measured	Calculated	Ratio
C. citriodora	1.43E-11	2.63E-11	0.54
E. marginata	2.58E-11	4.78E-11	0.54
E. pilularis	2.67E-11	2.62E-11	1.02
E. obliqua	4.08E-11	6.96E-11	0.59

We established that by correcting the diffusion coefficient calculations, using the ratios shown in Table 71, simulated and experimental core MC outputs more closely matched for each species. The correction factor was achieved by simply multiplying the tangential and radial macroscopic diffusivities described in the model by the corresponding correction ratio for each species, effectively correcting the calculated values.

Figure 76 shows an example of the MC simulation results for *C. citriodora* after the MC correction and using the diffusion coefficient corrections. A close match of MC core simulated and experimental outputs resulted.

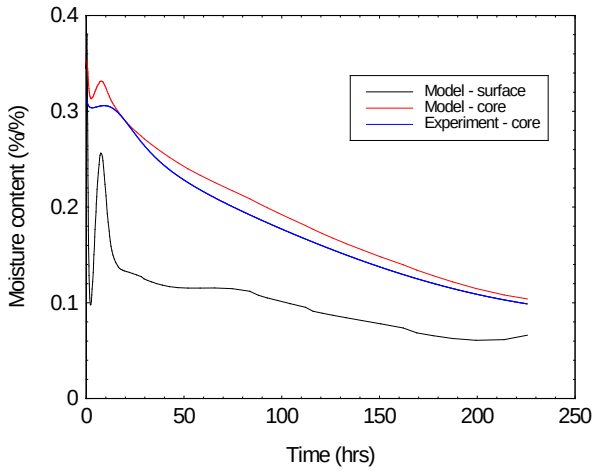

Figure 76. Transpore 2-D moisture content simulation results for *C. citriodora* using measured diffusion coefficient and adjusted MC

For subsequent simulations a pre-drying phase was introduced to accommodate the initial MC gradient set-up before drying, as previously described. Essentially, the pre-drying phase begins with cross-sections with no initial gradient, but with the previously established shifted initial average core MC. The simulation is then run under constant, mild drying conditions until the average cross-sectional MC reaches the experimental initial average MC, thus setting up a gradient in the cross-section reflecting the condition of material immediately prior to drying. The pre-drying conditions used were: 25 °C dry-bulb temperature, 20 °C wet-bulb temperature, 2 m/s airflow and ambient pressure (1 bar). After the pre-drying phase, the simulation automatically 'restarts' using the experimental drying conditions and the MC field established at the finalisation of the pre-drying phase.

The MC simulation results validated against the actual trial drying curves are presented in Figure 77 to Figure 80 and Table 72 for each species. The use of the pre-drying phase on matching the MC core simulated and experimental results shows a higher degree of accuracy than previous simulations. Additionally, the incorporation of a pre-drying phase reflects the actual situation during the start of industrial wood drying whereby a degree of MC gradient exists in board cross-sections.

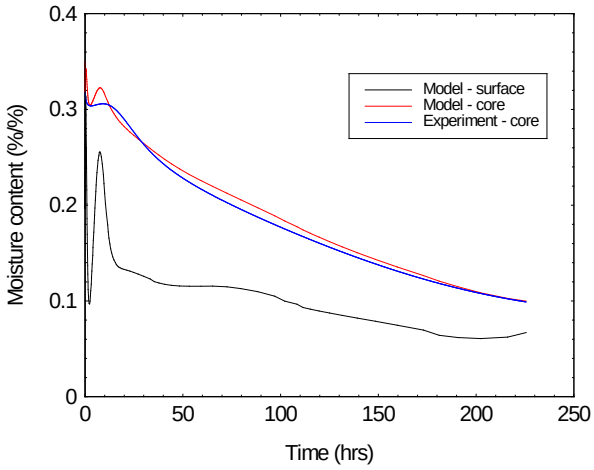

Figure 77. Transpore 2-D moisture content simulation results for *C. citriodora* using measured diffusion coefficient and pre-drying phase

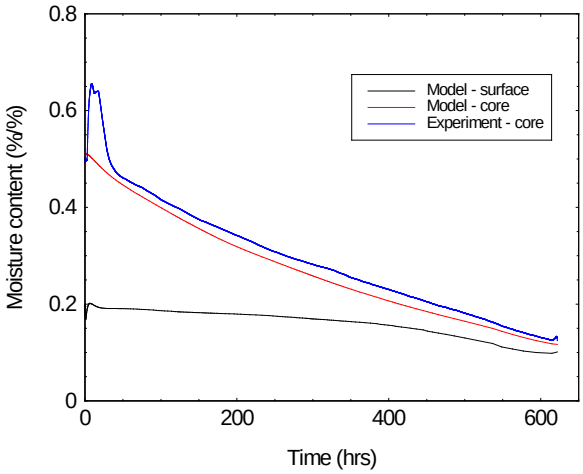

Figure 79. Transpore 2-D moisture content simulation results for *E.pilularis* using measured diffusion coefficient and pre-drying phase

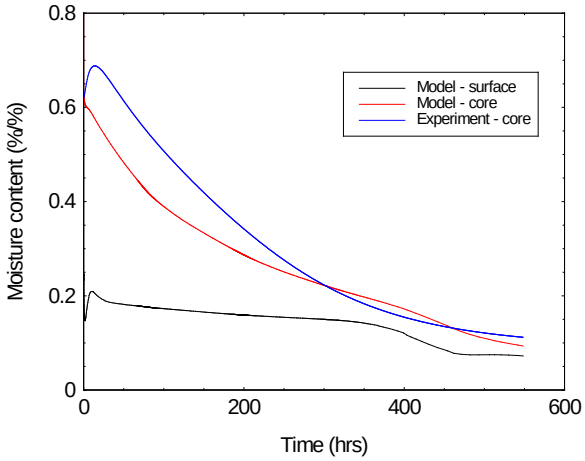

Figure 78. Transpore 2-D moisture content simulation results for *E. marginata* using measured diffusion coefficient and pre-drying phase

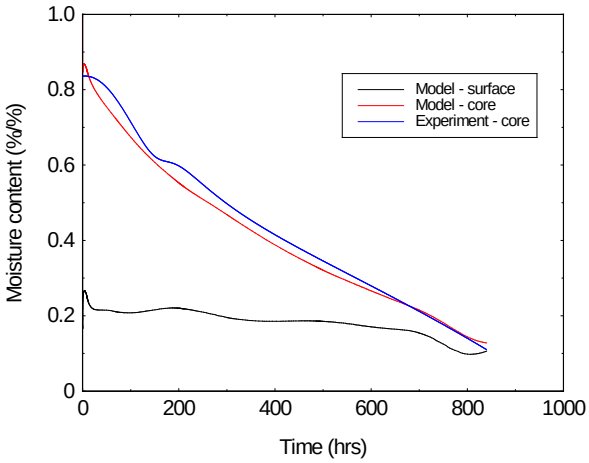

Figure 80. Transpore 2-D moisture content simulation results for *E.obliqua* using measured diffusion coefficient and pre-drying phase

Table 72. Simulation and experimental time comparisons versus MC

	Drying time (hrs)							
	C. citriodora		*E. marginata*		*E. pilularis*		*E. obliqua*	
MC (%)	Model	Experiment	Model	Experiment	Model	Experiment	Model	Experiment
50	-------	-------	104	87	32	39	297	203
30	15	14	230	247	264	239	570	538
20	75	78	326	405	459	419	717	726
15	132	139	410	461	558	536	787	790
11	197	216	548	535	610	588	815	831

Conventional drying simulation results

Using adjusted (measured) diffusion coefficient values, a simulation of conventionally drying *C. citriodora* was undertaken. The kiln drying schedule (dry and wet-bulb temperatures) was provided by Dale and Meyers sawmill, Queensland and is not published in this report due to commercial confidentiality. The air velocity was held at 2 m/s, common for this species, and the pressure held at ambient; 1000 mbar. All other simulation parameters were the same as those used to simulate vacuum drying for this species. The target final MC for this species is 11%, achieved after 504 hrs (21 days). We did not investigate conventional schedule simulations for the other species due to time constraints.

Figure 81 depicts the simulation results for MC. After 504 hours the final simulated MC was 11.1%, very close to the target. This signifies that the model, although developed for vacuum drying, can be readily used for conventional drying, the predominant drying method currently used by industry.

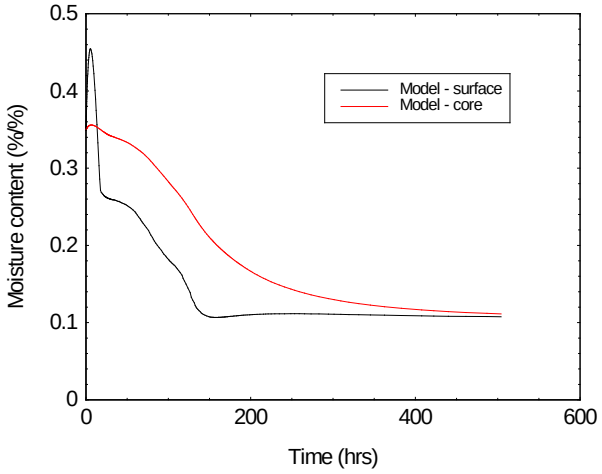

Figure 81. Transpore 2-D conventional drying moisture content simulation results for *C. citriodora* using measured diffusion coefficient and pre-drying phase

5 Discussion and conclusions

The principal objectives of this research were to:

- establish the viability of vacuum kiln drying Australian hardwood species compared with current conventional kiln drying methods,
- design a predictive drying model to accurately predict heat and mass transfer, and
- validate the drying model.

We achieved this through a series of end-matched conventional and vacuum drying trials, where a number of relevant wood, kiln and drying properties were measured for viability and model validation. Four trials for four species were conducted. We chose the species based on their wide ranging proximity, high commercial volume and vastly different wood properties and drying capabilities. The species were, *C. citriodora* (spotted gum), *E. marginata* (jarrah) *E. pilularis* (blackbutt) and *E. obliqua* (messmate).

In addition, to establish the economic viability of vacuum drying we prepared an economic model that provided a number of comparative case studies. Alongside this report, the economic model is also available as a useful tool for industry. In keeping with the structure of this report, the following project conclusions are presented under appropriate sub-headings.

5.1 Applied drying – Experimental drying trials

From the series of vacuum and conventional end-matched drying trials, we can form the following conclusions:

- The vacuum drying time was greatly reduced compared with end-matched conventional drying, where the best quality outcome vacuum drying times ranged between 41% and 66% of conventional kiln drying from green, depending on the species.
- For the most viable vacuum drying trials, the vacuum dried quality was either the same or better than the end-matched conventional drying counterpart, depending on the species.
- Unacceptable surface checking results were obtained for *E. pilularis* for every vacuum and conventional drying trial. However the percentage of boards making select grade for surface checking from the vacuum drying trials was considerably higher than for the conventional drying trials. We believe with further schedule adjustment acceptable surface checking resulting from vacuum drying can be obtained.
- Schedule adjustments greatly improved the dried quality between vacuum drying trials of the same species, resulting in us recommending the final vacuum drying schedule used for each species as a starting point for further vacuum drying.
- Twist was the major form of unacceptable distortion encountered for both vacuum and conventional trials across all species. Twist distortion was greatly reduced to within acceptable limits for vacuum drying trials by doubling the concrete stack weighting to 1000kg / m^3 between trials.
- A simple and efficient method was used to quantify the effect of reconditioning on collapse recovery using the image analysis software MeshPore. The reconditioning process was proved to effectively recover collapse eliminating ‘miss’ or ‘skip’ after dressing.
- For all trials, end splitting was significantly more prevalent in conventionally dried boards than vacuum dried boards. Reduction of end splitting could be a principal advantage over conventional drying. It is theorised that, due to overpressure, more longitudinal water flow occurs during vacuum drying, reducing MC gradients and associated stress at the board ends. This is a topic for further investigation.

5.2 Applied drying - Economic model

Using fundamental drying economics, we made and economic application with the ability to compare vacuum and conventional kiln drying from the green condition. We used this model to determine the economic viability of vacuum drying for each species over three different sized operations. We labelled the different sizes small, medium and large relating to wood capacities of 10, 35 and 50m^3. Kiln input data was provided by Brunner-Hildebrand, a project collaborator, and drying trial data were provided from the 'best outcome' applied drying trial for each species, based on a combination of the best drying quality and fastest drying time encountered. From the analysis the following conclusions can be made:

- For all sized operations, we found vacuum drying *E. marginata* and *E. pilularis* to be more economically viable than using current conventional methods.
- For large drying operations, we found vacuum drying *C. citriodora* and *E.obliqua* to be more economically viable than current conventional methods. This was not the case for the medium and small drying operations.
- The larger the drying operation the more economically viable vacuum drying becomes compared to conventional drying.
- The model is based on a number of assumptions and the case studies provided may not apply to all operations. The provision of the model as an application allows industry to tailor their own case studies to more closely simulate their own operation.

5.3 Drying modelling - Measurement of kiln conditions and wood drying properties

A number of specialised instruments were used on test and flying wood boards to measure wood shrinkage, moisture content and temperature, and kiln airflow during vacuum drying trials. Through continuous 'real–time' measurements, a greater understanding of the kiln conditions and wood properties during vacuum drying were obtained. The data produced is essential to input into and validate the modelling component of this project.

5.4 Drying modelling - Measurement of essential wood properties

We measured a number of wood properties that are essential provide the necessary structure for developing an accurate heat and mass transfer drying model. They were wood density, initial MC, fibre porosity, gas permeability, bound water diffusion and shrinkage. For many of these measurements sophisticated equipment was required. As a result of these measurements the following conclusions were made:

- Shrinkage data varied between species and was consistent with published data.
- Shrinkage values varied greatly between the tangential and radial directions, except for *C. citriodor*a, and shrinkage values between species differ due to variations in physical and chemical properties. In terms of shrinkage, *C. citriodora* is more isotropic compared with the other species tested.
- Collapse shrinkage was clearly evident for *Eucalyptus obliqua*, but not with other species, consistent with industrial seasoning experience. The wood-water relations of this species, free of collapse, was characterised by using thinner sample sections (in the radial-tangential plane) as theorised.
- A clear difference in fibre porosity, size, fibre cell wall thickness and orientation is evident between these species.
- A strong correlation was found between measured and calculated wood density, based on fibre porosity.
- *C. citriodora* diffusion coefficients were much lower in all directions compared with the other species, where *E. obliqu*a was the highest. The radial/tangential ratio of

diffusion coefficient for *C. citriodora* was approximately 1:1 indicating low diffusion isotropy in this plane. This is evident in many other wood property ratios measured for this species such as shrinkage and permeability.

- The ratio of longitudinal diffusion to both radial and tangential directions is much greater for *E. obliqua* than *C. citriodora*, indicating *E. obliqua's* greater propensity for drying in the longitudinal direction.
- The species investigated are highly impermeable compared to published data of exotic hardwood species and were at least a factor of 10 less permeable than the lowest published figure
- *C. citriodora* was the lowest permeability species measured, with the permeability order of the other species changing depending on wood direction.
- A fundamental technique was developed to increase the range of gas permeability measurements 4 orders of magnitude than previously measured using the same device.

5.5 Drying modelling - Vacuum drying modelling

Using the existing softwood drying model *Transpore 2D*, the model was re-coded and optimised in the Matlab environment, allowing peak performance with rapid convergence. The model is able to accurately simulate the heat and mass (water) transfer or flux in the radial and tangential wood directions. We conducted vacuum drying simulations for each species tested using the kiln drying and wood property parameters measured as part of this project. Additionally, we used the model to compare the conventional drying rate of *C. citriodora* using a known conventional schedule for this species. This was outside the proposed scope of this work. As a result of this modelling research the following conclusions can be made:

- The drying of these species is primarily limited by diffusion in the radial-tangential plane.
- Diffusion coefficient parameters seemed the most sensitive in regards to accurate heat and mass transfer modelling.
- Initial, uncorrected, simulations resulted in faster drying rates than experimental results.
- Accurate diffusion coefficient values have been characterised for each species in the radial, tangential and longitudinal directions. They were found to differ from theoretical calculations and have been successfully used to refine the model accuracy.
- Experimental material was found to be entering the kiln with moisture gradients due to manipulation of the boards prior to kiln drying. This seems to coincide with simulation results after approximately the first 16 hours of drying.
- The introduction of a pre-drying phase to simulate the initial setup of MC gradients prior to drying, and corrected radial and tangential macroscopic calculated diffusion coefficients resulted in a good agreement of simulated and experimental drying curves.
- Depending on the species, the model accurately predicted drying time form green to 11% MC within 91 to 98% of the actual drying trials.
- Using the model, including corrected diffusion coefficients, conventional kiln drying simulations of *C. citriodora* produced accurate determination of end-point MC after the same drying time as reported by industry.

6 Recommendations

The results of drying trials show that vacuum drying produces material of the same or better quality than is currently being produced by conventional methods in a much faster timeframe. Economic analysis indicates positive or negative results depending on the species and the size of drying operation. We recommend vacuum drying over conventional drying for all operation sizes, in terms of drying quality, time and economic viability, for *E. marginata* and *E. pilularis*. We also recommend vacuum drying over conventional drying for the same reasons for drying *C. citriodora* and *E. obliqua* in larger drying operations (kiln capacity 50 m^3 or above), but not for smaller operations at this stage. Further schedule refinement has the ability to reduce drying times further and may improve the vacuum drying viability of the latter species in smaller operations.

Anecdotal evidence suggests that vacuum drying viability is strengthened when drying thicker dimension timber as the difference in vacuum and conventional drying times is magnified. We recommend this topic for further investigation.

A comprehensive heat and mass transfer drying model has been developed with the ability to accurately simulate vacuum and conventional drying of Australian hardwood species. This has the ability to significantly reduce the time required for this type of research. We recommend developing the model to include a mechanical component with the ability to simulate drying shrinkage stress/strain to predict drying degrade such as checking, distortion and residual drying stress.

7 References

Blakemore, P. (2003), 'The use of handheld electrical moisture meters with commercially important Austrlian hardwoods.', Project no. PN01.1316, CSIRO report prepared for Forest and Wood Products Australia, viewed 11 March 2009, <http://www.fwpa.com.au>

Department of Primary Industries and Fisheries. (2008), viewed 7 March 2009, <http://www.dpi.qld.gov.au>

Forest Product Commission Western Ausrtalia. (2009), viewed 10 March 2009, <http://www.fpc.wa.gov.au>

ABARE. (2010), 'Australian forest and wood products statistics', viewed 23 May 2011, <http://abare/publications_html/afwps>

Aguiar, O. & Perré, P. (2000) The “flying wood” test used to study the variability of drying behaviour of oak. *Cost Action E15. 2nd Workshop: Advances in drying of wood, Sopron.*

Anon. (2011) Comparison of 2011 Australian Standing Offer Energy Prices. Office of the Tasmanian Economic Regulator. 30.

Avramidis, S. (2007) Chapter 6 - Bound water migration in wood. In: Perré, P. (Ed.) Fundamentals of wood drying, A.R.BO.LOR, Nancy. pp. 105-124.

Bird, R.B., Stewart, W.E. & Lightfoot, E.N. (1960) Transport Phenomena. John Wiley and Sons, Inc., New York.

Blakemore, P.A. & Langrish, A.G. (2008) Effect of collapse on fitted diffusion co-efficients for Victorian ash eucalypts. *Wood Sci. Technol.*, 42(535-549.

Bootle, K.R. (2004) Wood in Australia - Types, properties and uses. McGraw Hill, Sydney. 452.

Brandao, A. & Perré, P. (1996) The "Flying Wood" - A quick test to characterise the drying behaviour of tropical woods. In: *5th International IUFRO Wood Drying Conference*. Quebec, Canada,

Dadswell, H.E. (1972) The anatomy of eucalypt woods. 66. Commonwealth Scientific and Industrial Research Organisation. 1-40.

Dullien, F.A.L. (1992) Porous media: Fluid transport and pore structure. Academic Press Inc., New York.

Engwirda, R. (2009) Manager, Hurford Hardwood. Lismore, New South Wales. April 2009.

Hansmann, C., Wimmer, W.G. & Teischinger, A. (2002) Permeability of wood - A review. *Wood Research*, 47(4)**:** 1-16.

Innes, T.C. (1996) Improving seasoned hardwood timber quality with particular reference to collapse. *Engineering.* Hobart, University of Tasmania.

Innes, T.C., Bennet, P.J. & Lee, M.W. (2008) Processing backsawn Tasmanian regrowth *Eucalyptus obliqua*. *Tasforests*, 17(75-94)**:**

Leggate, W., Palmer, G., Mcgavin, R. & Muneri, A. (2000) Productivity, sawn recovery and potential rates of return from eucalypt plantations in queensland. In: *The future of eucalypts for wood products*. Launceston, Tasmania,

Malmquist, L. & Noack, D. (1960) Untersuchungen über die Trocknung empfindlicher Laubhölzer in reinemHeißdampf (ungesättigter Wasserdampf) bei Unterdruck. *Holz als Roh - und Werkstoff*, 18(5)**:** 171-180.

Mcmillen, J.M. (1963) Stresses in wood during drying. 1652. U.S. Department of Agriculture, Forest Service, Forest Products Laboratory.

Milota, M.R., Tschernitz, J.L., Verril, S.P. & Mianowski, T. (1995) Gas permeability of plantation loblolly pine. *Wood and Fibre Science*, 27(1)**:** 34-40.

Nolan, G., Innes, T.C., Redman, A.L. & Mcgavin, R. (2003) Australian hardwood drying best practice manual. Forest and Wood Products Research and Development Corporation, Melbourne.

Pearn, G. (2007) Personal communication, New South Wales, Boral Timber.

Perré, P. (1996) The Numerical Modelling of Physical and Mechanical Phenomena Involved in Wood Drying: an Excellent Tool for Assisting with the Study of New Processes. In: *5th Int. IUFRO Wood Drying Conference*. Quebec, Canada,

Perré, P. (2005a) Meshpore: A software able to apply image-based meshing techniques to anisotropic and heterogeneous porous media. *Drying Technology*, 23(1993-2006.

Perré, P. (2005b) *MeshPore*: a software able to apply image-based meshing techniques to anisotropic and heterogeneous porous media. *Drying Technology*, 23(9-11)**:** 1993-2006.

Perré, P. (2007a) Chapter 7 - Fluid Migration in Wood. In: Perré, P. (Ed.) Fundamentals of Wood Drying, A.R.BO.LOR, Nancy. pp. 125-156.

Perré, P. (2007b) Experimantal device for the accurate determination of wood-water relations on micro-samples. *Holzforschung*, 61(4)**:** 419-429.

Perré, P. (2010) Personal communication, Brisbane,

Perré, P. & Turner, J.W. (1999a) Transpore: A generic heat and mass transfer computational model for understanding and visualising the drying of porous media. *Drying Technology*, 17(7)**:** 1273-1289.

Perré, P. & Turner, J.W. (2008) A mesoscopic drying model applied to the growth rings of softwood: Mesh generation and simulation results. *Maderas, Ciencia y technologia*, 10(3)**:** 251-274.

Perré, P. & Turner, W. (1999b) A 3-D version of TransPore: a comprehensive heat and mass transfer computational model for simulating the drying of porous media. *Int. J. of Heat and Mass Transfer*, 42(4501-4521.

Redman, A.L. (2001) Improving quality of seasoned Tasmanian eucalypt species. *Faculty of Engineering.* Launceston, University of Tasmania.

Redman, A.L. (2007) Accelerated seasoning of plantaion grown *Eucalyptus cloeziana* and *Eucalyptus pellita* sawn timber. PN 07.3022. Forest and Wood Prupucts Australia. 1-30.

Redman, A.L. (2008) Charaterisation of wood properties and tranverse anatomy for vacuum drying modelling of commercially important Australian hardwood species. PG08.5097. Forest and Wood Products Australia. 1-82. http://fwpa.com.au.

Redman, A.L. (2010) Computational modelling of the vacuum drying of Austrlalian Hardwoods. Queensland Cyber Infrastructure Foundation. 1-43. http://www.qcif.edu.au.

Remond, R. (2010) Personal communication, Brisbane,

Rousset, P., Perre, P. & Girard, P. (2004) Modification of mass transfer properties in poplar wood (P. robusta) by a thermal treatment at high temperature. *Holz als Roh -und Workstoff*, 62(113-119.

Rozsa, A. & Mills, R.G. (1997) Index of kiln seasoning schedules. In: Waterson, G. C. (Ed.) Australian Timber Seasoning Manual, Third ed, Australian Furniture Research and Development Institute, Launceston. pp. 167-175.

Salin, J.G. (2010) Problems and solutions in wood drying modelling: history and future. *Wood Material Science and Engineering*, 5(123-134.

Savard, M., Lavoie, V. & Trembala, C. (2004) Technical and Economical Assessment of Superheated Steam Vacuum Drying of Northern Red Oak. In: *N.A.G.R.E.F. COST E15 Conference*. Forintel Canada Corp., Athens, Greece, 22-24 April.

Serway, R.A. (1998) Principles of physics. Saunders College Publishing, Florida.

Siau, J.F. (1979) The Effect of Temperature and Moisture Content on Physical Changes in Wood. In: *Rosen, H. N.; Simpson, W.; Wengert, E. M.; (Chairmen): Symposium on wood moisture content temperature and humidity relationships, Virginia Polytechnic Institute and State University, Blacksburg, Virginia, Oct. 29, 1979. 1979, 4 11; 31 ref.* Forest Products Laboratory, USDA Forest Service.; Madison, Wisconsin; USA,

Siau, J.F. (1984) Transport processes in wood. Germany, Springer-Verlag.

Standards Australia. (1997) *AS/NZS 1080.1: 1997 Timber-Methods of Test - Method 1: Moisture content* Australian and New Zealand Standard, distributed by SAI Global Limited.

Standards Australia. (1999) *AS 2796: 1999 Hardwood-Sawn and milled products*, Australian Standard, distributed by SAI Global Limited.

Standards Australia. (2000) *AS/NZS 1080.3:2000 Timber-Methods of test-Method 3: Density*, Australian and New Zealand Standard, distributed by SAI Global Limited.

Standards Australia. (2001) *AS/NZS 4787:2001 Timber-Assessment of drying quality*, Australian and New Zealand Standard, distributed by SAI Global Limited.

Turner, I.W. & Perré, P. (2004) Vacuum Drying of Wood with Radiative Heating: II. Comparison between Theory and Experiment. *AIChE Journal*, 50(1)**:** 108-118.

Whitaker, S. (1977) Simultaneous heat, mass and momentum transfer in porous media: A theory of drying. *Advances in Heat Transfer*, 13(119-203.

Acknowledgements

I would like to thank the following people and companies who, with their support, this research project was made possible.

Dr Henri Bailleres, Research Scientist Innovative Forest Products, DEEDI Queensland.

Robert McGavin, Research Scientist Innovative Forest Products, DEEDI Queensland.

Martin Davies, Research Scientist Innovative Forest Products, DEEDI Queensland.

Eric Littee, Research Technician Innovative Forest Products, DEEDI Queensland.

Daniel Field, Research Technician Innovative Forest Products, DEEDI Queensland.

Dr Patrick Perré, Professor, Head of LERMAB (Integrated research unit on wood science), AgroParisTech – ENGREF France.

Dr Ian Turner, Professor, School of Mathematical Sciences QUT, Queensland.

HPC Research Support, QUT, Queensland.

Queensland Cyber Infrastructure Foundation (QCIF), Queensland.

Ingo Wollocha, Sales Manager Brunner-Hildebrand, Germany.

Dale and Meyers management and staff, Maryborough, Queensland.

Burnett Sawmill management and staff, Bundaberg, Queensland.

Boral Timber management and staff, New South Wales.

Hurford Hardwood management and staff, Casino and Lismore, New South Wales.

Notaras and Sons management and staff, Grafton, New South Wales.

Gunns Timber management and staff, Manjimup, Western Australia.

Gunns Timber management and staff, Launceston, Tasmania.

ITC Limited management and staff, Huonville and Launceston, Tasmania.

FWPA management and staff, Australia.

8 Appendix1 – List of abbreviations

Latin letters

2D	two-dimensional	
3D	three-dimensional	
A	area	m^2
AE	acoustic emission	
Ag	green cross–sectional area	mm^2
A_i	image area	mm^2
A_k	activation energy	J
A_{nr}	non–reconditioned cross–sectional area	mm^2
A_r	reconditioned sample cross–sectional area	mm^2
A_{vj}	lumen area	μm^2
A_w	wood tissue area	μm^2
DMA	dynamic mechanical analysis	
AS	Australian Standard	
AS/NZS	Australian and New Zealand Standard	
BBT1..BBT4	blackbutt (*Eucalyptus pilularis*) end–matched drying trials 1 to 4	
c_p	specific heat	$J\ kg^{-1}\ K^{-1}$
C_L	amount of liquid tension collapse	%
c	molar concentration	$mol\ m^{-3}$
CF	collapse factor	
$\overline{\overline{\mathbf{D}}}$	diffusivity tensor	$m^2\ s^{-1}$
D	area of cross section less internal check area	m^3
DBT	dry bulb temperature	°C
DEEDI	Department of Employment, Economic Development and Innovation	
D_{gap}	gap between concave or convex faces	mm
D_{stress}	degree of residual drying stress	
E	modulus of elasticity	Pa
E*	complex modulus	Pa
E’	storage modulus	Pa
E”	loss modulus	Pa
EMC	equilibrium moisture content	%
ENGREF	l’École Nationale du Génie Rural des Eaux des Forêts	
ESEM	environmental scanning electron microscope	
e	sample thickness	m
FSP	fibre saturation point	

FWPA	Forest and Wood Products Australia	
G	area of green cross section	m^3
g	gravitational acceleration	$m\ s^{-2}$
HPC	High Performance Computing	
Hz	frequency	Hz
h	specific enthalpy	$J\ kg^{-1}$
h	heat transfer coefficient	$(W\ m^{-2}\ K^{-1})$
IP	intersection point	
l_{fi}	fibre lumen contour length	µm
l_{ij}	manually drawn contour length	µm
L	sample length	m
J	flux expression	
JAR1..JAR4	jarrah (*Eucalyptus marginata*) end–matched drying trials 1 to 4	
K	intrinsic permeability	m^2
$\overline{\overline{\mathbf{K}}}$	absolute permeability tensor	m^2
$\overline{\overline{\mathbf{k}}}$	relative permeability tensor	
k	Boltzmann's constant	
k_a	air permeability	m^2
k_L	deformation constant	
k_m	mass transfer coefficient	$m\ s^{-1}$
k_r	relative permeability	
L	Longitudinal	
L	sample thickness	m
l	length	m
M	molecular weight	$kg\ mol^{-1}$
MC	moisture content	
m	mass vapour transferred	
MES1..MES4	messmate (*Eucalyptus obliqua*) end–matched drying trials 1 to 4	
$\mathbf{n}$	unit normal	
ΔP	pressure difference	Pa
$\overline{P}$	average pressure	Pa
$\boldsymbol{P}$	pressure	Pa
PC	personal computer	
P	total liquid tension	$N\ m^{-2}$
P_l	pressure of the metastable liquid phase	Pa
P_K	pressure inside bubble	Pa
Q	flux	$m^2\ s^{-1}$
Q	the limit of plastic flow	$N\ m^{-2}$

QUT	Queensland University of Technology	
r	principle radii of curved surface	m
R	gas constant	J mol^{-1} K^{-1}
R	radial	
R&D	research and development	
S	volume saturation	
S_o	collapse free shrinkage	%
SPG1..SPG4	spotted gum (*Corymbia citriodora*) end–matched drying trials 1 to 4	
SRC	Salisbury Research Centre	
t	time	s
T	temperature	K
t_{ave}	average cell wall thickness	µm
T_d	board thickness dry	m
T_g	board thickness green	m
TG	glass transition temperature	°C
v	mass velocity vector	m s^{-1}
v	air velocity	m s^{-1}
v	Poisson's ratio	
V_g	green volume	m^3
V_S	volumetric shrinkage	m^3 m^{-3}
VSD	variable speed drive	
VOC	volatile organic compounds	
W	board width	m
WBD	Wet bulb depression	°C
W_d	board width dry	m
W_g	board width green	m
x	rectangular coordinate	m
X	molar fraction	(mol/mol)
X	magnification	
X	moisture content (dry basis)	kg kg^{-1}
Z_1	molecules per cm^3	cm^{-3}

Greek symbols

ε	volume fraction	
ε	strain	m m^{-1}
δ	phase angle	
δ	amplitude of deformation	
λ	molecular latent heat of evaporation	kJ kg^{-1}

λ	thermal conductivity	W m^{-1} K^{-1}
ρ	intrinsic averaged density	kg m^{-2}
ρ_0	wood density	kg m^{-2}
σ	surface tension	N m^{-1}
$\sigma(T)$	surface tension at temperature *T*	N m^{-1}
σ_x	stress	Pa
σ*	complex stress	Pa
σ’	elastic stress	Pa
σ”	viscous stress	Pa
τ	relaxation time of collapse process	s
μ	dynamic viscosity of air	Pa. s
φ	phase potential	
ϕ	porosity	m^3 m^{-3}
χ	depth scalar	m
ω	mass fraction	

Superscripts and subscripts

a	air
b	bound water
c	capillary
calc	calculated
crit	critical
e	enthalpy
eff	effective property
f	fibres
fsp	fibre saturation point
g	gas phase
i,j	structural direction of wood
L	longitudinal direction
l	liquid
r	relative
R	radial direction
s	solid phase
t	top
T	tangential direction
v	vapour phase
v_∞	vapour phase at boundary
v	vessels

w	liquid phase
wt	wood tissue
∞	value outside the boundary layer in the free stream